Quasi-Static Approximation for Numerical Computation of Plasmon Eigenfrequencies in Nanoparticles

by

Abdulhamed Alsisi

A thesis
presented to the University of Waterloo
in fulfillment of the
thesis requirement for the degree of
Master of Mathematics
in
Applied Mathematics

Waterloo, Ontario, Canada, 2014

Author's Declaration

I hereby declare that I am the sole author of this thesis. This is a true copy of the thesis, including any required final revisions, as accepted by my examiners.

I understand that my thesis may be made electronically available to the public.

Abstract

General physical properties of electrostatic (plasmon) resonances in nanoparticles are presented. Direct calculation of the resonance values of the permittivity of nanoparticles, and subsequently their resonance frequencies, through a boundary element method is discussed. An efficient numerical approach for the calculation of resonance frequencies of a spherical nanoparticle is developed and illustrated, which is compared with theoretical results. Results of numerical approach for a spherical nanoparticle in free space and on a silicon dioxide substrate are presented and discussed.

Acknowledgements

I would like to thank all the people who made this possible. First and foremost, thank you to my advisors, Professor Lilia Krivodonova and Professor Zoran Miskovic, for their expertise and encouragement. They patiently helped to improve my writing, and provided valuable guidance and discussion in solving problems. I would not have completed this thesis without their help. I would like to thank my committee members, Professor Hans De Sterck and Professor Mohammad Kohandel.

Special thanks also to Dr. Andree Susanto for his invaluable assistance in this work, especially during late nights squashing bugs in my code. And also for our incomparably long discussion.

I would like to express my appreciation to Amir Issaei for his support. I would to thank Dr. Ahmet Ozkan Ozer for our friendship and his help. I would like to thank Dr. Venkata Manem, Subasha Wickramarachchi, Daniel Otero-Fadul, Dr. Puneet Sharma, Dr. Dhanaraja Kasinathan, Helen Warren, Stephanie Martin, Maureen Fraser, Laura Frazee, lai junyu, and Dr. Hamid Molavian for all their help.

I would like to express my appreciation to Keenan Lyon and Arman Tavakoli for reading and reviewing my thesis giving valuable corrections.

Finally, I would like to acknowledge the support provided by my family during the preparation of this thesis, my father Hamza Alsisi, my mother Aisha Rashwan , my brothers Dr.Gassan Alsisi, Dr. Rayan Alsisi, and Dr.Mohammed Alsisi, my sister Dr.Areej Alsisi, my wife, and my angels Aisha and Hamza.

Dedication

This is dedicated to the ones I love. To my beloved parents, loving children, wife, dear brothers and sister.

Table of Contents

List of Tables

List of Figures

Chapter 1

Introduction

The interaction between light and matter has been an essential aspect of various scientific studies. This interaction has been the subject of study by various brilliant scientists, many of whom have produced impressive results.

In the past, many believed that the wavelength of light sets a fundamental threshold on the area of light's focus, as propagating waves cannot be focused down to a spot smaller than or approximately half of their wavelength [1]. Nevertheless, new developments have come to show that light is not restricted to freely propagating waves. Electromagnetic fields oscillating at optical frequencies can also exist in the form of transient waves bound to the surface of an object that contains quasi-free charge carriers, such as electrons in precious metals. The near field radiation of an object is not subject to the same diffraction limit as the far field radiation, and can be confined to dimensions as small as the atomic scale. Therefore, the purpose of nano-optics is to explore an effective method of directing optical energy into evanescent waves on metallic nanoparticles. Part of the power of surface plasmonics is they don't decay away from the surface, which is what "evanescent" means.

1.1 Surface Plasmons

Surface plasmons are quantized oscillations at an interface between two materials: a material with negative permittivity and free charge carriers, typically a metal, and a material with positive permittivity involving a collective oscillation of surface charges [2].

The first documented observation of a surface plasmon by R. Wood dates back to 1902 [3, 4]. Wood beamed an iridescent light on a metallic diffraction grating and observed narrow dark bands in the spectrum, which became known as anomalies [5]. L. Rayleigh [6] provided a physical interpretation of this occurrence, which was later refined by Fano [7, 5]. Fano concluded that these anomalies were associated with excitation of electromagnetic surface waves on the surface of the diffraction grating [3]. Extending on the work of Pines and Bohm, Ritchie [8] predicted existence of surface plasmons oscillation in 1957 [2], and Stern and Ferrell [9] coined the term "surface plasmon" [10]. Powell and Swan [11, 12] experimentally proved Ritchie's predictions a few years later [10]. In 1968 Otto [13], Kretschmann and Raether [14] documented excitation of surface plasmons [15].

Experimental progress in assessing the optical phenomena resulting from electromagnetic response of metals has led to the fast-growing research field of palsmonics.

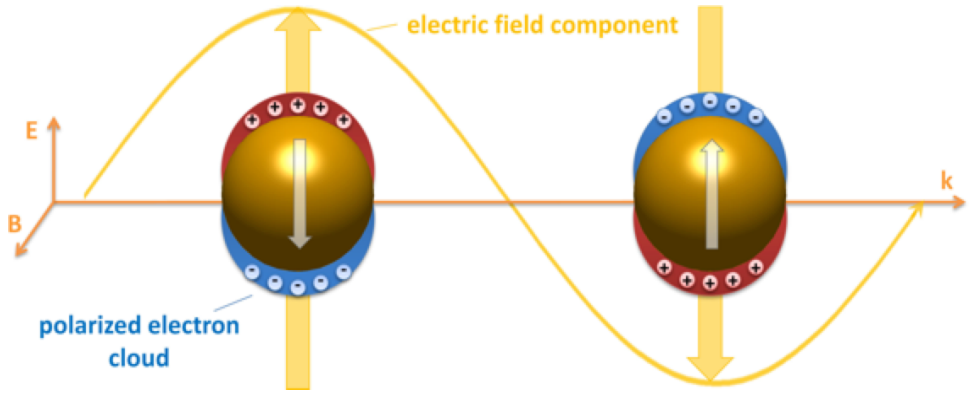

Figure 1.1: Excitation of particle's plasmons, adopted from [15]. Electric field caused by incoming electromagnetic waves. The yellow balls are nano-particles, typically metallic.

1.2 Plasmonics

The primary objective in plasmonics, which has played an enormous role in the field of nanophotonics, is to explore the interaction of electromagnetic fields with nanoparticles whose dimensions are smaller than their wavelength. This phenomenon is a result of the interaction between electromagnetic radiation and conduction electrons in small, mostly metallic, nanostructures. This in turn results in an enhanced optical near field of sub-wavelength dimension. Although surface plasmon polaritons and localized surface plasmons, the two main components of plasmonics, have been consistenetly mentioned in the scientific literature since the early twentieth century, the field of plasmonics has only recently witnessed great progression in research and application [16].

When incident light hits a metal nanoparticle, the electrons in the particle move to one side, as a result of electric field polarization, leaving behind positive charges on the opposite side, see Figure 1.1. Subsequently, because of attraction between negative and positive charges, the electron cloud oscillates from side to side at a certain frequency. If the frequency of incident electromagnetic wave matches one of the resonance frequencies of the particle, extensive oscillation of all of the free electrons in the metal will be produced. In turn, large electric fields are produced in the particle, influencing the electrons and reinforcing the oscillations. This excitation produced by oscillating charges inside the particle coupled with oscillating electromagnetic fields immediately outside the particle is commonly known as a plasmon resonance or localized surface plasmon [1].

Conduction electrons move rapidly on the order of femtoseconds (femtoseconds is 10^{-15} seconds) when an electric field is applied to a metal. This movement is rapid relative to the frequencies of microwaves and radio waves. Thus, metals can be viewed as perfect conductors. In metal objects whose dimensions are larger than the wavelength of a given electromagnetic wave, the incident light would not excite plasmons with high efficiency [1]. However, in nanoscale objects whose dimensions are smaller than the wavelength of electromagnetic waves, the coupling between light and plasmon resonance can be very strong. Hence, metal nanoparticles have the capability of pushing optics fully into the nanometer size range and, in turn, allowing ordinary light fields to generate strong evanescent waves that are confined on the nanoscale [1]. These materials have been nearly the exclusive subject of plasmonics research as they support high quality plasmon resonances at optical frequencies. The greater the number of electrons involved in a plasmon oscillation, the

greater the electrostatic restoring force, and the greater the resonance frequency.

When comparing various materials, losses in silver and gold are considered relatively low. In fact, silver has the lowest losses, and consequently the strongest plasmon resonances, of all known materials. Gold, on the other hand, is more stable chemically and physically than silver, and hence it is used more often [1].

Certain aspects of promising growth in the field of plasmonics are responsible for its current development, such as promise in the development of new super fast computer chips, new possibilities for treating cancer, ultra-sensitive molecular detectors and the ability of making things invisible with negative-refraction materials. Besides the aforementioned, the capability to manipulate and control light on the nanometer scale opens up a wide range of possibilities in terms of application of plasmonics that include data storage, optical data processing, quantum optics, optoelectronics, photovoltaics and quantum information processing [15].

1.3 Localized Surface Plasmon Resonance

The total excitation including both the charge motion and the associated electromagnetic field is called a Localized Surface Plasmon Resonance (LSPR) for the closed surface of a small particle. The curved surface of the particle applies a restoring force on the driven electrons resulting in the plasmon resonance and subsequently field amplification inside and in the near-field region outside the particle [17]. LSPRs have the ability to guide and enrich light fields. They are usually confined to length scales that are smaller than the diffraction limit, and hence are suitable for localization and enhancement of electromagnetic fields. LSPR has been a topic of study for many years, particularly considering the role that such excitation plays in scanning transmission electron microscopy, near field optical spectroscopy [10], and biosensor applications. More historical overview for the use of the phenomenon for biosensor applications is given in [5]. In recent years, the role of localized surface plasmons in nanostructures has become a topic of interest. Localized plasmons in nanostructures, as well as carbon based structures, can be excited through interaction with light. Hence, they can be detected in the form of pronounced optical resonances [17].

The resonances occur in nanoparticles at frequencies for which the following two conditions are satisfied: 1) the particle permittivity is negative, this is also due to a positive permittivity outside the particle. It is the interface that allows the plasmons to exist and not decay. Also, 2) the free-space wavelengths of electromagnetic radiation in the visible range are large in comparison with the nanoparticle's dimensions. The latter condition implies that these resonances are electrostatic in nature [18]. That means electrostatic resonance may occur only when the particle's permittivity is a function of frequency and its real part has negative values for some range of frequencies. For metals, this frequency range is below the plasma frequencies, a time-scale in plasma physics [5]. Each material has a unique plasma frequency that is determined by the volume density of electrons in the bulk of the material. For good conductors such as silver and gold, plasma frequencies are in the range of the visible frequency range, and this explains why silver and gold nanoparticles are usually employed in plasmon resonance studies and applications. However, for nanoparticles of various shapes, there may exist multiple resonant frequencies, which are determined by the geometrical factors [5].

The primary objective of this thesis is to study efficient numerical algorithms for calculating the permittivity values for which resonant frequencies occur on nanoparticles. We achieve this by transforming the partial differential equation describing the problem into an integral eigenvalue equation. The latter can be used to compute the resonance frequencies.

The first numerical simulation of this kind was accomplished by Ouyang and Isaacson [18]. The field has witnessed enormous progress after the publication of I. Mayergoyz, D. Fredkin and Z. Zhang's paper [5, 2, 19]. In their work, they referred to the prossess as "Electrostatic (plasmon) resonance in nanoparticles".

The numerical method used here is called the Boundary Element Method (BEM). BEM is a numerical method for solving linear partial differential equations encountered in mathematical physics and engineering [20]. The basic idea is to express the solution in terms of boundary distributions of fundamental solutions of the differential equation. The fundamental solutions are the Green's functions expressing the field due to a localized source. Then, we compute the densities of the distributions that satisfy the boundary conditions.

1.4 Electrostatic Approximation

The traditional approach in the literature in examining the electronic plasma resonance in nanoparticles neglects all losses and computes resonance frequencies for lossless systems [18]. This approach is based on a presumption that the nature of resonances in metallic nanoparticles is electrostatic, as in the case of interfaces, see [16]. These resonances take place at frequencies for which the particle permittivity is negative and the dimensions of the nanoparticle are much smaller than the wavelength. When the dielectric permittivity of metallic nanoparticles is negative, Poisson's equation for electrostatics combined with boundary conditions for our system has only the trivial solution, with frequencies corresponding to the above negative values are the resonance frequencies [5]. Because the surface plasmons are restrained to the surface, there is no decay away from it, meaning Laplace's equation is still valid. The metallic nanoparticles behave at optical frequencies as particles with dispersion. This means that the permittivity depends on frequency, and its real part assumes a negative value for some range of frequencies. In Appendix A, we show a simple derivation of the so-called Drude model for a frequency-dependent pemitiviity of a metal. This range of frequencies in metal particles is below the plasma frequencies. On the other hand, gold and silver nanoparticles, which are good conductors, provide a good sample for the observation of electrostatic, or plasmonic resonance as their frequencies are in the visible light frequency range [5]. To give more details we have to start from Maxwell's equations.

1.4.1 Maxwell's Equations

The interaction of metals with electromagnetic fields can be fully described by Maxwell's equations. Maxwell's equations are a set of fundamental equations governing all microscopic and macroscopic electromagnetic phenomena. In the differential form, they are written as:

$$\nabla \times \vec{E} = -\frac{\partial \vec{B}}{\partial t}, \tag{1.1}$$

$$\nabla \times \vec{H} = \frac{\partial \vec{D}}{\partial t} + \vec{J}, \tag{1.2}$$

$$\nabla \cdot \vec{D} = \rho, \tag{1.3}$$

$$\nabla \cdot \vec{B} = 0. \tag{1.4}$$

These equations are known individually as Faraday's law (1.14), Ampere's circuital law (1.15), and Gauss' law (1.3) and (1.4) for electricity and magnetism, respectively. These equations link the four fields i.e. $\vec{E}$ (the electric field), $\vec{H}$ (the magnetic field), $\vec{D}$ (electric flux density), and $\vec{B}$ (magnetic flux density), with the external electric charge and current densities ρ and $\vec{J}$.

Besides Maxwell's equations, the field vectors $\vec{E}$ and $\vec{H}$ are coupled with their respective flux densities by material constitutive relations, and can be linked via the polarization $\vec{P}$ and magnetization $\vec{M}$ by:

$$\vec{D} = \epsilon \vec{E} = \epsilon_0 \vec{E} + \vec{P}, \tag{1.5}$$

$$\vec{H} = \frac{1}{\mu}\vec{B} = \frac{1}{\mu_0}\vec{B} - \vec{M}, \tag{1.6}$$

where ϵ_0 and μ_0 are the dielectric permittivity and magnetic permeability of vacuum, respectively. In vacuum without external charge, we write these equations as:

$$\vec{D} = \epsilon_0 \vec{E}, \tag{1.7}$$

$$\vec{H} = \frac{1}{\mu_0}\vec{B}. \tag{1.8}$$

Placing (1.7) in (1.3) with $\rho = 0$ we get:

$$\nabla \cdot \vec{E} = 0. \tag{1.9}$$

Doing the same steps but this time by placing (1.7), (1.8) and (1.9) in (1.15), and setting $\vec{J} = 0$, we obtain

$$\nabla \times \vec{B} = \mu_0 \epsilon_0 \frac{\partial \vec{E}}{\partial t}. \tag{1.10}$$

Taking the curl of (1.14) and substituting equation (1.10) in the right hand side, we get the wave equation for $\vec{E}$

$$\nabla^2 \vec{E} - \frac{1}{c^2}\frac{\partial^2}{\partial t^2}\vec{E} = 0, \tag{1.11}$$

where $\frac{1}{c^2} = \mu_0 \epsilon_0$ and c is the speed of light in vacuum. Taking the Fourier transform with respect to the spatial coordinates and time, the fields can be turned into individual plane-wave components of wave vector $\vec{K}$ and angular frequency ω:

$$\left(\vec{K}^2 - \frac{c^2}{\omega^2}\right)\vec{E} = 0. \tag{1.12}$$

With the definitions $K = \lambda/(2\pi)$ and $\omega = 2\pi\nu$, we can say

$$\lambda = \frac{c}{\nu}, \tag{1.13}$$

where λ is the wavelength of light in the surrounding medium and ν is its frequency. Then if the wavelength is much bigger than, the diameter of the particle d, $\lambda \gg d$, Maxwell's equations can be simplified using the quasi-static approximation.

1.4.2 Quasi-static Approximation

The idea of the quasi-static approximation is that the particle is much smaller than the wavelength of light in the surrounding medium. The phase of the harmonically oscillating electromagnetic field is practically constant over the particle volume, so that one can calculate the spatial field distribution by assuming the simplified problem of a particle in an electrostatic field. Thus, the magnetic field is not important and can be neglected by assuming that the speed of light in (1.10) is infinite. Thus, we can rewrite Maxwell's equations (1.14) - (1.4) as

$$\nabla \times \vec{E} = 0, \tag{1.14}$$

$$\nabla \times \vec{H} = 0, \tag{1.15}$$

$$\nabla \cdot \vec{D} = \rho, \tag{1.16}$$

$$\nabla \cdot \vec{B} = 0. \tag{1.17}$$

Using $\nabla \times \vec{E} = 0$, we can calculate the electric field by finding the solution of Poisson equation for the electric potential

$$\vec{E}(\vec{r}, t) = -\nabla\Phi(\vec{r}, t). \tag{1.18}$$

In using (1.5) for a material with dielectric constant ϵ, we have

$$\vec{D} = \epsilon\vec{E} = -\epsilon\nabla\Phi. \tag{1.19}$$

Using equation (1.16) the Poisson equation is written as

$$\nabla \cdot (\epsilon\nabla\Phi) = -\rho. \tag{1.20}$$

In this thesis, I shall concentrate on solutions of the Poisson equation when there are no external sources of electric field, i.e. $\rho = 0$ in (1.20). We can use the resulting Laplace's equation because plasmon resonance occurs with no external charges added to the system. The resulting Laplace equation is going to be solved by implementing boundary conditions on a particle that is characterized by a frequency-dependent dielectric function $\epsilon(\omega)$. In this way, I shall deduce an eigenvalue problem that will give a set of frequencies ω for which the particle supports self-sustained oscillations of its charge carriers called plasmons.

1.5 Structure of the Thesis

This thesis is divided into three main parts. In Chapter 2, we will discuss two techniques for formulation of a Boundary Integral Equation (BIE). will provide a detailed derivation of BIE for a particle in free-space and half-space. At the beginning of Chapter 3 a short historical overview of BEM is given, from the first use to the modern perception. Then, we will present an implementation of BEM to the problem described in Chapter 2. In Chapter 4, we show the result of applying BEM with two different approaches.

1.5.1 Measurement Units

We have used International System of Units (SI) throughout the thesis.

Chapter 2

Boundary Integral Equation

There are two methods with which one can formulate elliptic boundary value problems as boundary integral equations (BIEs). The indirect method is expressed in terms of non-physical single and double layer potentials. The unknown density functions, that have been defined on the surface, are then determined by the given boundary data. The direct method involves the modeling of actual physical variables where the given boundary data is inserted into Green's representation formula, which in turn is solved for the unknown boundary data. Both versions involve the integration of Green's function for the operator modeling the behavior of the medium that is being treated, and both are especially well-suitable for the study of infinite domains. The principle of the indirect method consists in first determining the unknown density function as a solution of a boundary integral equation by means of the given boundary conditions. Then we can insert it into the associated potentials, which gives us the solution of the boundary value problem. For more details about the two techniques see [21, 22].

2.1 Direct Formulation

As discussed the direct formulation of BIE requires the implementation of the electrostatic potential $\Phi(\vec{r})$ and Green's function of the Poisson's equation in Green's identity. Steps of how to construct the direct formulation are presented in this section. Consider a closed domain V with boundary S, and consider the Poisson equation

$$\nabla^2\Phi(\vec{r}) = -\frac{1}{\epsilon}\rho(\vec{r}); \;\; \vec{r} \in V. \tag{2.1}$$

The solution $\Phi(\vec{r})$ of (2.1) represents the potential produced at a point $\vec{r}$ in a domain V due to a source of electric charge with volume density $\rho(\vec{r})$ distributed over V. We will only consider the Laplace equation for which $\rho(\vec{r}) = 0$, that is

$$\nabla^2\Phi(\vec{r}) = 0; \;\; \vec{r} \in V, \tag{2.2}$$

where ∇^2 is the Laplacian operator in three dimensions defined as

$$\nabla^2 \equiv \frac{\partial^2}{\partial x^2} + \frac{\partial^2}{\partial y^2} + \frac{\partial^2}{\partial z^2}. \tag{2.3}$$

To compute the solution of (2.2) we require boundary conditions, as follows

- Dirichlet boundary conditions;

$$\Phi(\vec{r}) = g(\vec{r}), \quad \vec{r} \in S, \tag{2.4}$$

where g is a given function.

- Neumann boundary conditions;

$$\frac{\partial \Phi}{\partial \hat{n}}(\vec{r}) \equiv \hat{n} \cdot \nabla \Phi(\vec{r}) = h(\vec{r}), \quad \vec{r} \in S, \tag{2.5}$$

where $\hat{n}$ is the outward unit normal at S and $h(\vec{r})$ is a given function.

- Mixed boundary conditions;

$$\begin{cases} \Phi(\vec{r}) = g(\vec{r}), & \vec{r} \in S_1, \\ \frac{\partial \Phi}{\partial \hat{n}} = h(\vec{r}), & \vec{r} \in S_2, \end{cases}$$

where g and h are given functions defined on disjoint parts S_1 and S_2 of the boundary, such that $S = S_1 \cup S_2$.

We cannot convert the ordinary differential equations (ODEs) or PDEs into BIEs without the fundamental solutions [21]. The fundamental solution of the Laplace equation is the solution of the singularly forced Poisson equation. Green's functions of Laplace equation in three dimensions form a particular class of harmonic functions that are singular at an arbitrary point $\vec{r}' = (x_0, y_0, z_0)$. Hence, by definition Green's functions satisfy the singularly forced Poisson equation

$$\nabla^2 G(\vec{r}, \vec{r}') + \frac{1}{\epsilon}\delta(\vec{r} - \vec{r}') = 0, \quad \forall \vec{r}, \vec{r}' \in \mathbb{R}^3, \tag{2.6}$$

where

- $\vec{r} = (x, y, z)$ is the variable "field point".
- $\vec{r}' = (x_0, y_0, z_0)$ is the fixed location of "singular point" or pole.
- $\mathbb{R}^3$ indicates the full there dimensions space.
- $\delta(\vec{r} - \vec{r}')$ is the Dirac delta function in three dimensions that represents a unit source at the source point $\vec{r}'$.
- ϵ is the permittivity of the medium.

The Dirac delta function $\delta(\vec{r} - \vec{r}')$ satisfies the following properties [20]:

1. $\delta(\vec{r} - \vec{r}')$ vanishes everywhere except at the point $x = x_0, y = y_0, z = z_0$, where it becomes infinite.
2. $\int_V \delta(\vec{r} - \vec{r}')dV = \begin{cases} 1, & \vec{r}' \in V, \\ 0, & \vec{r}' \notin V. \end{cases}$

3. $\int_V \delta(\vec{r}-\vec{r}\,')\Phi(\vec{r})dV = \begin{cases}\Phi(\vec{r}\,'), & \vec{r}\,' \in V,\\ 0, & \vec{r}\,' \notin V.\end{cases}$

The direct boundary integral equation (DBIE) can be found through the Green's second identity, shown below [23]. Let V be a domain with boundary surface S and $\hat{n}$ is the outward unit normal. Moreover, let $f(x,y,z)$ and $g(x,y,z)$ be two twice continuously differentiable scalar functions of position in V

$$\iiint_V \left(f\nabla^2 g - g\nabla^2 f\right) dV = \iint_S \left(f\nabla g - g\nabla f\right)\cdot \hat{n}\, dS. \tag{2.7}$$

Now we apply it to our problem in (2.2) to get

$$\iiint_V \left(G(\vec{r},\vec{r}\,')\nabla^2\Phi(\vec{r}) - \Phi(\vec{r})\nabla^2 G(\vec{r},\vec{r}\,')\right) dV = \oiint_S \left(G(\vec{r},\vec{r}\,')\frac{\partial\Phi}{\partial\hat{n}}(\vec{r}) - \Phi(\vec{r})\frac{\partial G}{\partial\hat{n}}(\vec{r},\vec{r}\,')\right) dS. \tag{2.8}$$

Applying equations (2.2) and (2.6), interchanging the roles of r and r', using the Maxwell's symmetry of the Green's function, and using the property (3) we obtain

$$\Phi(\vec{r}) = \oiint_S \left(G(\vec{r},\vec{r}\,')\frac{\partial\Phi}{\partial\hat{n}'}(\vec{r}\,') - \Phi(\vec{r}\,')\frac{\partial G}{\partial\hat{n}'}(\vec{r},\vec{r}\,')\right) dS'. \tag{2.9}$$

Since the Green's function $G(\vec{r},\vec{r}\,')$ is singular at the point $\vec{r}\,'$, we will construct a volume V_c that is bounded by a closed surface D inside the domain V, isolating the point $\vec{r}\,'$. This is required to obtain a uniquely defined electric field within the source region. Then the new domain of integration is now $V - V_c$ with boundary $S + D$. For simplicity we can write the potential $\Phi(\vec{r})$ with evaluation inside, outside and on the boundary as [20, 21, 24];

$$C(\vec{r})\Phi(\vec{r}) = \oiint_S \left(G(\vec{r},\vec{r}\,')\frac{\partial\Phi}{\partial\hat{n}'}(\vec{r}\,') - \Phi(\vec{r}\,')\frac{\partial G}{\partial\hat{n}'}(\vec{r},\vec{r}\,')\right) dS', \tag{2.10}$$

where the coefficient $C(\vec{r})$ is given by

$$C(\vec{r}) = \begin{cases}1, & \vec{r} \in V,\\ \frac{1}{2}, & \vec{r}\in S,\\ 0, & \vec{r}\notin V\cup S,\end{cases} \tag{2.11}$$

with

$$\iint_S \frac{\partial G}{\partial\hat{n}'}(\vec{r},\vec{r}\,')dS' = \begin{cases}1, & \vec{r} \in V_c,\\ \frac{1}{2}, & \vec{r}\in D,\\ 0, & \vec{r}\notin V_c\cup D,\end{cases} \tag{2.12}$$

2.2 Indirect Formulation

In the indirect formulation one can use the fundamental solutions (Green's function) to construct BIEs straightforwardly without using the Green's identities. Indirect boundary

integral equations (IBIEs) are defined in terms of single and double layer potentials. IBIE defines density functions on the surface of the domain. These density functions have no direct physical meanings. We introduce the following definitions of the single and double layer potential respectively [21]:

$$\Phi(\vec{r}) = \iint_S G(\vec{r}, \vec{r}\,')\sigma(\vec{r}\,')dS(\vec{r}\,'),\ \forall \vec{r} \in V \tag{2.13}$$

$$\Phi(\vec{r}) = \iint_S \frac{\partial G}{\partial \hat{n}'}(\vec{r}, \vec{r}\,')\mu(\vec{r}\,')dS(\vec{r}\,'),\ \forall \vec{r} \in V, \tag{2.14}$$

where σ and μ are the surface densities of charges and point dipoles, respectively, which are distributed across the boundary S. In the following, we shall only be working with the expression in Eq. (2.13).

We are interested here in IBIEs, for which we can use the fundamental solutions (Green's functions) to construct BIEs directly, without using Green's identities. BIE formulation for Green's functions for free space and half space is represented here in detail. In the next section we represent the problem of the thesis topic and give a brief background of the physics involved with the topic.

2.3 Boundary Integral Equation Formulation for the Free-space Green's Function

If the size of metallic nanoparticles is much smaller than the wavelength of the electromagnetic field of the incident light, we can employ the quasistatic approximation [19, 18]. It means our solutions are given by the Poisson or Laplace equation for electrostatic potential $\Phi(\vec{r})$, where $\vec{r}$ is a point in $\mathbb{R}^3$, rather than the Helmholtz equation for the scalar and vector potentials of the wave equation, but keeps the full frequency-dependent dielectric function in the evaluation of the boundary condition [19].

Let a nanoparticle occupy volume $V_- \subset \mathbb{R}^3$ with boundary S separating it from $V_+ = \mathbb{R}^3 \backslash V_-$, and consider it to be a dielectric object of arbitrary shape with relative permittivity ϵ_-. We are interested in ϵ_- for which a source free electromagnetic field exists. For a metallic particle in the air, we have

$$\epsilon_+ = 1, \tag{2.15}$$

$$\epsilon_- = 1 - \frac{\omega_p^2}{\omega^2}, \tag{2.16}$$

where ω_p is a given constant called plasma frequency for the material and ω is an unknown frequency, see Appendix (A).

Suppose $\vec{r}_Q$ and $\vec{r}_M$ are two points on the boundary S and suppose $\hat{n}$ is the outer unit normal vector at $\vec{r}_Q$ as shown in the Figures 2.1 and 2.2. An electric potential $\Phi(\vec{r})$ can be introduced. This potential must satisfy a boundary value problem where the Laplace equation

$$\nabla^2 \Phi(\vec{r}) = 0 \tag{2.17}$$

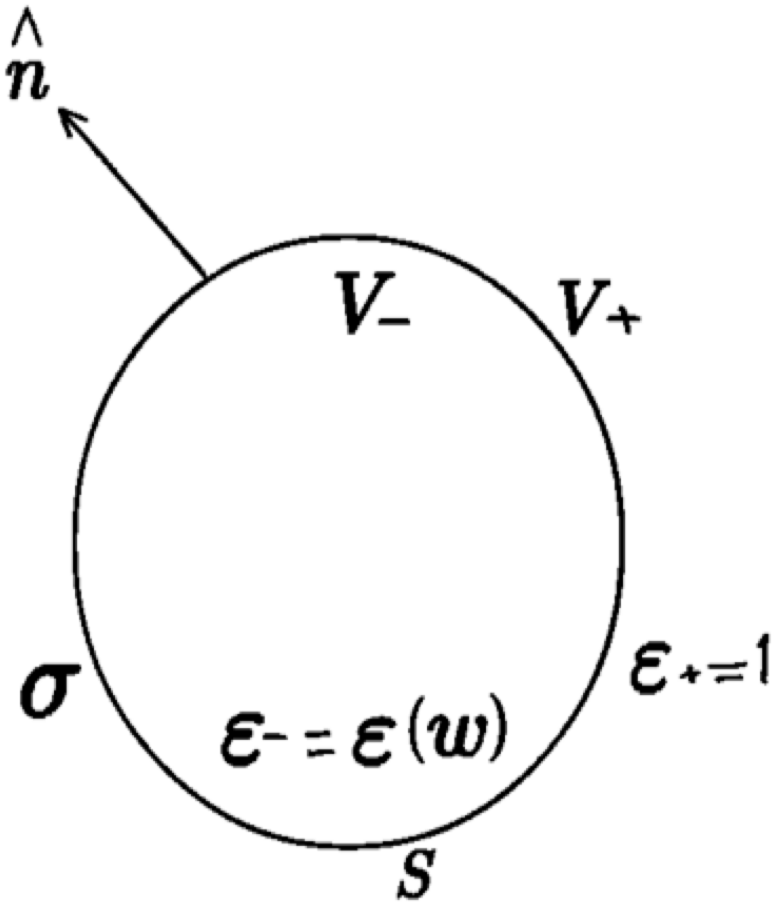

Figure 2.1: The dielectric nanoparticle bounded by surface S

is to be solved in $\mathbb{R}^3 \backslash S$ with the condition $\Phi(\vec{r}) \to 0$ as $\|\vec{r}\| \to \infty$. Let

$$\Phi(\vec{r}) = \begin{cases} \Phi_-(\vec{r}) & \text{if} \quad \vec{r} \in V_-, \\ \Phi_+(\vec{r}) & \text{if} \quad \vec{r} \in V_+. \end{cases}$$

Boundary conditions at points $\vec{r}_Q \in S$ are

$$\Phi_+(\vec{r}_Q) = \Phi_-(\vec{r}_Q) \tag{2.18}$$

$$\epsilon_+ \hat{n} \cdot \nabla \Phi_+(\vec{r}_Q) = \epsilon_- \hat{n} \cdot \nabla \Phi_-(\vec{r}_Q) \tag{2.19}$$

The quantity $\epsilon \hat{n} \cdot \nabla \Phi$ is called the potential flux. Conditions (2.18) and (2.19) imply that the potential and the potential flux are continuous across the boundary S. To find resonant frequencies ω, we will derive an eigenvalue problem for ϵ_- by using an integral equation for the solution of (2.17) that satisfies the boundary conditions (2.18) and (2.19).

2.3.1 The Free-space Green's Function

The Green's function is based on the solution of the partial differential equation (PDE) subject to a singular forcing (the electric field arising from a point charge, or displacement field arising from a point forcing). Typically, the solution is infinite at the point of application of the singular load. We will derive the Green's function for the Poisson equation (1.20) in free space, where $\epsilon = \epsilon_0$. From the definition of the Green's function, we have

$$\nabla^2 G(\vec{r}, \vec{r}\,') = \frac{-1}{\epsilon_0} \delta(\vec{r} - \vec{r}\,'), \tag{2.20}$$

where $\vec{r}$,$\vec{r}\,' \in \mathbb{R}^3$ and the gradient taken at point $\vec{r}$. The Dirac delta function $\delta(\vec{r} - \vec{r}\,')$ represents a unit source at the source point $\vec{r}$, and $G(\vec{r}, \vec{r}\,')$ represents the response at the field point $\vec{r}\,'$ that is due to that source [21].

Let r represent the radial distance

$$r = \|\vec{r} - \vec{r}\,'\| = \sqrt{(x - x')^2 + (y - y')^2 + (z - z')^2}, \tag{2.21}$$

and assume that $G(\vec{r}, \vec{r}\,')$ only depends on r away from the source ($r \neq 0$), i.e. $G(\vec{r}, \vec{r}\,') = G(\|\vec{r} - \vec{r}\,'\|) = G(r)$ and since the forcing function is zero ($\nabla^2 G(\vec{r}, \vec{r}\,') = 0$), then (2.20) yields [25]

$$\frac{1}{r^2} \frac{d}{dr} (r^2 \frac{dG}{dr}) = 0, \text{ for } \quad r \neq 0. \tag{2.22}$$

The general solution of (2.22)

$$G(r) = \frac{c_1}{r} + c_2. \tag{2.23}$$

We will determine the constants that account for the singularity at the source by integrating equation (2.20) and using the Gauss' theorem around a small sphere of radius r centered at the origin

$$\iiint \nabla^2 G \, dV = \frac{-1}{\epsilon_0},$$

$$\iiint \nabla \cdot (\nabla G)\, dV = \oiint \nabla G \cdot \hat{n}\, dS = \frac{-1}{\epsilon_0}.$$

The Green's function normal $\nabla G \cdot \hat{n}$ is $\frac{\partial G}{\partial r}$. On the sphere the radius is constant, so that

$$4\pi r^2 \frac{\partial G}{\partial r} = \frac{-1}{\epsilon_0},$$

since the surface area of a sphere is $4\pi r^2$. Taking the limit of an infinitesimally small sphere, we can express the singularity condition as [25]

$$\lim_{r \to 0} r^2 \frac{\partial G}{\partial r} = \frac{-1}{4\pi\epsilon_0}. \tag{2.24}$$

Comparing (2.23) and (2.24), we have

$$c_1 = \frac{1}{4\pi\epsilon_0}.$$

c_2 is an arbitrary constant. For convenience, we let $c_2 = 0$ [25], giving

$$G(\vec{r}, \vec{r}\,') = \frac{1}{4\pi\epsilon_0 r}. \tag{2.25}$$

Hence, infinite space Green's functions are singular at the concentrated source.

Now, we define $\sigma(\vec{r_Q})$ as the surface density of charges on S. It is an unknown function that is distributed over the boundary S of the particle and only depends on $\vec{r}_Q$. We can derive a solution of (2.17) using IBEM. As we discussed previously, we need to define a single-layer potential [21] as

$$\Phi(\vec{r}) = \oiint_S G(\vec{r}, \vec{r}_M)\sigma(\vec{r}_M)\, dS_M, \tag{2.26}$$

$\sigma(\vec{r}_M)$ is surface density, where $\vec{r}_M$ is a point on S. From equation (2.25) we obtain:

$$\Phi(\vec{r}) = \frac{1}{4\pi\epsilon_0} \oiint_S \frac{\sigma(\vec{r}_M)}{\|\vec{r} - \vec{r}_M\|}\, dS_M, \tag{2.27}$$

where dS_M is an infinitesimal surface element around the point $\vec{r}_M$, whereas $\vec{r}$ may be in either V_+ or V_- and may approach S from either side. It is clear that this potential Φ satisfies equation (2.17) and the boundary condition (2.18).

Next, we recall that the normal components of electric field of surface electric charges are given by

$$\hat{n} \cdot \nabla\Phi_\pm(\vec{r_Q}) = \lim_{h \to 0^+} \hat{n} \cdot \nabla\Phi(\vec{r}_\pm), \tag{2.28}$$

where $\vec{r}_\pm = \vec{r}_Q \pm h\hat{n}$ as in Figure 2.2, h is the height between $\vec{r}_+$, $\vec{r}_Q$, and $\vec{r}_-$.

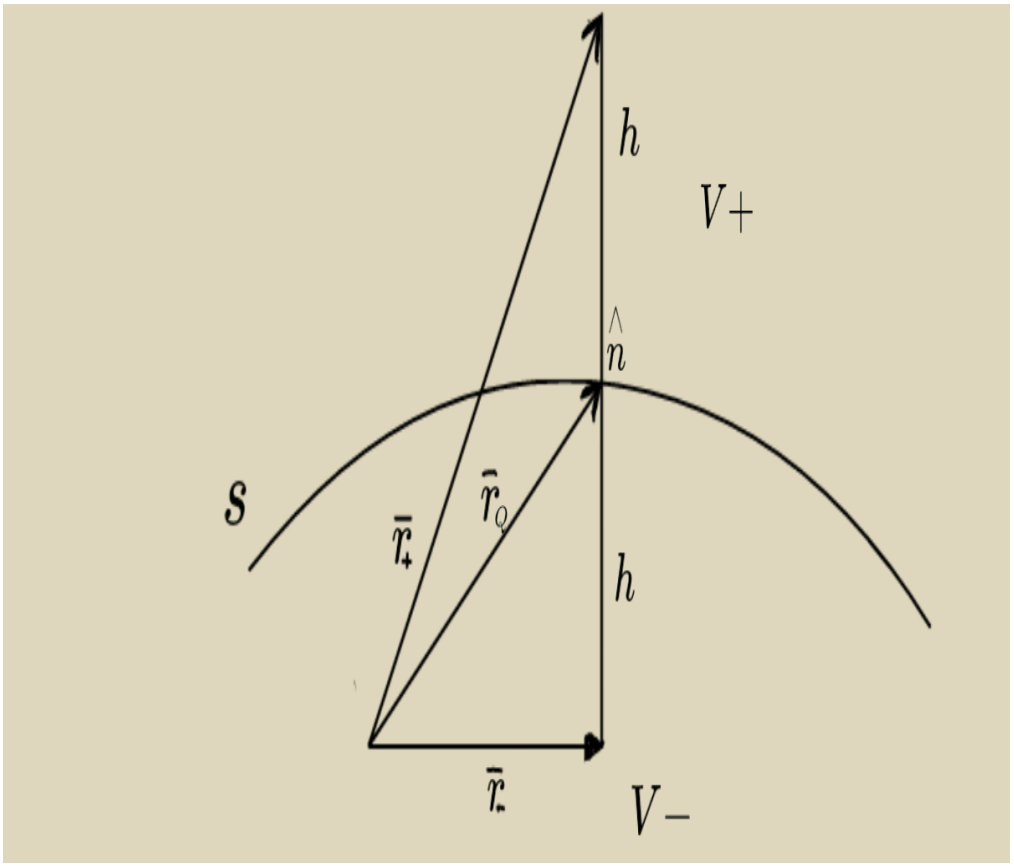

.

Figure 2.2: A diagram explaining the limiting procedure outlined in equation (2.28)

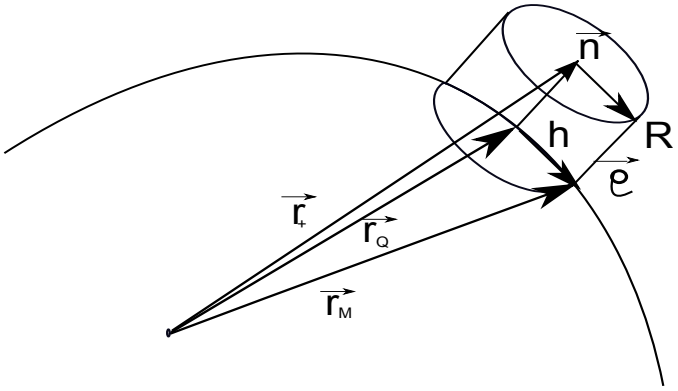

Figure 2.3: A diagram explaining the pill-box integration procedure outlined in equation (2.32)

It can be shown that

$$\begin{aligned}\hat{n}\cdot\nabla\Phi_{\pm}(\vec{r}_Q) &= \oiint_S \lim_{h\to 0^+} \hat{n}\cdot\nabla G(\vec{r},\vec{r}_M)\Big|_{\vec{r}=\vec{r}_Q\pm h\hat{n}}\,\sigma(\vec{r}_M)\,dS_M \\ &= -\frac{1}{4\pi\epsilon_0}\oiint_S \hat{n}_Q\cdot\frac{\vec{r}_Q-\vec{r}_M}{||\vec{r}_Q-\vec{r}_M||^3}\sigma(\vec{r}_M)\,dS_M \mp \frac{1}{2\epsilon_0}\sigma(\vec{r}_Q). \end{aligned} \tag{2.29}$$

By using

$$\nabla_{\vec{r}} G(\vec{r},\vec{r}\,') = -\frac{1}{4\pi\epsilon_0}\frac{\vec{r}-\vec{r}\,'}{||\vec{r}-\vec{r}\,'||^3} \tag{2.30}$$

and letting $\vec{r}\,' = \vec{r}_M$, $\vec{r} = \vec{r}_Q \pm h\hat{n}$, we obtain:

$$\begin{aligned}\hat{n}\cdot\nabla_r G(\vec{r},\vec{r_M})\Big|_{\vec{r}=\vec{r}_Q\pm h\hat{n}} &= -\hat{n}\cdot\frac{\vec{r}_Q-\vec{r}_M\pm h\hat{n}}{||\vec{r}_Q-\vec{r}_M\pm h\hat{n}||^3} \\ &\approx -\hat{n}_Q\cdot\frac{\vec{r}_Q-\vec{r}_M}{||\vec{r}_Q-\vec{r}_M||^3} \mp \frac{h}{||\vec{r}_Q-\vec{r}_M\pm h\hat{n}||^3}. \end{aligned} \tag{2.31}$$

Now, consider a pill-box region of radius R on surface S centered at point $\vec{r}_Q$. By defining $\varrho = ||\vec{r}_Q - \vec{r}_M|| < R$, and assuming that R is sufficiently small, one can show that the second term in equation (2.31) behaves as Dirac Delta function of ϱ in the limit $h \to 0$. Then, the second term in the integral at the first line in equation (2.29), may be integrated using polar coordinates with $dS_M = 2\pi\varrho\, d\varrho$ so that

$$\begin{aligned}
\frac{1}{4\pi\epsilon_0}\lim_{h\to 0^+}\oiint_S \frac{\mp h}{||\vec{r}_Q - \vec{r}_M{}' \pm h\hat{n}||^3}\sigma(\vec{r}_M)\, dS_M &\approx \mp\frac{\sigma(\vec{r}_Q)}{4\pi\epsilon_0}\lim_{h\to 0^+}\iint_{\Delta S}\frac{h}{||\vec{r}_Q - \vec{r}_M \pm h\hat{n}||^3}\, dS_M \\
&= \mp\frac{\sigma(\vec{r}_Q)}{4\pi\epsilon_0}\lim_{h\to 0^+} 2\pi\int_0^R \frac{h}{(\varrho^2+h^2)^{\frac{3}{2}}}\varrho\, d\varrho \\
&= \mp 2\pi\frac{\sigma(\vec{r}_Q)}{4\pi\epsilon_0}\lim_{h\to 0^+} h\left(\frac{1}{h} - \frac{1}{\sqrt{R^2+h^2}}\right) \\
&= \mp\frac{1}{2\epsilon_0}\sigma(\vec{r}_Q), \qquad (2.32)
\end{aligned}$$

where ΔS is the pill-box lower and upper top surface area.

Finally, substituting equation (2.29) into (2.19) gives an eigenvalue integral equation for $\sigma(\vec{r}_Q)$ with λ being an eigenvalue,

$$\sigma(\vec{r}_Q) = \frac{\lambda}{2\pi}\oiint_S \sigma(\vec{r}_M)\frac{\vec{r}_{MQ}\cdot\hat{n}_Q}{\|\vec{r}_{MQ}\|^3}\, dS_M, \qquad (2.33)$$

where $\vec{r}_{MQ} = \vec{r}_Q - \vec{r}_M$, and using the ϵ_- and ϵ_+ from (2.15) and (2.16)

$$\lambda = \frac{\epsilon_- - \epsilon_+}{\epsilon_- + \epsilon_+} = \frac{-\frac{\omega_p^2}{\omega^2}}{2 - \frac{\omega_p^2}{\omega^2}}. \qquad (2.34)$$

2.4 Boundary Integral Equation Formulation for the Half-space Green's Function

Here we wish to model a situation when the nanoparticle is placed close to a planar surface of a substrate, as often occurs in experiments. Hence, we need to derive Green's function for Poisson equation in the presence of two semi-inifinte dielectric regions.

We consider planar boundary $\widetilde{S}$ between two regions with relative dielectric constants ϵ_1 and ϵ_2 using the cylindrical coordinates $(\vec{r}, z)$ with $\vec{r} \in \mathbb{R}^2$, so that

$$\epsilon_r(z) = \begin{cases} \epsilon_1 & \text{if } z > 0, \\ \epsilon_2 & \text{if } z < 0. \end{cases}$$

Now, we need to define Green's function for the situation in Figure 2.4, so

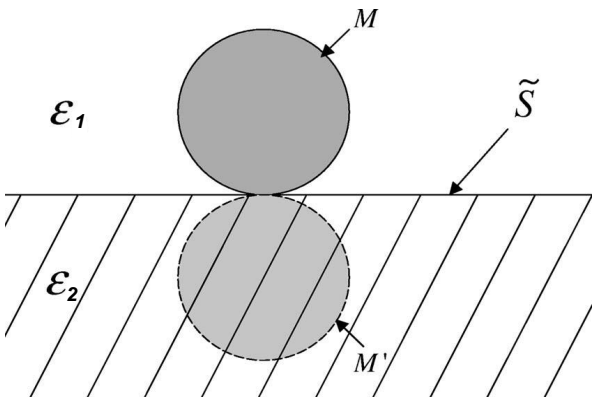

Figure 2.4: Nanoparticle on substrate. The dashed particle is the mirror image of the actual particle on the substrate[18].

$$\nabla \cdot (\epsilon_r(z)\nabla\Phi) = -\frac{1}{\epsilon_0}\rho, \tag{2.35}$$

where $\rho(\vec{r}, z)$ is the external change distribution fully localized in region 1 ($z > 0$). We will solve Poisson equation (2.35) for potential $\Phi(\vec{r}, z)$ by assuming

$$\Phi(\vec{r}, z) = \begin{cases} \Phi_1(\vec{r}, z) & \text{if } z > 0, \\ \Phi_2(\vec{r}, z) & \text{if } z < 0, \end{cases}$$

subject to the boundary conditions

$$\begin{aligned} \Phi_1(\vec{r}, 0) &= \Phi_2(\vec{r}, 0), \\ \epsilon_1 \frac{\partial \Phi_1(\vec{r}, 0)}{\partial z} &= \epsilon_2 \frac{\partial \Phi_2(\vec{r}, 0)}{\partial z}, \end{aligned} \tag{2.36}$$

as well as $\Phi_1(\vec{r}, z) \to 0$ as $z \to \infty$, $\Phi_2(\vec{r}, z) \to 0$ as $z \to -\infty$.
We define Fourier transform in the plane parallel to the boundary,

$$\Phi_j(\vec{r}, z) = \int e^{i\vec{g}\cdot\vec{r}} \widetilde{\Phi}_j(\vec{g}, z) \frac{d^2\vec{g}}{4\pi^2},$$

where $j = 1, 2$, and

$$\rho(\vec{r}, z) = \int e^{i\vec{g}\cdot\vec{r}} \widetilde{\rho}(\vec{g}, z) \frac{d^2\vec{g}}{4\pi^2}.$$

Now, we get to solve two Helmholtz equations

$$\begin{aligned} \widetilde{\Phi}_1''(z) - g^2\widetilde{\Phi}_1(z) &= -\frac{1}{\epsilon_1\epsilon_0}\widetilde{\rho}(z) \\ \widetilde{\Phi}_2''(z) - g^2\widetilde{\Phi}_2(z) &= 0, \end{aligned} \tag{2.37}$$

where we adopt a shorthand notation $\widetilde{\Phi}_j''(z) \equiv \frac{\partial^2}{\partial z^2}\widetilde{\Phi}_j(\vec{g}, z)$ and $\widetilde{\rho}(z) \equiv \widetilde{\rho}(\vec{g}, z)$. Equations (2.37) are subject to the same boundary conditions as in (2.36).

Then, we express Green's function as

$$G(\vec{r} - \vec{r}', z, z') = \int e^{i\vec{g}\cdot(\vec{r}-\vec{r}')} \widetilde{G}(z, z') \frac{d^2\vec{g}}{4\pi^2}, \tag{2.38}$$

where

$$\widetilde{G}(z, z') \equiv \widetilde{G}(\vec{g}; z, z') = \begin{cases} \widetilde{G}_1(z, z') & \text{if } z > 0 \\ \widetilde{G}_2(z, z') & \text{if } z < 0 \end{cases}$$

satisfying

$$\frac{\partial^2\widetilde{G}_1}{\partial z^2} - g^2\widetilde{G}_1 = -\frac{1}{\epsilon_1\epsilon_0}\delta(z - z') \tag{2.39}$$

for source at $z' > 0$ and

$$\frac{\partial^2\widetilde{G}_2}{\partial z^2} - g^2\widetilde{G}_2 = 0, \tag{2.40}$$

subject to boundary conditions $\widetilde{G}_1 \to 0$ as $z \to \infty$, $\widetilde{G}_2 \to 0$ as $z \to -\infty$, as well as

$$\begin{aligned} \widetilde{G}_1(0,z') &= \widetilde{G}_2(0,z'), && (2.41)\\ \epsilon_1 \frac{\partial \widetilde{G}_1}{\partial z}\bigg|_{z=0} &= \epsilon_2 \frac{\partial \widetilde{G}_2}{\partial z}\bigg|_{z=0}. && (2.42) \end{aligned}$$

Assuming

$$\widetilde{G}_1(z,z') = \begin{cases} \widetilde{G}_>(z,z') & \text{if} \quad 0 \le z' < z, \\ \widetilde{G}_<(z,z') & \text{if} \quad 0 \le z < z', \end{cases} \tag{2.43}$$

with the matching conditions due to continuity and the jump at $z = z'$,

$$\widetilde{G}_>(z',z') = \widetilde{G}_<(z',z'), \tag{2.44}$$

$$\frac{\partial \widetilde{G}_>}{\partial z}\bigg|_{z=z'} - \frac{\partial \widetilde{G}_<}{\partial z}\bigg|_{z=z'} = -\frac{1}{\epsilon_1 \epsilon_0}, \tag{2.45}$$

we may write

$$\widetilde{G}_>(z,z') = A(z')e^{-gz} + \beta(z')e^{gz}, \tag{2.46}$$

where $\beta(z') = 0$ to ensure $\widetilde{G}_> \to 0$ as $z \to \infty$,

$$\widetilde{G}_<(z,z') = B(z')e^{gz} + C(z')e^{-gz}, \tag{2.47}$$

and

$$\widetilde{G}_2(z,z') = D(z')e^{gz} + \ell(z')e^{-gz}, \tag{2.48}$$

where $\ell(z') = 0$ to ensure $\widetilde{G}_2 \to 0$ as $z \to -\infty$.
We need to find A, B, C, D. From (2.41)

$$B + C = D. \tag{2.49}$$

From (2.42)

$$\begin{aligned} \epsilon_1 \frac{\partial \widetilde{G}_<}{\partial z}\bigg|_{z=0} &= g\epsilon_1(B(z') - c(z')), \\ \epsilon_2 \frac{\partial \widetilde{G}_2}{\partial z}\bigg|_{z=0} &= g\epsilon_2 D(z'), \\ \epsilon_1(B - C) &= \epsilon_2 D. && (2.50) \end{aligned}$$

From (2.44) and (2.45)

$$Ae^{-gz'} = Be^{gz'} + Ce^{-gz'}, \tag{2.51}$$

$$-g(Ae^{-gz'}) - g(Be^{gz'} - Ce^{-gz'}) = -\frac{1}{\epsilon_1 \epsilon_0}. \tag{2.52}$$

From (2.49-2.52) we find

$$A = \frac{1}{2g\epsilon_1\epsilon_0}\left(e^{gz'} + \frac{\epsilon_1-\epsilon_2}{\epsilon_1+\epsilon_2}e^{-gz'}\right), \tag{2.53}$$

$$B = \frac{e^{-gz'}}{2g\epsilon_1\epsilon_0}, \tag{2.54}$$

$$C = \frac{2\pi}{g\epsilon_1}\left(\frac{\epsilon_1-\epsilon_2}{\epsilon_1+\epsilon_2}e^{-gz'}\right). \tag{2.55}$$

Next, substitute A, B and C in equations (2.46),(2.47)

$$\widetilde{G}_>(z,z') = \frac{1}{2g\epsilon_1\epsilon_0}\left(e^{-g(z-z')} + \frac{\epsilon_1-\epsilon_2}{\epsilon_1+\epsilon_2}e^{-g(z+z')}\right), \tag{2.56}$$

$$\widetilde{G}_<(z,z') = \frac{1}{2g\epsilon_1\epsilon_0}\left(e^{g(z-z')} + \frac{\epsilon_1-\epsilon_2}{\epsilon_1+\epsilon_2}e^{-g(z+z')}\right), \tag{2.57}$$

$$\tag{2.58}$$

giving

$$\widetilde{G}_1(z,z') = \frac{1}{2g\epsilon_1\epsilon_0}\left(e^{-g|z-z'|} + \frac{\epsilon_1-\epsilon_2}{\epsilon_1+\epsilon_2}e^{-g(z+z')}\right), \tag{2.59}$$

where $z>0, z'>0$. Noting that

$$\int \frac{1}{g}e^{i\vec{g}\cdot\vec{r}}\,e^{-g|z|}\frac{d^2\vec{g}}{4\pi^2} = \frac{1}{2\pi}\frac{1}{\sqrt{\|\vec{r}\|^2+z^2}},$$

we obtain

$$G_1(\vec{r}-\vec{r}',z,z') = \frac{1}{4\pi\epsilon_0}\left[\frac{1}{\epsilon_1}\frac{1}{\sqrt{(\vec{r}-\vec{r}')^2+(z-z')^2}} + \frac{1}{\epsilon_1}\frac{\epsilon_1-\epsilon_2}{\epsilon_1+\epsilon_2}\frac{1}{\sqrt{(\vec{r}-\vec{r}')^2+(z+z')^2}}\right]. \tag{2.60}$$

Let $\epsilon_1 = 1$ and $\epsilon_2 = \epsilon$ be relative permittivity of the substrate, and exchanging $\vec{r}$ and $\vec{r}'$ with $\vec{r}_Q$ and $\vec{r}_M$ respectively. Then

$$G_1(\vec{r}_Q,\vec{r}_M) = \frac{1}{4\pi\epsilon_0}\left(\frac{1}{r_{MQ}} - \frac{\epsilon-1}{\epsilon+1}\frac{1}{r_{M'Q}}\right), \tag{2.61}$$

where $r_{M'Q} = \|\vec{r}_Q - \vec{r}_{M'}\|$ and M' is the image of M with respect to the substrate plane $\widetilde{S}$. After that, we can modify equation (2.33) for a nanoparticle in the region 1 as follows

$$\sigma(\vec{r}_Q) = \frac{\lambda}{2\pi}\iint_S \sigma(\vec{r}_M)\hat{n}_Q\cdot\nabla_{\vec{r}_Q}[G_1(\vec{r}_Q,\vec{r}_M)]\,dS_M, \tag{2.62}$$

where λ is given by formula (2.34).

We need to apply the boundary condition (2.19) in order to derive the boundary integral equation for the half space Green's function. We start from the potential equation and use

the Green's function in equation (2.61)

$$\Phi(\vec{r}) = \frac{1}{4\pi\epsilon_0} \oiint_S \frac{\sigma(\vec{r_M})}{\|\vec{r} - \vec{r}_M\|} dS_M - \frac{1}{4\pi\epsilon_0} \frac{\epsilon - 1}{\epsilon + 1} \oiint_S \frac{\sigma(\vec{r_M})}{\|\vec{r} - \vec{r}_{M'}\|} dS_M. \tag{2.63}$$

The boundary conditions are applied in multiple steps for simplicity

$$\begin{aligned} \hat{n} \cdot \nabla\Phi_{\pm}(\vec{r})\Big|_{\vec{r}\to\vec{r}_Q\in S} &= -\frac{1}{4\pi\epsilon_0} \lim_{h\to 0^+} \oiint_S \hat{n} \cdot \frac{\vec{r} - \vec{r}_M}{||\vec{r} - \vec{r}_M||^3}\Big|_{\vec{r}=\vec{r}_Q\pm h\hat{n}} \sigma(\vec{r}_M)\, dS_M \\ &+ \frac{1}{4\pi\epsilon_0} \frac{\epsilon - 1}{\epsilon + 1} \lim_{h\to 0^+} \oiint_S \hat{n} \cdot \frac{\vec{r} - \vec{r}_{M'}}{||\vec{r} - \vec{r}_{M'}||^3}\Big|_{\vec{r}=\vec{r}_Q\pm h\hat{n}} \sigma(\vec{r}_M)\, dS_M. \end{aligned}$$

The first part of the left hand side have been derived earlier (see equation (2.29)). Now applying equation (2.19) we get

$$(\epsilon_+ - \epsilon_-) \frac{-1}{4\pi\epsilon_0} \oiint_S \hat{n}_Q \cdot \left(\frac{\vec{r}_Q - \vec{r}_M}{||\vec{r}_Q - \vec{r}_M||^3} - \frac{\epsilon - 1}{\epsilon + 1} \frac{\vec{r}_Q - \vec{r}_{M'}}{||\vec{r}_Q - \vec{r}_{M'}||^3} \right) \sigma(\vec{r}_M)\, dS_M - \frac{1}{2\epsilon_0}(\epsilon_+ - \epsilon_-)\sigma(\vec{r}_Q) = 0 \tag{2.64}$$

We can modify and write this equation as

$$\sigma(\vec{r}_Q) = \frac{\lambda}{2\pi} \oiint_S \sigma(\vec{r}_M) \left(\frac{\hat{n}_Q \cdot \vec{r}_{MQ}}{||\vec{r}_{MQ}||^3} - \frac{\epsilon - 1}{\epsilon + 1} \frac{\hat{n}_Q \cdot \vec{r}_{M'Q}}{||\vec{r}_{M'Q}||^3} \right) dS_M, \tag{2.65}$$

where λ is given by formula (2.34). This eigenvalue equation will be solved computationally in great detail in the following chapter.

2.5 Mie Theory of Plasmon Eigenfrequencies of a Sphere

One reliable technique that has been consistently used for the study of the interaction of light with small particles is the Mie Theory. Named after Gustav Mie, the theory provides an analytical solution for light scattering from spherical particles [15]. The derivation of Mie's formal solution can be found in [26, 27].

We will calculate the plasmon eigenfrequencies ω for a metallic sphere of radius R in vacuum. This can be done analytically by using spherical harmonics $Y_{lm}(\theta, \varphi)$, (for more details see Appendix A.2). Here, $\theta \in [0, \pi]$ and $\varphi \in [0, 2\pi)$ are the angles that define the spherical coordinates (r, θ, φ). A detailed explanation and rigorous definition of these functions can be found in [28]. We expand the Green's function $G(\vec{r}, \vec{r}')$ for the Poisson equation in the spherical coordinates for points $\vec{r} = (r, \theta, \varphi)$ and $\vec{r}' = (r', \theta', \varphi')$

$$G(\vec{r}, \vec{r}') = \frac{1}{\|\vec{r} - \vec{r}'\|} = \sum_{l=0}^{\infty} \sum_{m=-l}^{l} \frac{4\pi}{2l + 1} \frac{r_<^l}{r_>^{l+1}} Y_{lm}(\theta, \varphi) Y_{lm}^*(\theta', \varphi'), \tag{2.66}$$

where $r_> = max(r, r')$ and $r_< = min(r, r')$ [28]. Substituting (2.66) into (2.27) with $\vec{r}' =$

$\vec{r}_M = (R, \theta', \varphi')$ and letting $dS_M = R^2 \sin\theta' d\theta' d\varphi'$, we can express the potential Φ as

$$\Phi(\vec{r}) = \begin{cases} \Phi_+(\vec{r}) & \text{if} \quad r > R, \\ \Phi_-(\vec{r}) & \text{if} \quad r < R, \end{cases}$$

where

$$\Phi_+(\vec{r}) = \sum_{l=0}^{\infty} \sum_{m=-l}^{l} \frac{4\pi}{2l+1} \frac{R^{l+2}}{r^{l+1}} \sigma_{lm} Y_{lm}(\theta, \varphi), \tag{2.67}$$

$$\Phi_-(\vec{r}) = \sum_{l=0}^{\infty} \sum_{m=-l}^{l} \frac{4\pi}{2l+1} \frac{r^{l}}{R^{l-1}} \sigma_{lm} Y_{lm}(\theta, \varphi) \tag{2.68}$$

with

$$\sigma_{lm} = \int_0^{\pi} \int_0^{2\pi} \sigma(\theta', \varphi') Y^*_{lm}(\theta', \varphi') \sin\theta' d\theta' d\varphi' \tag{2.69}$$

being the coefficients in an expansion of the surface charge density $\sigma(\vec{r}_M) = \sigma(\theta', \varphi')$ in terms of spherical harmonics, see equations (2.75) and (2.76) below.

Equations (2.67) and (2.68) show that the potential is continuous across the spherical surface $r = R$, and from the boundary condition (2.19) we get

$$-\epsilon_+ \frac{\partial \Phi_+}{\partial r}\bigg|_{r=R} = \sum_{l=0}^{\infty} \sum_{m=-l}^{l} \frac{4\pi}{2l+1} (l+1) \sigma_{lm} Y_{lm}(\theta, \varphi) \tag{2.70}$$

and

$$\epsilon_- \frac{\partial \Phi_-}{\partial r}\bigg|_{r=R} = \sum_{l=0}^{\infty} \sum_{m=-l}^{l} \frac{4\pi}{2l+1} l \sigma_{lm} Y_{lm}(\theta, \varphi). \tag{2.71}$$

Combining these two equations

$$\sum_{l=0}^{\infty} \sum_{m=-l}^{l} \frac{4\pi}{2l+1} \left[l\epsilon_- + (l+1)\epsilon_+ \right] \sigma_{lm} Y_{lm}(\theta, \varphi) = 0, \tag{2.72}$$

yields

$$\left[l\epsilon_- + (l+1)\epsilon_+ \right] = 0 \quad \forall l, \tag{2.73}$$

which, for $\epsilon_+ = 1$ and $\epsilon_- = 1 - \frac{\omega_p^2}{\omega^2}$, gives the set of plasmon frequencies

$$\omega_l = \omega_p \sqrt{\frac{l}{2l+1}}, \quad l = 0, 1, 2, ... \tag{2.74}$$

Notice that the frequency ω_l of the l-th eigenmode is $(2l+1)$-fold degenerate. This degeneracy is a consequence of a high symmetry on a sphere [28].

It is instructive to test equation (2.33) for a sphere of radius R. We should therefore

expand the charge density as

$$\sigma(\vec{r}_Q) = \sigma(\theta, \varphi) = \sum_{l=0}^{\infty} \sum_{m=-l}^{l} \sigma_{lm} Y_{lm}(\theta, \varphi), \tag{2.75}$$

$$\sigma(\vec{r}_M) = \sigma(\theta', \varphi') = \sum_{l=0}^{\infty} \sum_{m=-l}^{l} \sigma_{l'm'} Y_{l'm'}(\theta', \varphi'). \tag{2.76}$$

Noting that

$$\frac{\vec{r}_{MQ} \cdot \hat{n}_Q}{||\vec{r}_{MQ}||^3} = -\frac{\partial}{\partial r} G(\vec{r}, \vec{r}') \bigg|_{r \to R, r'=R} \tag{2.77}$$

with $G(\vec{r}, \vec{r}')$ given in (2.66), a question arises whether to use the form with $r > r' = R$ or $r < r' = R$. We define it via the arithmetic mean,

$$\frac{\vec{r}_{MQ} \cdot \hat{n}_Q}{||\vec{r}_{MQ}||^3} = -\frac{1}{2} \frac{\partial}{\partial r} G(\vec{r}, \vec{r}') \bigg|_{r \to R^+, r'=R} - \frac{1}{2} \frac{\partial}{\partial r} G(\vec{r}, \vec{r}') \bigg|_{r \to R^-, r'=R}. \tag{2.78}$$

Breaking this equation for simplicity, when $r' = R$, $r > R$:

$$\frac{\partial}{\partial r} \frac{R^l}{r^{l+1}} \bigg|_{r=R} = \frac{-(l+1)}{R^2},$$

and again when $r' = R$, $r < R$:

$$\frac{\partial}{\partial r} \frac{r^l}{R^{l+1}} \bigg|_{r=R} = \frac{l}{R^2}.$$

Now we can solve (2.78) straightforwardly

$$\frac{\vec{r}_{MQ} \cdot \hat{n}_Q}{||\vec{r}_{MQ}||^3} = -\sum_{l=0}^{\infty} \sum_{m=-l}^{l} \frac{4\pi}{2l+1} \frac{l - (l+1)}{2R^2} Y_{lm}(\theta, \varphi) Y^*_{lm}(\theta', \varphi'). \tag{2.79}$$

Substituting (2.76) and (2.79), and using the normalisation and orthogonality relation of spherical harmonics

$$\int_0^{2\pi} \int_0^{\pi} Y^*_{lm}(\theta', \varphi') Y_{l'm'}(\theta', \varphi') \sin\theta' \mathrm{d}\theta' \mathrm{d}\varphi' = \delta_{ll'} \delta_{mm'},$$

in the right-hand side of equation (2.33) yields

$$\sigma(\vec{r}_Q) = \sum_{l=0}^{\infty} \sum_{m=-l}^{l} \sigma_{lm} Y_{lm}(\theta, \varphi) \frac{\lambda}{2l+1}. \tag{2.80}$$

Comparing this result with equation (2.75), one derives an eigenvalue equation

$$\lambda = 2l + 1, \tag{2.81}$$

which is consistent with equation (2.34) upon using equation (2.74). In the discussion of

our computational results for a spherical nanoparticle in the following section, we shall present results for the eigenvalues of λ and compare them with the values in equation (2.81) that result from the Mie theory.

Chapter 3

Boundary Element Method

3.1 Introduction

The boundary element method (BEM) is a numerical method for solving differential equations formulated through the use of boundary integral equations (BIEs) and produces a system of linear algebraic equations with a full matrix [21]. BEM, which involves some discretization, is also known as the boundary integral equation method (BIEM) or, in computational electromagnetics, method of moments (MoM), though the latter is not always tantamount to BEM. This method is most suitable for linear, elliptic and homogenous partial differential equations addressing boundary-value problems in the case that a homogenous source is absent [20]. One unique aspect of BEM is that only the boundary of the problem needs to be discretized [29]. This is the main benefit that BEM formulation introduces; it does not require the computation of requisite functions throughout the domain of the solution but rather just the boundary of the domain. Hence, once the unknown boundary distribution is determined, the solution can be generated straightforwardly [20]. In other words, only the curve boundaries for two-dimensional problems and the surfaces for three-dimensional problems need to be discretized when using BEM. This aspect of BEM makes it stand out from other numerical methods such as the finite element method (FEM) and finite difference method (FDM), as it makes BEM more appropriate for exterior problems. BEM can also effectively solve problems with singularities or discontinuities that occur in the domain. Another benefit of the boundary element method is the fact that the boundary's functions and its normal derivatives are solved for simultaneously and with the same degree of accuracy [24].

For instance, for an infinite domain two-dimensional problem one can notice the differences in discretization of the domain between FEM and BEM see Figure 3.1 and Figure 3.2. In order to use FEM the domain has to be meshed to some distance from the circle. The disadvantage of doing so is the question how big the distance should be and consequently how large the mesh will be. Thus, the method would consume time computing approximations in meshing the part of the domain, which is not what we are interested in. In order to apply BEM to the same problem, we just need to discretize the boundary of the domain. In short, in BEM the domain discretization is a computationally inexpensive problem. The method works well on an infinite or semi-infinite domain, whereas in FEM the infinite or semi-infinite domain is a computationally expensive problem and the method works better in finite domains.

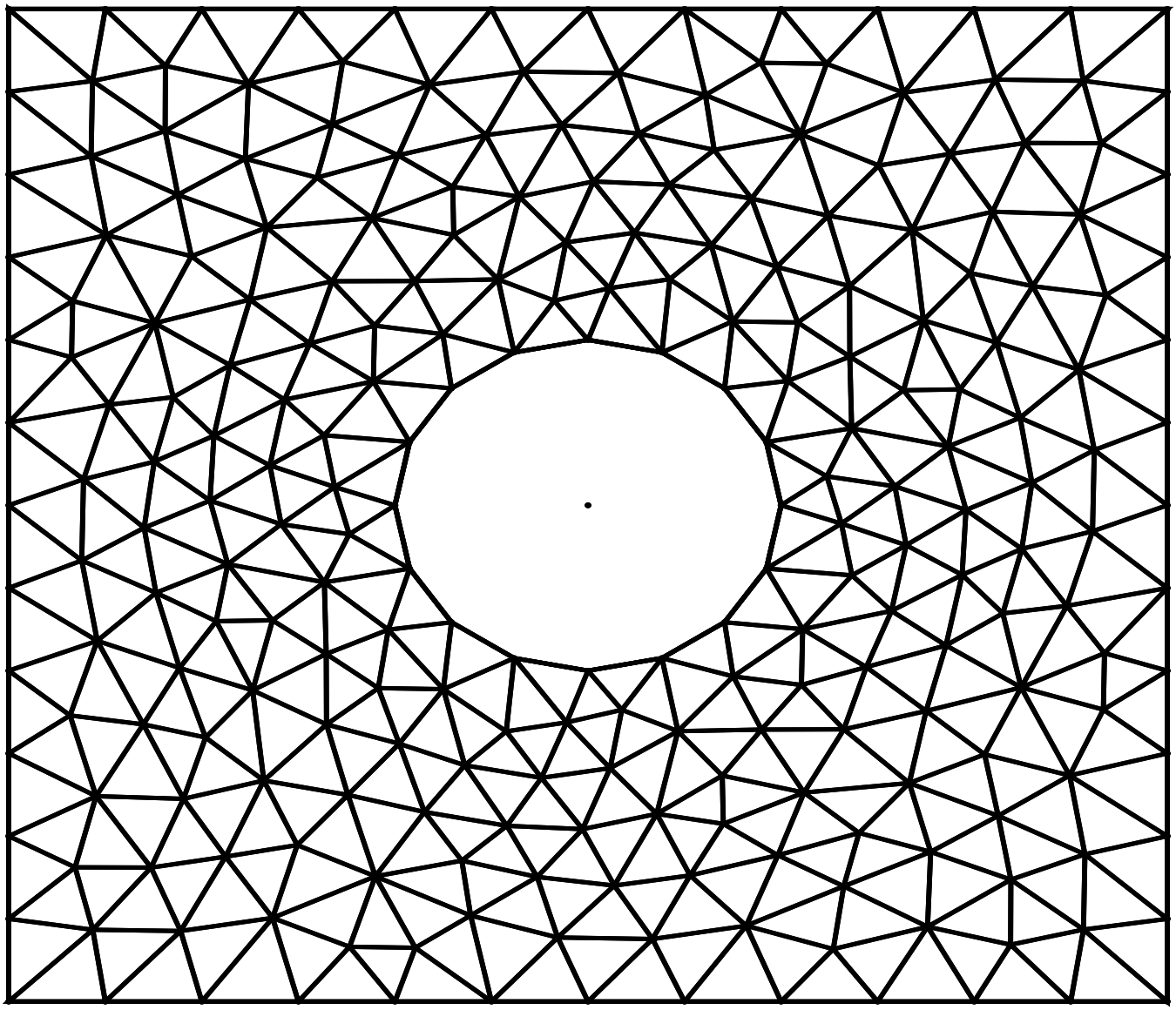

Figure 3.1: A two dimensional problem with a domain that extends to infinity. In the FEM, a mesh is generated for a finite area in the domain. One issue is how large should this area be, it is not possible to extend in the computation the mesh to infinity. Therefore, a finite area has to be selected. In contrast, in the BEM only the inner circle is discretized see Figure 3.2.

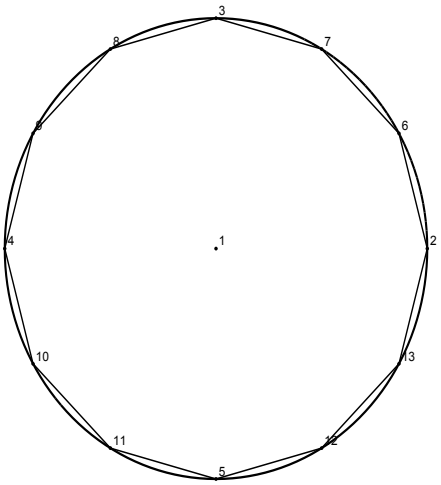

Figure 3.2: A two dimensional problem with a domain that extends to infinity. In this problem the interior of the circle is not included. One feature of BEM is that only the boundary of the circle needs to be discretized. This is in contrast to FEM see Figure 3.1. Therefore BEM has an advantage over FEM with respect to mesh discretization.

One major setback in using BEM is that it can only be applied to partial differential equations whose fundamental solution is known. These fundamental solutions are not readily available for all PDEs [30]. The lack of some of the required fundamental solutions has contributed to the slow progress of BEM in its early years. Nevertheless, in more recent times, BEM has witnessed major progress as fundamental solutions have become well understood. For instance, the Laplace equation and other boundary value problems (BVPs), whose fundamental solutions are known, can be formulated as boundary integration equations. Hence, once all the data becomes available through boundary integral equations, the solution to a BVP can be obtained by applying Green's identity [24].

The use of BEMs goes back to the late nineteenth and early twentieth centuries. In 1886, Somigliana used direct BEM formulation to present a displacement and stresses integral equation. The first indirect BEM formulation was in 1903 by Fredholm [24]. The first major development in application of BEM was reported in the 1960s when a two-dimensional problem was formulated into boundary integral equations that were discretized and solved by Jawson and Symm [24]. Their formulation could not be labeled direct BEM due to the fact that the functions had to be differentiated or integrated to attain physical quantities. The first direct formulation was put in use by Rizzo who also used BEM to discretize integral equations in a two-dimensional elastostatic problem [21]. Boundary integral equations were first put to use to solve three-dimensional problems by Cruse [24]. Although boundary integral equations had been utilized by various scholars in the 1960s, the term boundary element method was only introduced for the first time in 1978 by CA Brebbia.

3.2 Discretization

BEM implementation includes discretization of the surface surrounding a chosen control volume in three dimensions into flat or curved elements, presenting local approximations for the unknown functions in the local surface coordinates and, lastly, generating and solving systems of linear equations for the coefficients of the local expansions.

The integral equation (2.33) expresses the value of the density function $\sigma(\vec{r}_Q)$ at any point $\vec{r}_Q$ in terms of its values and a normal derivative at the boundary. A discretisation of this equation leads to the BEM system of algebraic equations. The physical boundary S is partitioned into N parts S_j, $j = 1, 2, ..., N$, see Figure 3.3. We have used standard unstructured triangular meshing; other meshing systems can be used (e.g., quadrilateral or mixed), however triangles are generally beneficial when fitting a mesh to a complex geometry. Each partition is represented by flat triangular elements, each defined by a group of element nodes. The collection of the elements defines an unstructured surface grid defined by the global grid nodes.

We approximate the distributions σ with constants over each element. For high-order methods one needs to involve linear, quadratic, or higher order polynomial expansions of the surface functions over the individual boundary elements.

Meshes have been generated using GMSH [31], an open source finite element mesh generator. GMSH transforms a geometry (.geo) file into a mesh (.msh) file containing an unstructured triangular mesh. Then, a MATLAB code that we wrote reads the mesh cre-

Figure 3.3: Mesh for center of the sphere connected to the centroid of the triangle under consideration. For this example, let us call the resulting vector $\mathbf{r}_1$, We compute the following quantity.

ated by GMSH and generates a data structure representing mappings between the elements and vertices.

3.3 Implementation of BEM for the Free-space Green's Function

Here we represent an implementation study for the free space BIE described in the previous chapter. Using equation (2.33), let us partition S into N small pieces S_M and rewrite it as

$$\sigma(\vec{r}_Q) \approx \frac{\lambda}{2\pi} \sum_{M=1}^{N} \int_{S_M} \sigma(\vec{r}_M) \frac{\vec{r}_{MQ} \cdot \hat{n}_Q}{\|\vec{r}_{MQ}\|^3} \, dS_M. \tag{3.1}$$

We assume that points $\vec{r}_Q$ and $\vec{r}_M$ are the centroid points of triangles S_Q and S_M respectively and we approximate both the $\sigma(\vec{r}_M)$ and the kernel $(\frac{\vec{r}_{MQ} \cdot \hat{n}_Q}{\|\vec{r}_{MQ}\|^3})$ with constant functions over each triangle. Points $\vec{r}_Q$ and $\vec{r}_M$ are also used as collocation points, that is,

the points where the integral equation is applied. The BEM is then applied at the Q-th point and integration over S is estimated by the sum of the integrations on all N triangles. We have changed the notation here to write the problem in matrix form and to match our code, from Q and M to i and j, respectively, and we replaced $\vec{r}$ with $\mathbf{r}$. For instance, we replaced $\sigma(\vec{r}_Q)$ and $\sigma(\vec{r}_M)$ with σ_i and σ_j, respectively, with an understanding that σ_i is an approximate of $\sigma(\vec{r}_Q)$. We denote the area of the triangle S_j by ΔS_j. Hence, we obtain approximately

$$\sigma_i = \frac{\lambda}{2\pi} \sum_{j=1}^{N} \sigma_j \frac{(\mathbf{r}_i - \mathbf{r}_j) \cdot \mathbf{n}_i}{\|\mathbf{r}_i - \mathbf{r}_j\|^3} \Delta S_j, \tag{3.2}$$

We can write the sum in (3.2) as

$$\sigma_i = F_{i,j} \Delta S_j \sigma_j, \tag{3.3}$$

where

$$F_{i,j} = \frac{(\mathbf{r}_i - \mathbf{r}_j) \cdot \mathbf{n}_i}{\|\mathbf{r}_i - \mathbf{r}_j\|^3}. \tag{3.4}$$

Combining the vectors for $i = 1, \ldots, N$, we can rewrite (3.2) in a matrix form as

$$\sigma = \frac{\lambda}{2\pi} \mathbf{A}\ \sigma, \tag{3.5}$$

where

$$\sigma = \begin{pmatrix} \sigma_1 \\ \sigma_2 \\ \vdots \\ \sigma_N \end{pmatrix}$$

and

$$\mathbf{A} = \begin{bmatrix} F_{1,1} \cdot \Delta S_1 & F_{1,2} \cdot \Delta S_2 & \cdots & F_{1,N} \cdot \Delta S_N \\ F_{2,1} \cdot \Delta S_1 & F_{2,2} \cdot \Delta S_2 & \cdots & F_{2,N} \cdot \Delta S_N \\ \vdots & \vdots & \ddots & \vdots \\ F_{N,1} \cdot \Delta S_1 & F_{N,2} \cdot \Delta S_2 & \cdots & F_{N,N} \cdot \Delta S_N \end{bmatrix}. \tag{3.6}$$

3.3.1 Non-Singular Triangles

If the kernel is non-singular over the surface of a triangle, which are the elements of $\mathbf{A}$ when $i \neq j$, the integral (3.1) can be computed in straightforward manner. To do so, we need to compute the outward normal $\mathbf{n}_i$ and the area of triangles ΔS_j. Let us assume that S_j is described by vertices (x_1, y_1, z_1), (x_2, y_2, z_2), and (x_3, y_3, z_3), see Figure 3.4. Then, $\mathbf{n}$ can be computed as

$$\mathbf{n} = \frac{\vec{v_1} \times \vec{v_2}}{\|\vec{v_1} \times \vec{v_2}\|}, \tag{3.7}$$

where $\vec{v_1} = (x_2 - x_1, y_2 - y_1, z_2 - z_1), \vec{v_2} = (x_3 - x_1, y_3 - y_1, z_3 - z_1)$ are vectors along the sides of the triangle which the normal is computed. However, this formula gives both inward and outward unit normals. This problem is difficult to resolve in general. Here, we

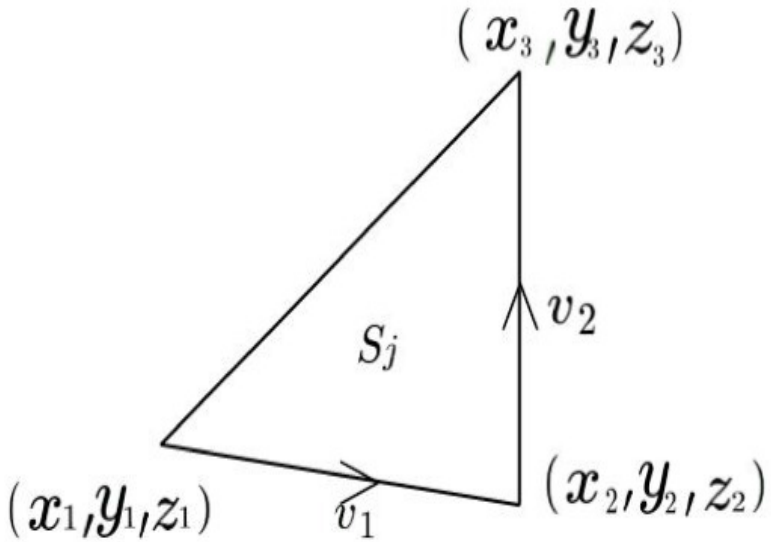

Figure 3.4: An element (triangle) S_j described by its vertices. The figure shows how the vectors used in computing the normal vector $\mathbf{n}$.

adopt the following approach.

$$a = \mathbf{n} \cdot \mathbf{r}_1 \tag{3.8}$$

we pick a point inside of our physical solid, e.g. $\mathbf{r}_1$ which is a centroid point of the same triangle. If $a > 0$ then $\mathbf{n}$ is the outward normal, otherwise we set $\mathbf{n} = -\mathbf{n}$. The area of triangle ΔS_j is given by

$$\Delta S_j = \frac{1}{2} \|\vec{v_1} \times \vec{v_2}\|. \tag{3.9}$$

Next, using these two formulas, we can solve straightforwardly equation (3.2) for non singular triangles. Part of the code for the outward-pointing unit normal and the area of triangle is given below:

```
% x1,y1,z1... these are vertices from
%the mesh file for the surface triangles

vec1 = [x1-x2;
    y1-y2;
    z1-z2];

vec2 = [x1-x3;
    y1-y3;
    z1-z3];

cross_prod = cross(vec1,vec2);

n = cross_prod/norm(cross_prod,2);
a = dot(n,r_1);
if  a < 0
    n = -n;
```

```
end

cross_prod = cross(vec1,vec2);
area_value_1(k) = 0.5*norm(cross_prod,2);
```

3.3.2 Singular Triangles

An issue arises when $\mathbf{r}_i$ and $\mathbf{r}_j$ are in the same triangle, which results in singularities because of the way the kernel is formulated. This happens only from the free space Green's function. Since the issue is when the two points are in the same triangle, the denominator in (3.2) is equal to zero so the function $F_{i,i}$ is undefined, that is, the singularity occurs along the diagonal of the matrix $\mathbf{A}$. One way to solve this is by simply setting the diagonal elements of the matrix $\mathbf{A}$ equal to zero [20]. For simplicity, we called this approximation Approach A.

$$\mathbf{A_{i,i}} = 0. \tag{3.10}$$

3.3.3 Approach B

I. Mayergoys *et al* [18] showed an efficient approach to approximate the diagonal elements. This approach is presented here; we called it Approach B. We begin by defining solid angle as a dimensionless unit angle in three dimensional space that an object subtended by a point creates. It is the area on the surface of a sphere divided by the radius squared of that sphere; for more details see [32]. In Figure 3.5 we show three different cases of the solid angle, and since we are using BEM we will consider only Case 1 in future derivations. Referring to equation (2.33) and from the definition of the solid angle, see Figure 3.6 for more details, notice that

$$d\omega = \frac{\vec{r}_{MQ} \cdot \hat{n}_Q}{\|\vec{r}_{MQ}\|^3} dS_Q, \tag{3.11}$$

is an infinitesimal solid angle that the surface element dS_Q at point $\vec{r}_Q$ occupies when viewed from point $\vec{r}_M$. When both points $\vec{r}_M$ and $\vec{r}_Q$ are on a closed surface S, and we integrate with respect to $\vec{r}_Q$ to get

$$\oint_S \frac{\vec{r}_{MQ} \cdot \hat{n}_Q}{\|\vec{r}_{MQ}\|^3} dS_Q = 2\pi. \tag{3.12}$$

On the other hand, one can see that $\lambda = 1$ is an eigenvalue; however, it is clear from equation (2.34) that this eigenvalue corresponds to $\epsilon_- \to -\infty$ and $\omega \to 0$, which corresponds to static polarization of the nanoparticle.. Thus, this eigenvalue is irrelevant to the topic of this thesis. From equation (3.12) and by integrating both sides of equation (2.33) with respect to dS_Q, and knowing that $\lambda \neq 1$ for plasmon resonance we get

$$\oint_S \sigma(\vec{r}_M)\, dS_M = 0. \tag{3.13}$$

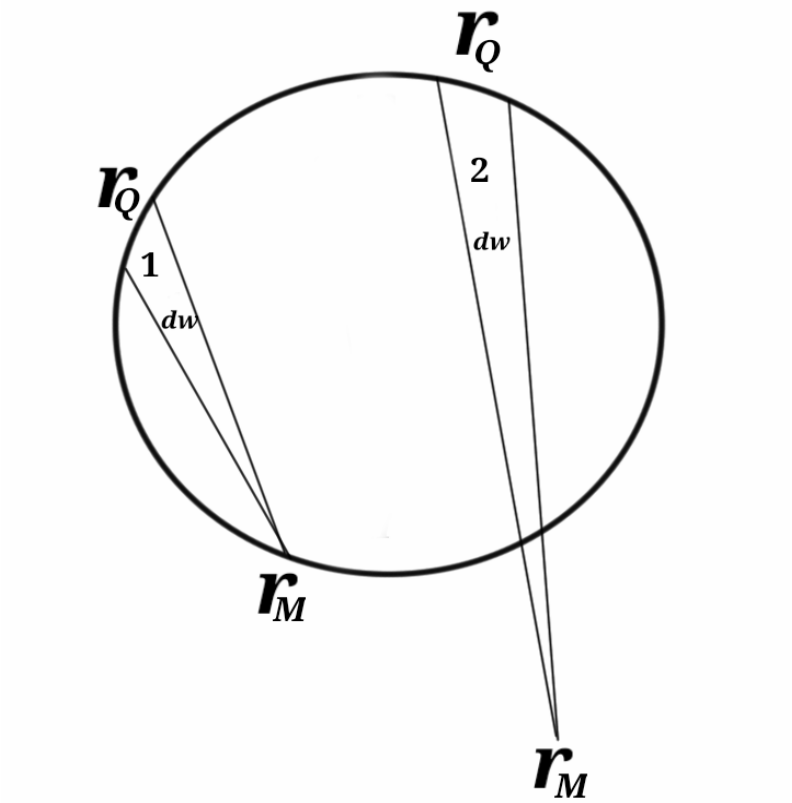

Figure 3.5: A diagram explaining the solid angle $d\omega$ that the surface element dS_Q at the point $\vec{r}_Q$ occupies when viewed from the point $\vec{r}_M$. Cases 1,2 respond to different views of the solid angle, Case 1 for two points on the surface of a sphere, and Case 2 for a point on the surface viewed by an outside point.

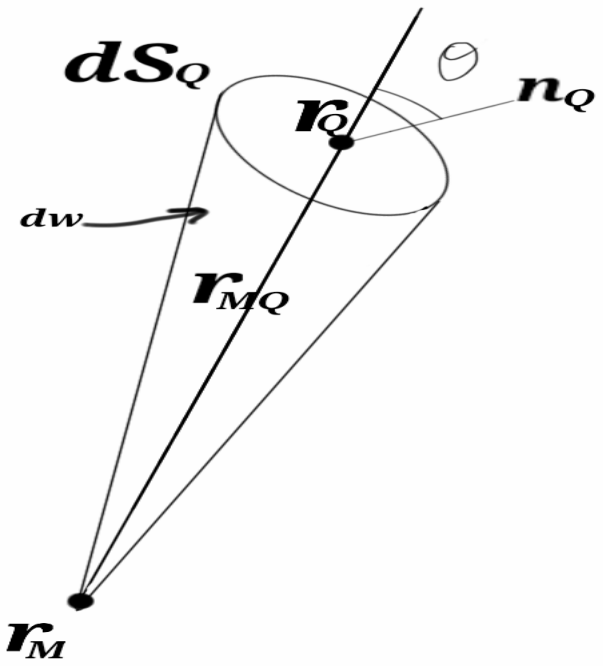

Figure 3.6: A diagram explaining the solid angle $d\omega$ that the surface element dS_Q at the point $\vec{r}_Q$ occupies when viewed from the point $\vec{r}_M$.

Note that, physically, this means that the total charge is zero. Now, we integrate equation (3.1) over the surface element S_i and change the order of integration in the right hand side integral

$$\int_{S_i} \sigma(\vec{r}_Q)\ dS_Q = \frac{\lambda}{2\pi} \sum_{j=1}^{N} \int_{S_j} \sigma(\vec{r}_M) \left[\int_{S_i} \frac{\vec{r}_{MQ} \cdot \hat{n}_Q}{\|\vec{r}_{MQ}\|^3} dS_Q \right] dS_M. \tag{3.14}$$

We define solid angle occupied by the surface element S_i when viewed from point $\vec{r}_M$

$$\omega_i(M) = \int_{S_i} \frac{\vec{r}_{MQ} \cdot \hat{n}_Q}{\|\vec{r}_{MQ}\|^3}\ dS_Q. \tag{3.15}$$

(3.14) can be presented as follows:

$$\int_{S_i} \sigma(\vec{r}_Q)\ dS_Q = \frac{\lambda}{2\pi} \sum_{j=1}^{N} \int_{S_j} \sigma(\vec{r}_M)\omega_i(M)\ dS_M. \tag{3.16}$$

By introducing new variables

$$X_i = \int_{S_i} \sigma(\vec{r}_Q)\ dS_Q, \tag{3.17}$$

integrals in the right-hand side of equation (3.16) can be approximated using the mean value theorem as follows:

$$\int_{S_j} \sigma(\vec{r}_M)\omega_i(M)\ dS_M \approx \omega_i(M_j) \int_{S_j} \sigma(\vec{r}_M)\ dS_M = \omega_{ij} X_j. \tag{3.18}$$

where M_j is some middle point of surface element S_j. Since the solid angles $\omega_i(M)$ are smooth functions of M and the kernel in equation (2.33) is singular, the approximation (3.18) is more accurate than the direct discretization of the integral in equation (2.33). By substituting formulas (3.17) and (3.18) into (3.16), we find

$$X_i = \frac{\lambda}{2\pi} \sum_{j=1}^{N} \omega_{ij} X_j. \tag{3.19}$$

The fundamental advantage of discretization of (3.19) is that the evaluation of singular integrals in calculations of ω_{ii} can be avoided completely by using the following equation. From (3.12) and (3.15), we find

$$\sum_{i=1}^{N} \omega_{ij} = 2\pi. \tag{3.20}$$

Thus, we can write

$$\omega_{ii} \approx 2\pi - \sum_{i=1_{i\neq j}}^{N} \omega_{ij}. \tag{3.21}$$

3.4 Implementation of BEM for the Half-space Green's Function

In this section we represent the implementation of BEM for the half-space Green's function. We follow the same steps we did in previous section. From equation (2.65) let us partition S into N small pieces S_j and rewrite it as follows:

$$\sigma(\vec{r}_Q) \approx \frac{\lambda}{2\pi} \sum_{j=1}^{N} \int_{S_j} \sigma(\vec{r}_M) \left(\frac{\hat{n}_Q \cdot \vec{r}_{MQ}}{||\vec{r}_{MQ}||^3} - \frac{\epsilon - 1}{\epsilon + 1} \frac{\hat{n}_Q \cdot \vec{r}_{M'Q}}{||\vec{r}_{M'Q}||^3} \right) dS_M. \tag{3.22}$$

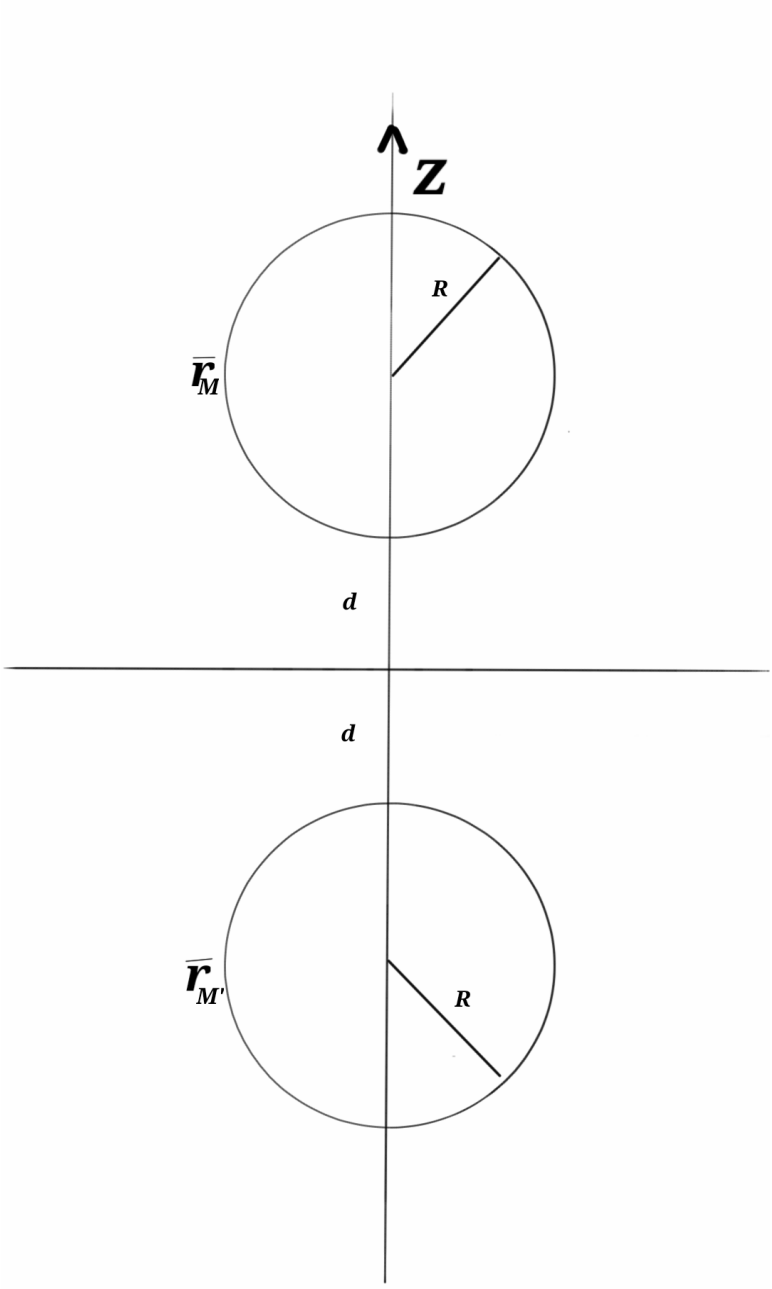

Figure 3.7: A diagram explaining the nanoparticles on substrate outlined in Section(2.4). As shown $\vec{r}_Q = (x_Q, y_Q, z_Q)$ and $\vec{r}_M = (x_M, y_M, z_M)$ are two points on the boundary S, $\vec{r}_{M'} = (x_M, y_M, -2d - 2z_M) \notin S$ is an image of $\vec{r}_M$ and d is the distance between the center of the nanoparticle and the surface $\widetilde{S}$ of the substrate.

Again we used the same assumption that points $\vec{r}_Q$ and $\vec{r}_M$ are the centroid points of each small triangle S_j and we first approximate both the $\sigma(\vec{r}_M)$ and the kernel $(\frac{\vec{r}_{MQ} \cdot \hat{n}_Q}{\|\vec{r}_{MQ}\|^3})$ with constant functions over each triangle.The element containing the j-th point is denoted S_j. These points are also used as the collocation points, that is, the points where the integral equation is applied. The BEM is then applied at the i-th point and integration over S is estimated by the sum of the integrations on all N triangles. Using the previously defined

convention for notation, we obtain from (3.22)

$$\sigma_i = \frac{\lambda}{2\pi} \sum_{j=1}^{N} \sigma_j \left[\frac{(\mathbf{r}_i - \mathbf{r}_j) \cdot \mathbf{n}_i}{\|\mathbf{r}_i - \mathbf{r}_j\|^3} - \frac{\epsilon - 1}{\epsilon + 1} \frac{\mathbf{n}_i \cdot (\mathbf{r}_i - \mathbf{r}'_j)}{||\mathbf{r}_i - \mathbf{r}'_j||^3} \right] \Delta S_j, \tag{3.23}$$

where $\mathbf{r}_i = (x_i, y_i, z_i)$, $\mathbf{r}_j = (x_j, y_j, z_j)$ and $\mathbf{r}'_j = (x_j, y_j, -2d - z_j)$, while d is the distance between the center of the nanoparticle and the origin as described in Figure 3.7. We can write the sum by combining the vectors for i in (3.23) as a matrix $\mathbf{A}$

$$\mathbf{A} = \begin{bmatrix} F_{1,1} \cdot \Delta S_1 & F_{1,2} \cdot \Delta S_2 & \cdots & F_{1,N} \cdot \Delta S_N \\ F_{2,1} \cdot \Delta S_1 & F_{2,2} \cdot \Delta S_2 & \cdots & F_{2,N} \cdot \Delta S_N \\ \vdots & \vdots & \ddots & \vdots \\ F_{N,1} \cdot \Delta S_1 & F_{N,2} \cdot \Delta S_2 & \cdots & F_{N,N} \cdot \Delta S_N \end{bmatrix}, \tag{3.24}$$

where

$$F_{i,j} = \frac{(\mathbf{r}_i - \mathbf{r}_j) \cdot \mathbf{n}_i}{\|\mathbf{r}_i - \mathbf{r}_j\|^3} - \frac{\epsilon - 1}{\epsilon + 1} \frac{\mathbf{n}_i \cdot (\mathbf{r}_i - \mathbf{r}'_j)}{||\mathbf{r}_i - \mathbf{r}'_j||^3}. \tag{3.25}$$

Now, we write (3.23) in a matrix form as

$$\sigma = \frac{\lambda}{2\pi} \mathbf{A} \sigma, \tag{3.26}$$

where

$$\sigma = \begin{pmatrix} \sigma_1 \\ \sigma_2 \\ \vdots \\ \sigma_N \end{pmatrix}.$$

Notice here that $F_{i,j}$ contains two parts, the first is the same as that we solved formally. Thus, we treat it the same way using approach B for the singularity terms. However, the second part of $F_{i,j}$ is non-singular for all the N. Following the same steps we integrate equation (3.22) over S_i

$$\int_{S_i} \sigma(\vec{r}_Q)\, dS_Q = \frac{\lambda}{2\pi} \sum_{j=1}^{N} \int_{S_j} \sigma(\vec{r}_M) \left[\omega_i(M) - \frac{\epsilon - 1}{\epsilon + 1} \omega(M') \right] dS_M, \tag{3.27}$$

where $\omega_i(M)$ is (3.15) and

$$\omega_i(M') = \int_{S_i} \frac{\vec{r}_{M'Q} \cdot \hat{n}_Q}{\|\vec{r}_{M'Q}\|^3}\, dS_Q, \tag{3.28}$$

is the solid angle subtended by the surface element S_i when viewed from the point M' that is the mirror image of the point M in the substrate surface plane. We can write

$$X_i = \frac{\lambda}{2\pi} \sum_{j=1}^{N} \left[\omega_{ij} - \frac{\epsilon - 1}{\epsilon + 1} \omega'_{ij} \right] X_j, \tag{3.29}$$

where X_i and X_j defined in equation (3.17) and equation (3.18) respectively.

3.5 Eigenvalues' Sensitivity and Accuracy

Equation (3.5) is an eigenvalue problem type of equation. In general we are looking for a solution that satisfies

$$(\mathbf{A} - \lambda I)\,\mathbf{X} = 0, \tag{3.30}$$

where I is the identity matrix, $\mathbf{A}$ is a square matrix and $\mathbf{X}$ is a nonzero vector. There are many approaches to find the eigenvalues. we have used here the MATLAB function *eig* to find the eigenvalues. The sensitivity of the eigenvalues of a matrix depends on perturbations. We are interested to know how sensitive are our calculations of the eigenvalues, presented here some derivations of that. These derivations have been done before in numerous of texts, (for more information and rigorous derivations see [33]). Rewriting (3.30) as

$$\lambda = \mathbf{X}_{-1}\mathbf{A}\mathbf{X}. \tag{3.31}$$

Let $\epsilon_{machine}$ denote the roundoff error cause by the perturbations

$$\lambda + \tilde{\lambda} = \mathbf{X}_{-1}\,(\mathbf{A} + \epsilon_{machine})\,\mathbf{X}. \tag{3.32}$$

Yields

$$\tilde{\lambda} = \mathbf{X}_{-1}\epsilon_{machine}\mathbf{X}, \tag{3.33}$$

Taking matrix norms

$$\|\tilde{\lambda}\| \leq \|\mathbf{X}_{-1}\|\|\epsilon_{machine}\|\|\mathbf{X}\| = K(\mathbf{X})\|\epsilon_{machine}\|, \tag{3.34}$$

where $K(\mathbf{X})$ is the matrix condition number. This condition number of $\mathbf{X}$ which is the matrix of eigenvectors not the condition of $\mathbf{A}$ nor of $\tilde{\lambda}$. Thus, this analysis does not say much about the sensitivity of eigenvalues. In order to investigate the sensitivity of an individual eigenvalue, we should involves the left eigenvectors y. With some simple derivations, one can define the eigenvalue condition number [33] as

$$k(\lambda_j, \mathbf{A}) = \|y\|\|x\|. \tag{3.35}$$

Since $\|x\| \leq \|\mathbf{X}\|$ and $\|y\| \leq \|\mathbf{X}\|$, we have

$$k(\lambda_j, \mathbf{A}) = K(\mathbf{X}). \tag{3.36}$$

The condition number of the eigenvector matrix is an upper bound for the individual eigenvalue condition numbers.

Chapter 4

Computational results

The two approaches described in the previous chapter have been tested on an example of spherical particle for which the analytical solution using the Mie theory may be used as a benchmark comparison data.

4.1 Eigenvalues for Nanosphere Particle in Free Space

The mesh used in calculation is shown in Figure 3.3, while the results of numerical computations are presented in Tables 4.1,4.2. We have used a unit sphere discretized into three different meshes; one with 792 triangles ($N = 792$), the second with 3168 triangles ($N = 3168$) and the third with 12672 triangles ($N = 12672$). As we previously discussed, the mesh was created using the free software GMSH. We have used unstructured flat triangular mesh. Then, we have performed computation using the two approaches combined with the GMSH data file using MATLAB.

We demonstrate sample tables of computation results for both approaches. For approach B, the complete results on 792-triangle mesh are compared with the first 792 eigenvalues on 3168-triangle mesh (shown in Appendix C). In Table 4.1, we present some of the results of the Approach A computation using the three discretization of the unit sphere. The initial mesh consists of 792 flat triangles. It is refined once by splitting each triangle into 4 (see Figure 4.1) to obtain a $N = 3168$ element mesh. This process is repeated one more time to produce $N = 12672$ element mesh. Note that the new vertices introduced in B are located on the surface of the particle and not on the old edge. In this approach we set the value of singular integrals to be zero, i.e. the diagonal elements in matrix $\mathbf{A}$ is 0. The computed result for this approach is not accurate. We also observe that the error is large for larger eigenvalues. Increasing the number of triangles has helped to reduce the error but it remains large.

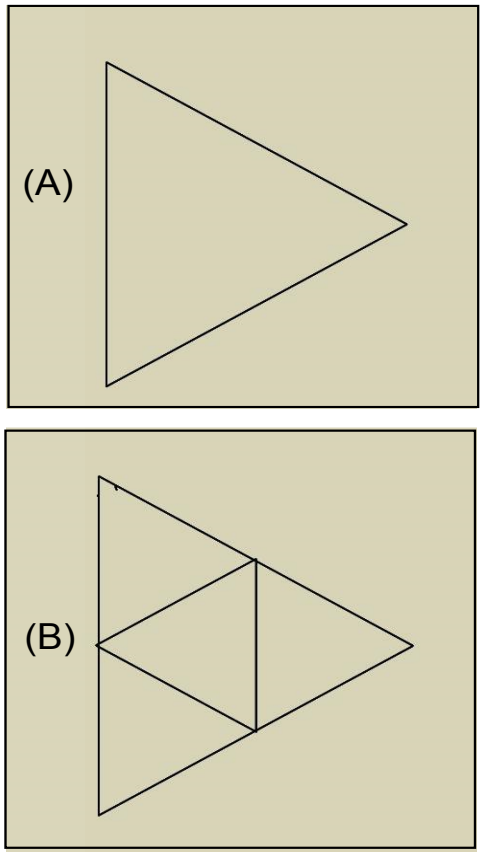

Figure 4.1: Mesh refinement by triangle splitting. (B) is a refinement of (A).

Eigenvalues for a single nanosphere				
Mode number	Exact Values	N = 792	N = 3168	N = 12672
1	3	3.379	3.185	3.091
2	3	3.384	3.187	3.092
3	3	3.386	3.188	3.092
4	5	6.126	5.526	5.254
5	5	6.139	5.53	5.255
6	5	6.199	5.55	5.268
7	5	6.223	5.557	5.266
8	5	6.234	5.561	5.263
9	7	9.438	8.082	7.51
10	7	9.471	8.09	7.513
11	7	9.486	8.095	7.515
12	7	9.579	8.12	7.541
13	7	9.644	8.142	7.533
14	7	9.644	8.143	7.533
15	7	9.725	8.164	7.524
16	9	13.31	10.83	9.847
17	9	13.52	10.89	9.919
18	9	13.6	10.91	9.908
19	9	13.63	10.91	9.9
20	9	13.71	10.94	9.893
21	9	13.8	10.96	9.885
22	9	13.86	10.98	9.869
23	9	13.97	11	9.877
24	9	14.08	11.03	9.874
25	11	18.02	13.85	12.29
26	11	18.33	13.92	12.41
27	11	18.46	13.95	12.31
28	11	18.51	13.96	12.32
29	11	18.72	14.02	12.33
30	11	18.84	14.04	12.37
31	11	19.06	14.06	12.35
32	11	19.06	14.09	12.35
33	11	19.34	14.15	12.36
34	11	19.57	14.18	12.39
35	11	19.71	14.22	12.4
36	13	23.96	17.17	14.84
37	13	24.02	17.19	14.85
38	13	24.26	17.26	14.87
39	13	24.47	17.32	15.03
40	13	24.96	17.37	14.89

Table 4.1: computational results with approach A

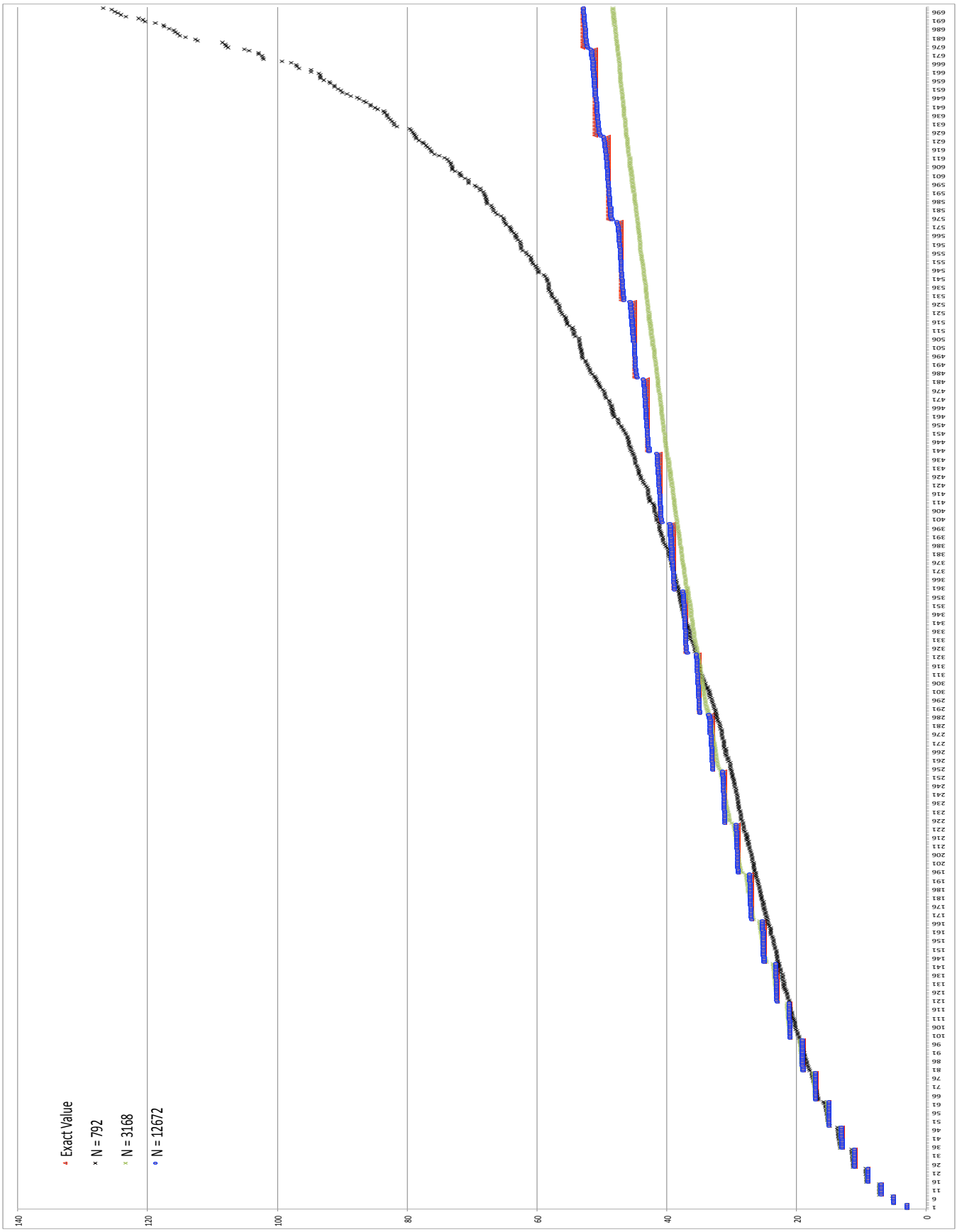

Figure 4.2: Eigenvalues chart comparing exact values with computational values obtained on three meshes.

In Table 4.2 and Figure 4.2, we present the results of approach B computation using the same three meshes. In this approach we have approximated the singularity of the diagonal elements by replacing them with the outcome of summing each of the row values and subtracting them from 2π (see equation (3.21)), as was discussed in Chapter 3. The computation results for this approach are a significantly improvement from Approach A. We can see that the error is reduced; even for large eigenvalues the approach is still close to the theoretical value. In Section 3.5 we introduced the condition number of eigenvalues and round-of errors. For simplicity, we rewrite it again here as

$$\epsilon_j \leq k(\lambda_j, A)\epsilon_{machine}, \tag{4.1}$$

knowing that $\epsilon_{machine} \approx 10^{-16}$ and using MATLAB function *condeig* we found the condition number for each computed eigenvalue (see Table 4.3). We notice from Table 4.3 that the condition numbers for eigenvalues are between 1.01 and 39.8. Substituting these numbers in (4.1) we observe that the roundoff error effects on the accuracy of the eigenvalues is negligible.

Eigenvalues for a single nanosphere				
Mode number	Exact Values	N = 792	N = 3168	N = 12672
1	3	3.027	3.007	3.002
2	3	3.029	3.007	3.002
3	3	3.03	3.008	3.002
4	5	5.06	5.017	5.004
5	5	5.065	5.018	5.005
6	5	5.101	5.026	5.007
7	5	5.111	5.029	5.007
8	5	5.116	5.03	5.008
9	7	7.114	7.034	7.009
10	7	7.13	7.038	7.01
11	7	7.132	7.038	7.01
12	7	7.173	7.049	7.013
13	7	7.188	7.053	7.014
14	7	7.218	7.061	7.016
15	7	7.249	7.067	7.017
16	9	9.069	9.032	9.009
17	9	9.163	9.06	9.016
18	9	9.173	9.06	9.017
19	9	9.227	9.072	9.019
20	9	9.276	9.085	9.023
21	9	9.295	9.091	9.024
22	9	9.306	9.091	9.024
23	9	9.355	9.104	9.027
24	9	9.429	9.123	9.032
25	11	10.98	11.03	11.01
26	11	11.08	11.06	11.02
27	11	11.13	11.07	11.02
28	11	11.17	11.08	11.02
29	11	11.24	11.1	11.03
30	11	11.3	11.11	11.03
31	11	11.36	11.13	11.04
32	11	11.44	11.14	11.04
33	11	11.49	11.16	11.04
34	11	11.55	11.18	11.05
35	11	11.59	11.19	11.05
36	13	12.83	13.02	13.01
37	13	12.91	13.03	13.01
38	13	12.97	13.07	13.03
39	13	13.04	13.09	13.03
40	13	13.16	13.12	13.04

Table 4.2: Computational results with approach B

Condition Number for Eigenvalues										
1.00673902	1.03292932	1.07758881	1.14201104	1.19705258	1.29095884	1.39202776	1.51784516	1.64977518	1.95828602	2.40569357
1.00692859	1.03325419	1.07795778	1.14324975	1.20050211	1.29211972	1.39328927	1.51808638	1.65233243	1.96766315	2.42124847
1.0075649	1.03333735	1.07913977	1.14344019	1.20148468	1.29308192	1.39358018	1.52645992	1.65715029	1.96766315	2.42124847
1.00779526	1.03352013	1.07991819	1.14452217	1.20347434	1.29651164	1.39971423	1.52988481	1.6796411	1.97673312	2.43731648
1.0085808	1.03397913	1.08047929	1.14474195	1.20587712	1.29799945	1.40021295	1.53188385	1.68079677	1.97973764	2.43740726
1.00883994	1.03418726	1.08087791	1.14575815	1.20804994	1.30022283	1.40330432	1.53425116	1.68079677	1.98120411	2.4587735
1.0088658	1.03451685	1.08193777	1.14591746	1.20837951	1.30041936	1.40358846	1.53457676	1.68118465	1.99012682	2.48420807
1.00914612	1.03479669	1.08209783	1.14592693	1.21076265	1.30119947	1.40371487	1.53618918	1.6840756	1.99306608	2.49788152
1.00920627	1.03561292	1.08221815	1.14593921	1.21120451	1.30184755	1.40595006	1.53638187	1.68695315	1.99831949	2.50240708
1.00956591	1.03567172	1.085055	1.14610801	1.21450355	1.30416135	1.40747534	1.53667101	1.68695315	1.99831949	2.52932978
1.00991139	1.03571653	1.08565968	1.14622306	1.2158966	1.30639381	1.41343792	1.53667101	1.69154332	2.00486864	2.54101611
1.01059843	1.03657622	1.08622167	1.14666787	1.21756033	1.30646243	1.41343792	1.54172417	1.69181016	2.02637767	2.55201168
1.01079178	1.0390522	1.08674065	1.14674283	1.21803845	1.30784071	1.41356448	1.54218132	1.69520062	2.02946431	2.55719452
1.01130328	1.03963201	1.08680127	1.14688369	1.21956114	1.30823787	1.4145052	1.54879778	1.70272642	2.03088948	2.5788281
1.01180125	1.03985176	1.08757114	1.14867202	1.2196904	1.30968272	1.41499352	1.54958754	1.70459666	2.03910667	2.60266163
1.01230374	1.04118676	1.08766403	1.14936901	1.2238247	1.31035432	1.41559259	1.55126763	1.70566086	2.04200457	2.6154705
1.0128117	1.04260156	1.08823835	1.15062817	1.22515895	1.31406612	1.41560619	1.55162976	1.70947215	2.04707772	2.61773208
1.01363923	1.04329367	1.08854934	1.15149194	1.22828965	1.31503999	1.41932495	1.55513715	1.71258251	2.04773971	2.62312042
1.01369194	1.04474154	1.08858881	1.15152845	1.22847388	1.31538846	1.42141979	1.56059316	1.71503288	2.0526173	2.62312042
1.01397064	1.04717769	1.09305972	1.15456498	1.22985604	1.31580703	1.42534238	1.56238799	1.7208923	2.05411441	2.62496216
1.01418393	1.04767237	1.09336596	1.1547424	1.23274516	1.31629631	1.42534238	1.56423111	1.72139249	2.06225569	2.66789021
1.01418422	1.04798252	1.09478381	1.15488242	1.23444275	1.3164519	1.42653636	1.56493294	1.73265145	2.06225569	2.71176186
1.0142307	1.04798252	1.09490238	1.15764691	1.23464313	1.31662359	1.42938037	1.56493294	1.73701262	2.07139288	2.71192752
1.01436996	1.04821655	1.0949623	1.15795398	1.23488966	1.31697881	1.43468718	1.56770803	1.73763411	2.08211781	2.71192752
1.01472491	1.04827511	1.09824179	1.15838727	1.23488966	1.3175793	1.43762503	1.56770803	1.7403136	2.08670488	2.74659329
1.01475479	1.04937464	1.10023955	1.15990879	1.23534148	1.31883771	1.44073113	1.56796565	1.74281811	2.09023365	2.75632399
1.01521297	1.0496056	1.10275061	1.16123705	1.23549174	1.32162518	1.44777602	1.5705128	1.7448668	2.09617137	2.75724707
1.01561757	1.05041571	1.10323692	1.16281196	1.23741275	1.32162518	1.44993278	1.57273894	1.74487078	2.10296598	2.75724707
1.01572773	1.05160549	1.10342047	1.16307987	1.23762428	1.32338422	1.45233442	1.57343054	1.75134427	2.11449586	2.7777314
1.01594323	1.05209647	1.10381802	1.16433462	1.23934286	1.32574698	1.45329831	1.57343054	1.75134427	2.1180679	2.77923851
1.01595977	1.05310872	1.10481345	1.16433462	1.24025964	1.32660051	1.45563399	1.57579043	1.76155536	2.1180679	2.804757
1.01634775	1.05318029	1.10487816	1.16441021	1.24039694	1.32667052	1.45800404	1.57608363	1.7666112	2.12463467	2.83236941
1.01689739	1.05334954	1.10565614	1.16565162	1.24250954	1.32667052	1.45867697	1.57679113	1.77846521	2.14593752	2.84002533
1.01693858	1.05349876	1.10625547	1.16570087	1.24347853	1.32811	1.46052659	1.57791855	1.77846521	2.15239081	2.86548629
1.01717298	1.05411092	1.10667307	1.16580453	1.2440254	1.32942482	1.46343205	1.57791855	1.77961044	2.15275137	2.86548629
1.01733162	1.05576353	1.10765818	1.16670568	1.24404047	1.3318437	1.46469189	1.57808505	1.78545473	2.15321928	2.86831561
1.01782848	1.05696884	1.10823694	1.16724039	1.24520868	1.33370888	1.46576365	1.58225048	1.79987655	2.15585978	2.89593804
1.01804751	1.05727705	1.1101582	1.16780709	1.25184811	1.33480254	1.47117799	1.58225048	1.80129624	2.15950861	2.92894826
1.01867227	1.05826678	1.11304932	1.16874248	1.25354601	1.33612687	1.47172032	1.5948179	1.81289125	2.16632489	2.93820619
1.0201208	1.05879876	1.11392806	1.16901001	1.25375392	1.33675755	1.4729945	1.59594707	1.81423656	2.18057777	2.96744718
1.02128722	1.05936357	1.11482597	1.16936333	1.25390664	1.33675755	1.47485606	1.59594707	1.81827485	2.18057777	2.96744718
1.02144772	1.05968641	1.11704708	1.16992819	1.25428056	1.33814598	1.47538217	1.59862179	1.82175154	2.192787	2.98603833
1.02156354	1.06023202	1.11735773	1.17141468	1.25549021	1.34053722	1.47538217	1.59862179	1.82669387	2.20391878	2.98603833
1.02169862	1.06053153	1.11833969	1.17146849	1.25549021	1.34405008	1.48532263	1.61485829	1.83728339	2.20555574	2.9890829
1.02195262	1.06055702	1.11919199	1.17262382	1.25635369	1.34405008	1.48570869	1.61790093	1.83728339	2.20750162	2.99815858
1.02204709	1.06055858	1.12043883	1.17290413	1.25668108	1.34570793	1.48999491	1.61976379	1.8417169	2.20750162	3.04584145
1.02254551	1.06235467	1.12062639	1.17405748	1.25736263	1.34603539	1.49014014	1.62070956	1.84281812	2.21109089	3.05459442
1.02262911	1.06294783	1.12196221	1.17452425	1.2582954	1.34737259	1.49052805	1.62134395	1.84720602	2.21840519	3.06099522
1.02273666	1.06416711	1.12404882	1.17525853	1.26087287	1.34786049	1.4942618	1.62228963	1.85107234	2.21840519	3.06839719
1.02398859	1.06442246	1.12452238	1.17602292	1.26922119	1.35170715	1.49546324	1.62398921	1.85109308	2.22241796	3.08110026
1.02442159	1.06450446	1.12470959	1.17610076	1.27055232	1.3532791	1.49546324	1.62462804	1.85989965	2.24111185	3.11544455
1.0263683	1.06585724	1.12542099	1.17675827	1.27090002	1.35907008	1.49700105	1.63145784	1.86457288	2.27564849	3.12615867
1.02657513	1.0665344	1.12606768	1.17685615	1.27199439	1.36022819	1.49846339	1.63306403	1.87074948	2.27564849	3.13235404
1.02670871	1.06794958	1.12657773	1.1769541	1.27212707	1.36296636	1.49846339	1.63580256	1.87074948	2.2844087	3.13235404
1.02773825	1.06796434	1.12803218	1.17697641	1.27304632	1.36336155	1.501047	1.63580256	1.87230668	2.2844087	3.15484786
1.02792743	1.06807356	1.12922512	1.17758789	1.27515613	1.36553304	1.50134697	1.63760854	1.88911069	2.28677784	3.19366514
1.02841103	1.06816078	1.13038564	1.18008061	1.27565232	1.36955524	1.50155445	1.6399613	1.8910801	2.28677784	3.29594159
1.02880121	1.06816107	1.13136972	1.18066225	1.28212845	1.37439908	1.50366421	1.6399613	1.89938668	2.30178175	3.35878076
1.02948216	1.06834607	1.13183615	1.1828219	1.28361721	1.37601299	1.50366421	1.64358301	1.89974612	2.31450508	3.51315742
1.02976808	1.06914253	1.13510054	1.18550846	1.28398178	1.3771405	1.50688766	1.64539954	1.9070909	2.31450508	3.58941143
1.03024284	1.06916511	1.13535288	1.18690512	1.28540972	1.3771405	1.5084135	1.64604636	1.91794036	2.33099575	3.61116507
1.03145277	1.07118251	1.13563562	1.1888921	1.2877437	1.37819388	1.50963231	1.64652284	1.91794036	2.33797339	3.69128081
1.03167125	1.07197857	1.13651813	1.19144302	1.2877437	1.37836576	1.51004914	1.64652284	1.93233964	2.35008368	3.72266045
1.03189057	1.07241541	1.13958064	1.1938494	1.28790819	1.37939936	1.51159288	1.64717111	1.93406124	2.36347136	3.72347023
1.03202642	1.07270543	1.13982937	1.19458358	1.28805531	1.38262189	1.51317324	1.64717111	1.93505175	2.36347136	3.76172702
1.03260824	1.07352144	1.13988996	1.19546893	1.28814243	1.38354222	1.51684445	1.64805954	1.94392216	2.36869775	3.82498678
1.03288266	1.0742776	1.14082924	1.19602803	1.29002826	1.38770187	1.51684445	1.64935296	1.94799208	2.3791259	3.82498678
1.0328899	1.07508274	1.14141177	1.19626076	1.29042411	1.39072066	1.51782607	1.64977518	1.94799208	2.38616743	3.85157878
3.85157878	4.09792011	4.60028528	4.82882133	4.86887498	5.98262363	6.80916747	10.0653682	11.6048548	14.1780679	25.7542282
3.88389098	4.09792011	4.62399619	4.84187918	5.62363843	5.98262363	6.80916747	10.0841813	11.7285863	17.9146046	25.7542282
3.95378328	4.2940296	4.69353784	4.84187918	5.66722959	6.22850163	7.57740065	11.1753591	11.7285863	18.2754321	39.7694848
4.07278761	4.31843372	4.82882133	4.8574514	5.77812583	6.36112093	8.62456201	11.1753591	14.1780679	18.2754321	39.7694848

Table 4.3: Condition numbers for eigenvalues, from top to bottom and from left to right.

In Figure 4.3, we show some of the computational results for all the meshes we also plot. The results are based on the mesh $N = 12672$ and corresponding exact values. The results from the other meshes as well for comparison. As demonstrated in Figure 4.3 the results with $N = 12672$ are accurate for a high number of eigenvalues as opposed to coarser mesh. The results are limited to the number of elements in the mesh, as shown in these figures increasing the number of elements in the mesh results in significant improvement of the computational results.

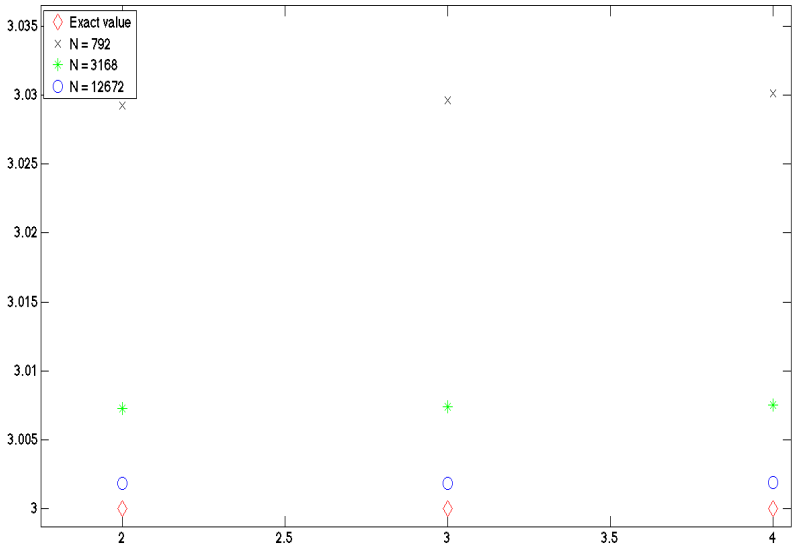
Exact value
N = 792
N = 3168
N = 12672
3.035
3.03
3.025
3.02
3.015
3.01
3.005
3
2
2.5
3
3.5
4

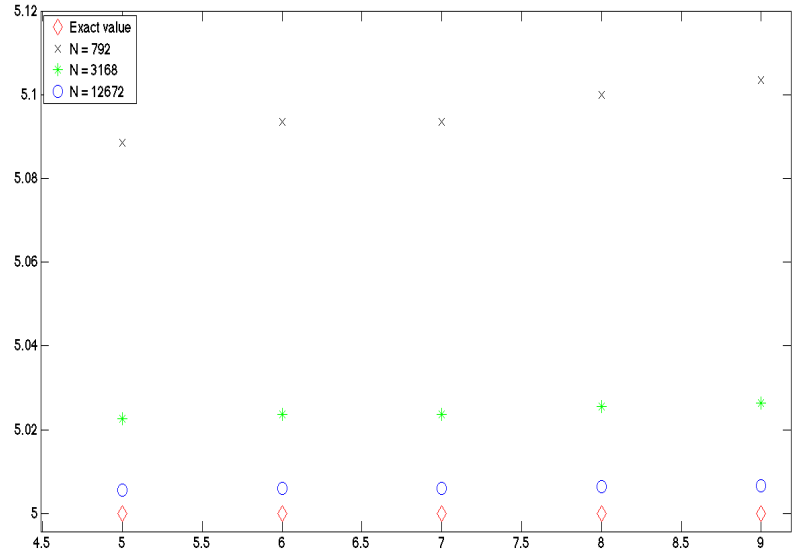
Exact value
N = 792
N = 3168
N = 12672
5.12
5.1
5.08
5.06
5.04
5.02
5
4.5
5
5.5
6
6.5
7
7.5
8
8.5
9

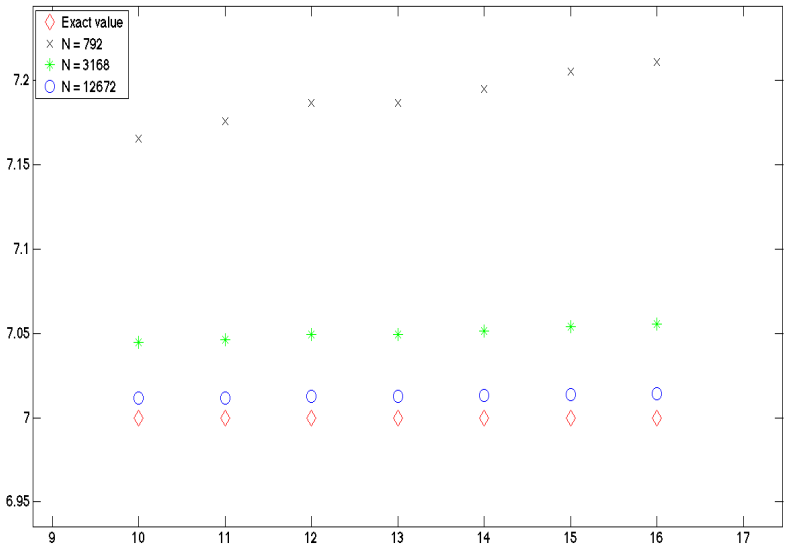
Exact value
N = 792
N = 3168
N = 12672
7.2
7.15
7.1
7.05
7
6.95
9
10
11
12
13
14
15
16
17

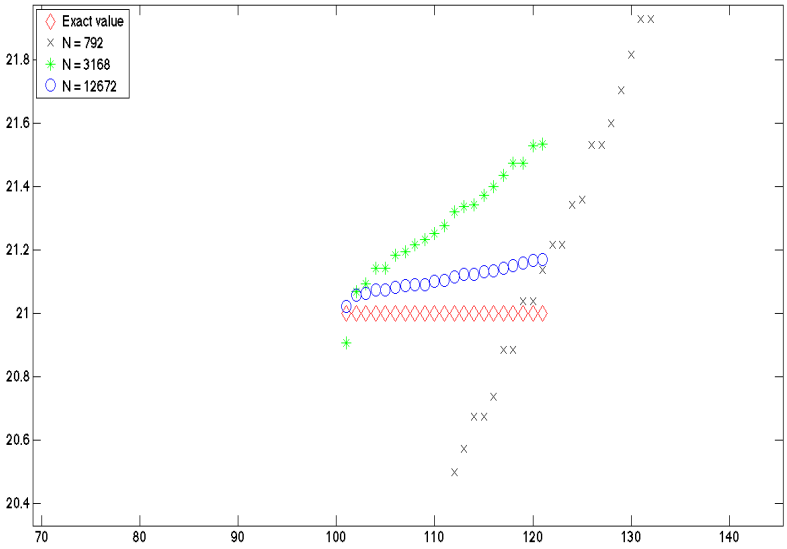
Exact value
N = 792
N = 3168
N = 12672
21.8
21.6
21.4
21.2
21
20.8
20.6
20.4
70
80
90
100
110
120
130
140

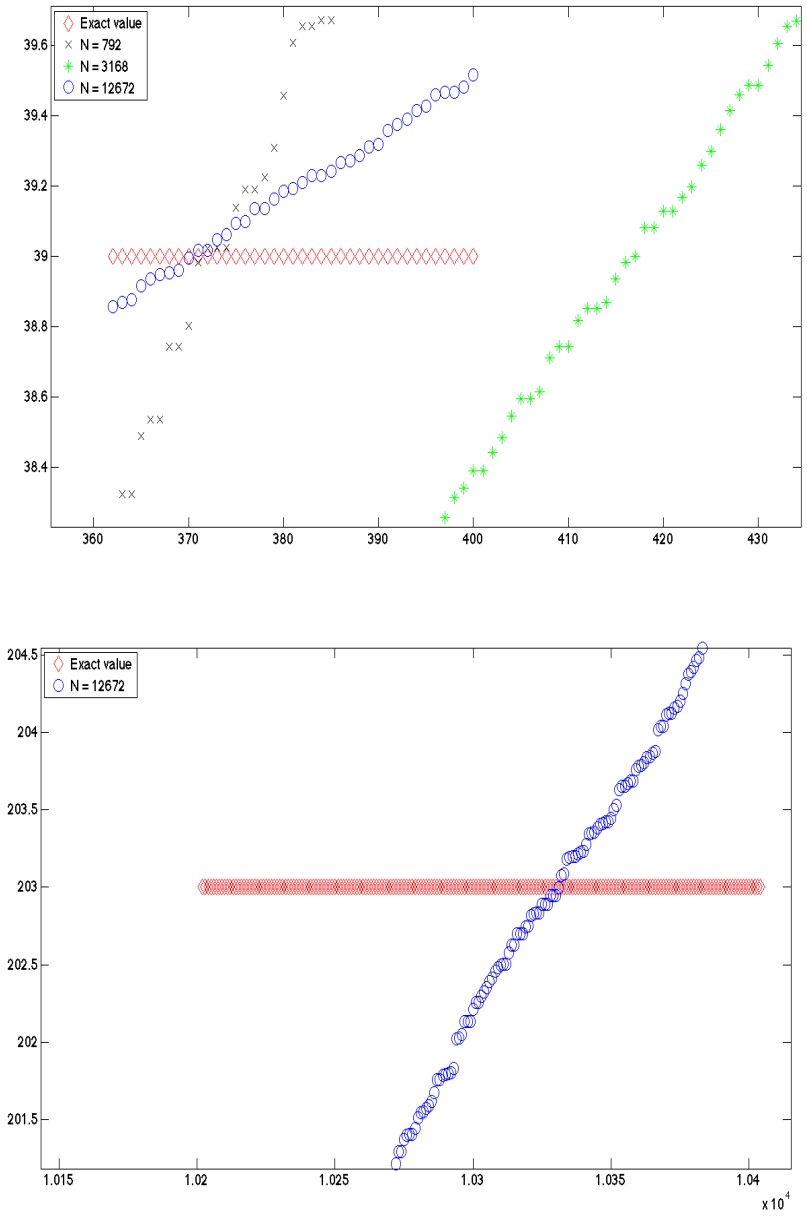

Figure 4.3: Eigenvalues for nanosphere in free space; comparison of results of exact values and computational values on three meshes. The exact values are $\lambda = 3, 5, 7, 21, 39, 203$. We see that the results on the mesh with $N = 12672$ are more accurate than the others.

In this thesis we seek the values of ω, writing equation (2.34) in terms of ω

$$\omega = \omega_p \sqrt{\left(\frac{1}{2} - \frac{1}{2\lambda}\right)}, \tag{4.2}$$

where ω_p as defined previously, is a given constant called the plasma frequency for the material, for gold and silver given in the Appendix A. λ is the eigenvalue discussed above, we notice from the equation (4.2) that for small eigenvalues, for which accurate computational results were presented, the error of the frequency ω is much smaller. Moreover, for high eigenvalues where the error increases, the resulting frequency yields an insignificant error.

4.2 Eigenvectors for Nanosphere Particle in Free Space

In this section we show the surface charge densities plotted on the same discretized sphere we used to compute eigenvalues on. From equation (3.5), the surface charge densities are the eigenvectors corresponding to the eigenvalues we presented in the previous section. We have used the eigenvectors on the mesh with $N = 12672$ and compared them with the associated Legendre polynomials in Table 4.4. The color coding is chosen so that the extreme red shows regions on the sphere with the largest positive components of the eigenvector σ and the extreme blue shows regions with the largest negative elements of that vector. Physically, those colors correspond to the regions with an excess density of electrons and the regions depleted of electrons, similar to those in Figure 1.1. In Figure 4.4 we show the surface charge densities σ_1, σ_2, and σ_3 corresponding to the eigenvalues $\lambda = 3$ compared with the associated Legendre polynomials P_1^0 and P_1^1. We see that the computed eigenvectors are quite similar to the associated Legendre polynomials, apart from different orientations. We recall that the Mie theory implies that the three eigenvectors with $l = 1$ are degenerate with respect to arbitrarily chosen axes of symmetry. Here we see that the computed eigenvectors are no longer degenerate because of slight differences in their corresponding computed eigenvalues, and that removal of degeneracy is reflected in different orientations of the axes in the first three spheres in Figure 4.4.

The surface charge densities σ_4, σ_5, σ_6, σ_7 ,and σ_8 corresponding to the eigenvalues $\lambda = 5$ are presented in Figure 4.5 and compared with the associated Legendre polynomials P_2^0 and P_2^1 and P_2^2.

$l = 0$	$P_0^0 = 1$
$l = 1$	$P_1^0 = \cos(\theta)$ $P_1^1 = \sin(\theta)$
$l = 2$	$P_2^0 = \frac{1}{2}(3\cos^2(\theta) - 1)$ $P_2^1 = 3\sin(\theta)\cos(\theta)$ $P_2^2 = 3\sin^2(\theta)$

Table 4.4: Associated Legendre polynomials P_l^m

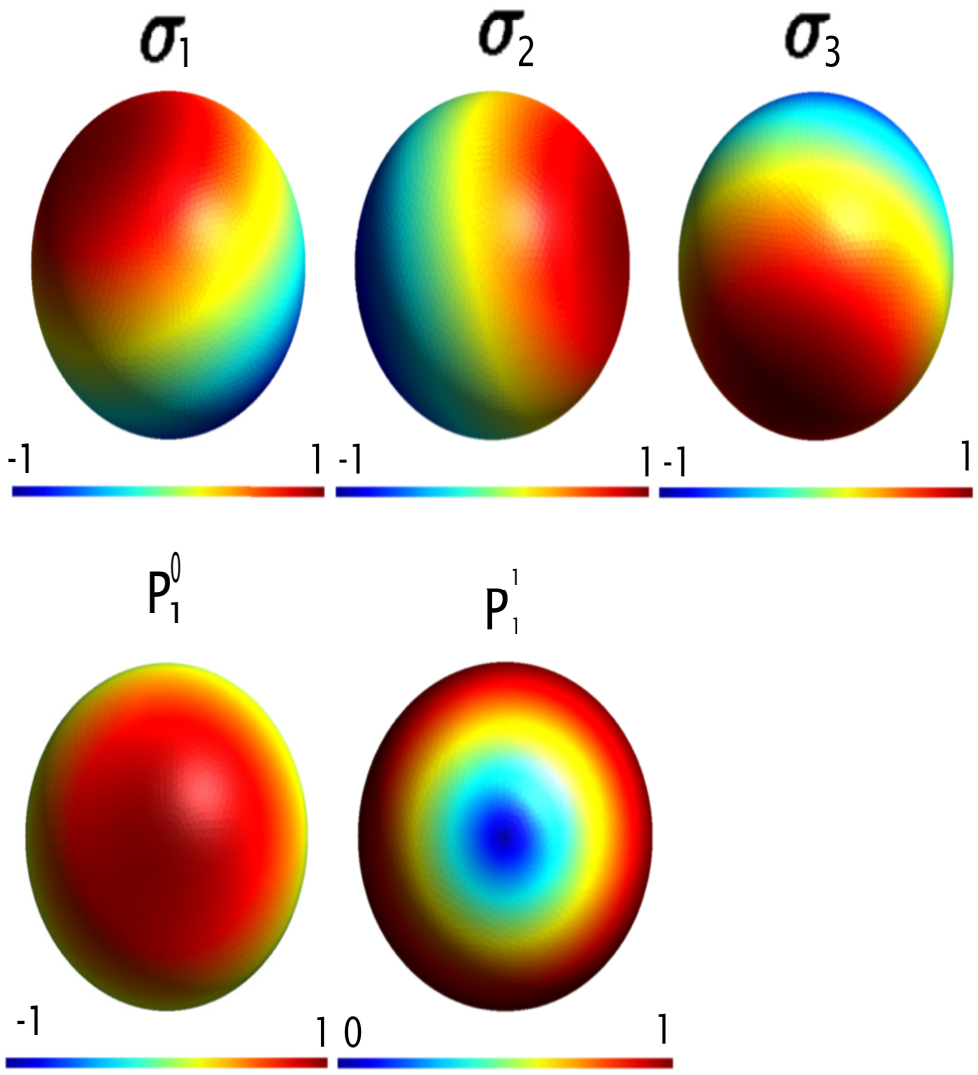

Figure 4.4: Starting from the upper left the first three figures represent the surface charge densities σ_1, σ_2, and σ_3, respectively, that correspond to the eigenvectors of the eigenvalues $\lambda_1 = 3$, $\lambda_2 = 3$, and $\lambda_3 = 3$. Next, the last two figures represent the associated Legendre polynomials P_1^0 and P_1^1.

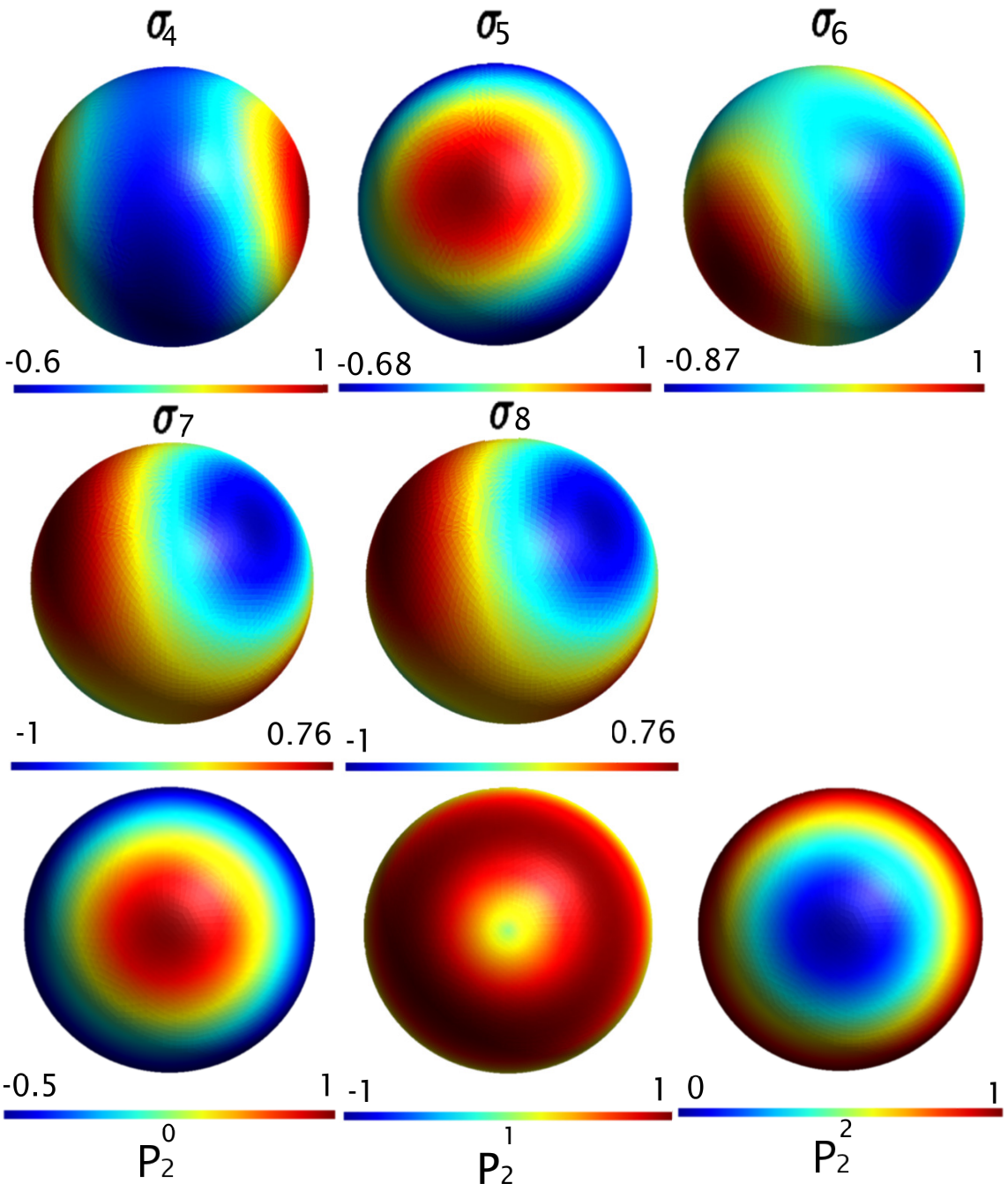

Figure 4.5: Starting from the upper left the first five figures represent the surface charge densities σ_4, σ_5, σ_6, σ_7, and σ_8, respectively which correspond to the eigenvectors of the eigenvalues λ_4 to λ_8. Next, the last three figures represent the associated Legendre polynomials P_2^0 and P_2^1 and P_2^2.

4.3 Nanosphere Particle Located on a Dielectric Substrate Computed Eigenvalues

In this section we present the results for the eigenvalue problem described in detail in Section 3.4. To do so, we need to know the value of ϵ in equation (3.29). We consider the

nanospherical particle on silicon dioxide substrates (SiO_2) which is of high technological interest; for more detail see [34]. For this case, $\epsilon = 3.9$, which is the relative permittivity for SiO_2. We choose the distance form the center of the sphere to the substrate to be equal to its radius, so that the sphere "sits" on the substrate. A sample of the results of numerical computations are presented in Table 4.5. Again, we have used a unit sphere discretized into the meshes used in Section 4.1. We used the approach B to create the first part of equation (3.29), which we have approximated the singularity comes from that part of the diagonal elements by replacing them with outcome of summing each row value and subtract them from 2π. In Figure 4.6, we show the eigenvalues chart for nanoparticles on SiO_2, which shows the results of three computational values of three meshes. The results of $N = 792$ are the base of the comparison.

Number	N = 792	N = 3168	N = 12672
1	0.449	0.114	0.028
2	0.462	0.114	0.028
3	0.469	0.115	0.028
4	0.477	0.116	0.029
5	0.482	0.117	0.029
6	0.489	0.119	0.029
7	0.507	0.123	0.03
8	0.547	0.133	0.033
9	1.023	0.801	0.2
10	2.043	0.812	0.201
11	2.182	0.827	0.205
12	2.201	0.844	0.211
13	2.678	0.852	0.211
14	2.735	0.871	0.216
15	2.759	0.913	0.228
16	2.879	0.994	0.251
17	2.993	1.033	0.419
18	3.072	1.591	0.433
19	3.241	1.652	0.436
20	3.432	1.685	0.447
21	3.829	1.748	0.46
22	3.913	1.886	0.464
23	4.217	1.902	0.484
24	4.259	1.952	0.519
25	4.439	1.993	0.546
26	4.881	1.999	0.562
27	5.038	2.148	0.567
28	5.136	2.178	0.579
29	5.231	2.287	0.58
30	5.381	2.333	0.596
31	5.569	2.339	0.617
32	5.788	2.435	0.639
33	5.912	2.492	1.002
34	6.286	2.55	1.359
35	6.434	2.665	1.39
36	6.59	2.773	1.422
37	6.774	3.008	1.435
38	6.822	3.028	1.447
39	6.962	3.25	1.515
40	7.275	3.301	1.56

Table 4.5: Eigenvalues for a single nanosphere on SiO_2.

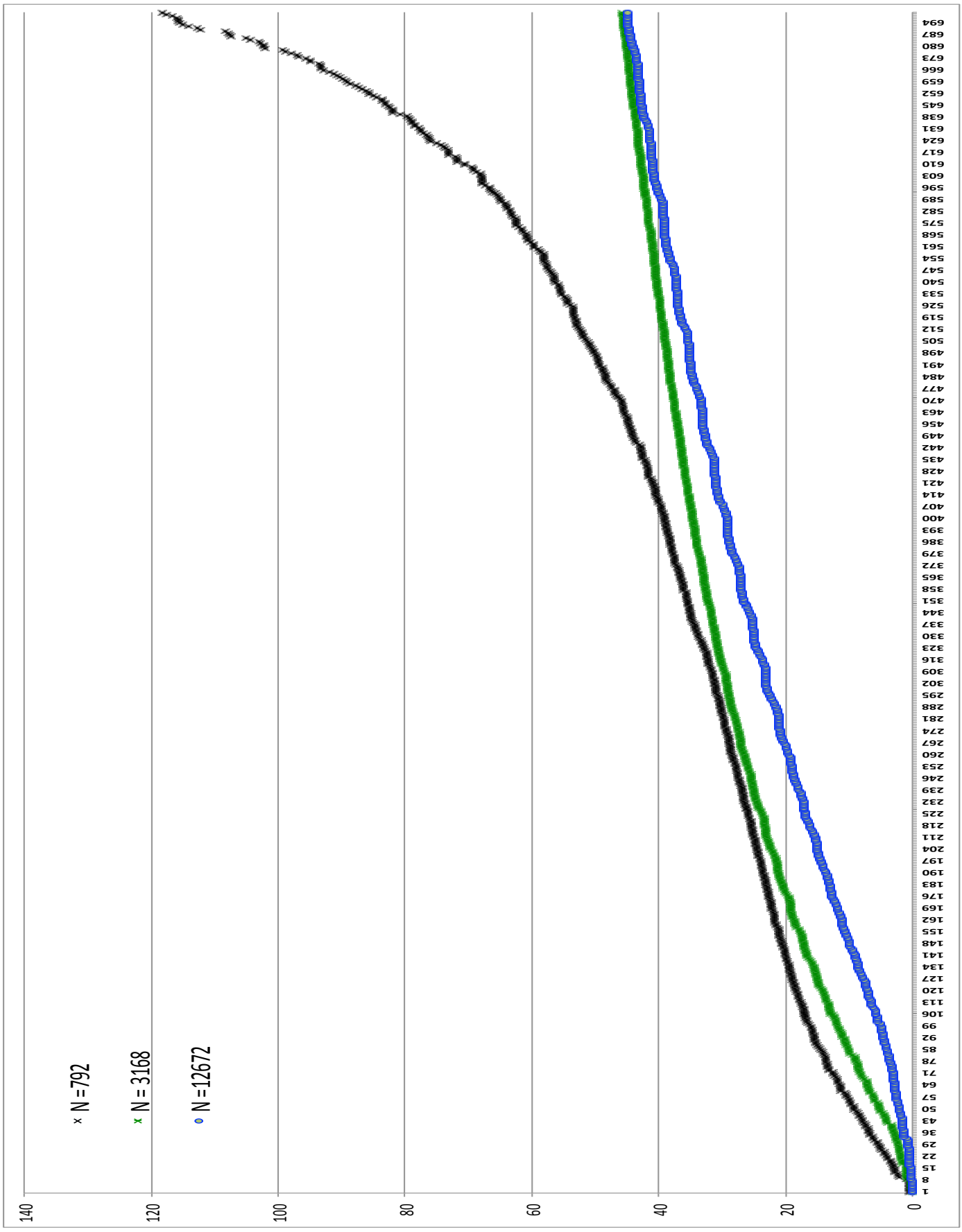

Figure 4.6: Eigenvalues chart for nanoparticle on a SiO_2, which shows the results of three computational values of three meshes.

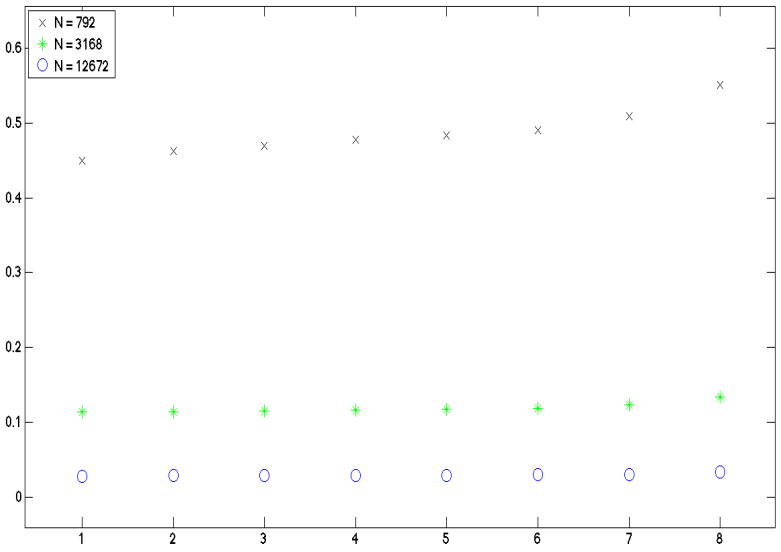
N = 792
N = 3168
N = 12672
0.6
0.5
0.4
0.3
0.2
0.1
0
1
2
3
4
5
6
7
8

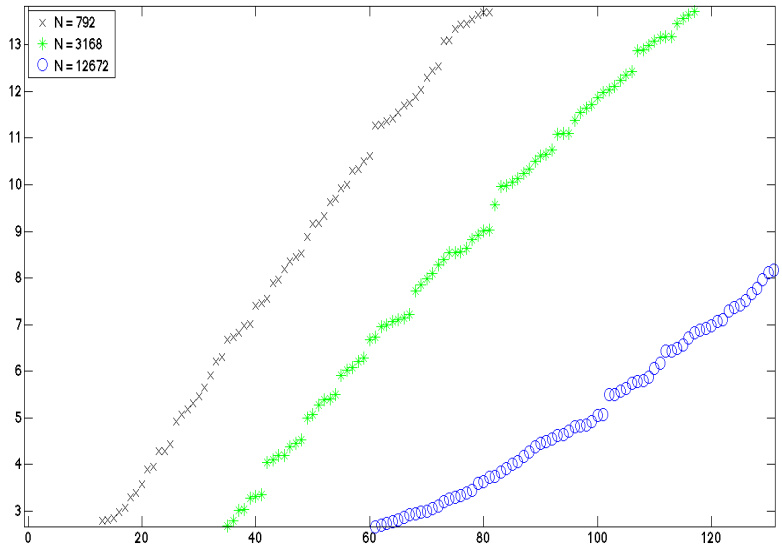
N = 792
N = 3168
N = 12672
13
12
11
10
9
8
7
6
5
4
3
0
20
40
60
80
100
120

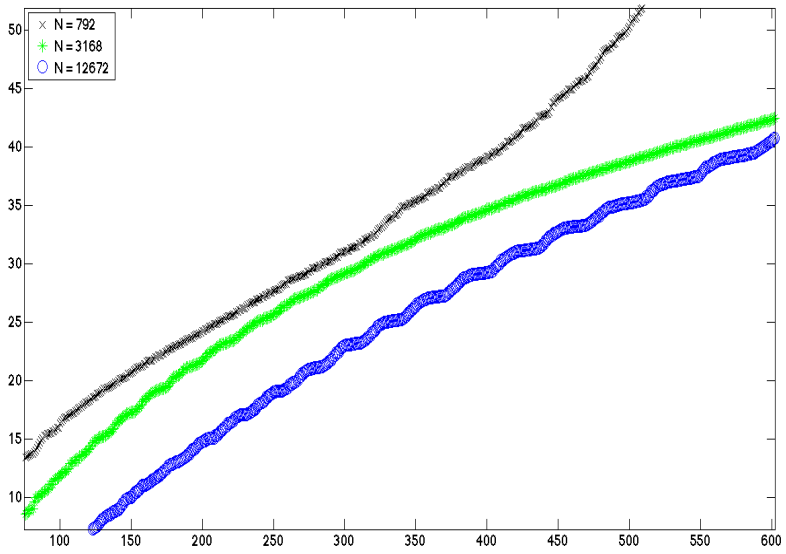
N = 792
N = 3168
N = 12672
50
45
40
35
30
25
20
15
10
100
150
200
250
300
350
400
450
500
550
600

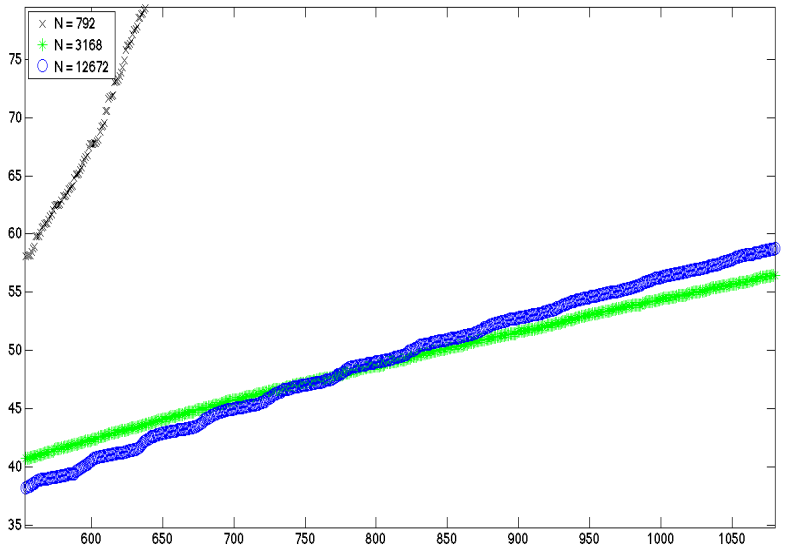
N = 792
N = 3168
N = 12672
75
70
65
60
55
50
45
40
35
600
650
700
750
800
850
900
950
1000
1050

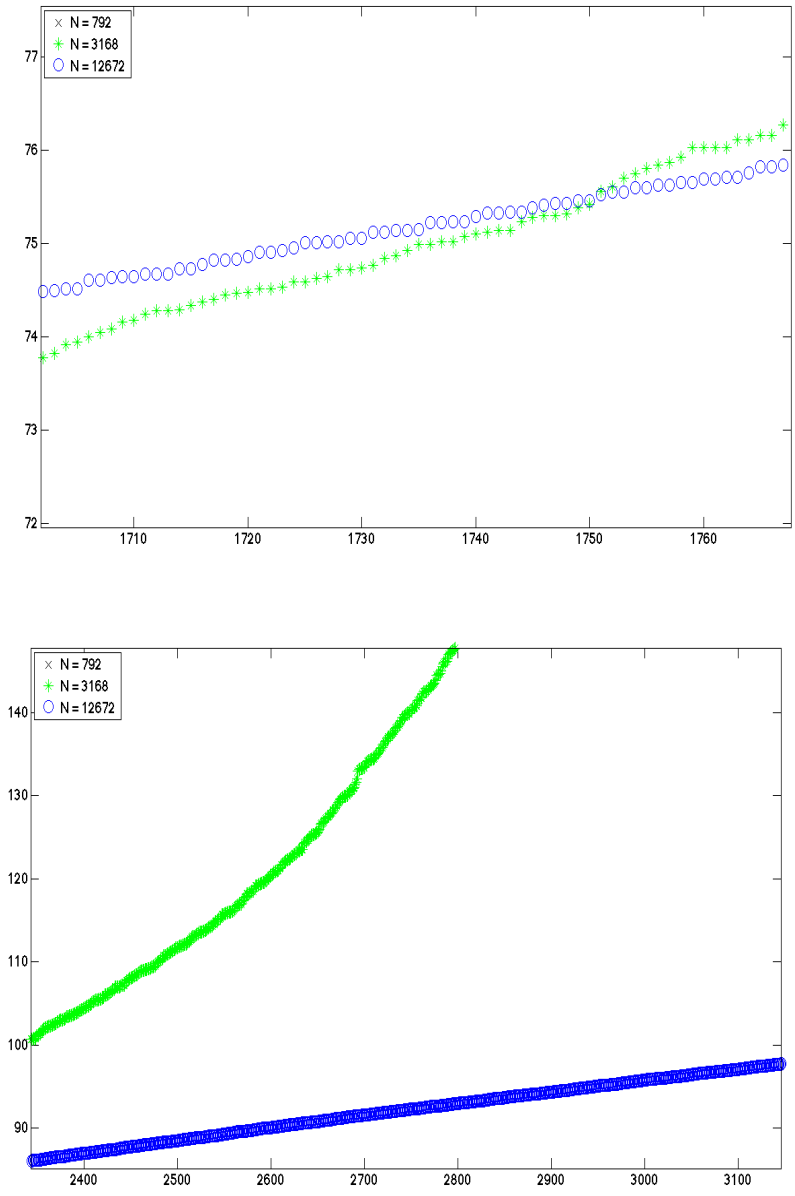

Figure 4.7: Eigenvalues for nanoparticle on a SiO_2 substrate. It shows that the results for $N = 12672$ are more accurate than the others even with higher eigenvalues.

Figure 4.7 shows the results for three meshes and explains how accurate the results are with $N = 12672$. We notice that the results with $N = 3168$ are still near the results with $N = 12672$ when the eigenvalues are small. However, with higher eigenvalues we notice the divergence between the meshes. The figure shows the results with $N = 792$ far from the other results. It shows how accurate the results with $N = 12672$ for higher eigenvalues.

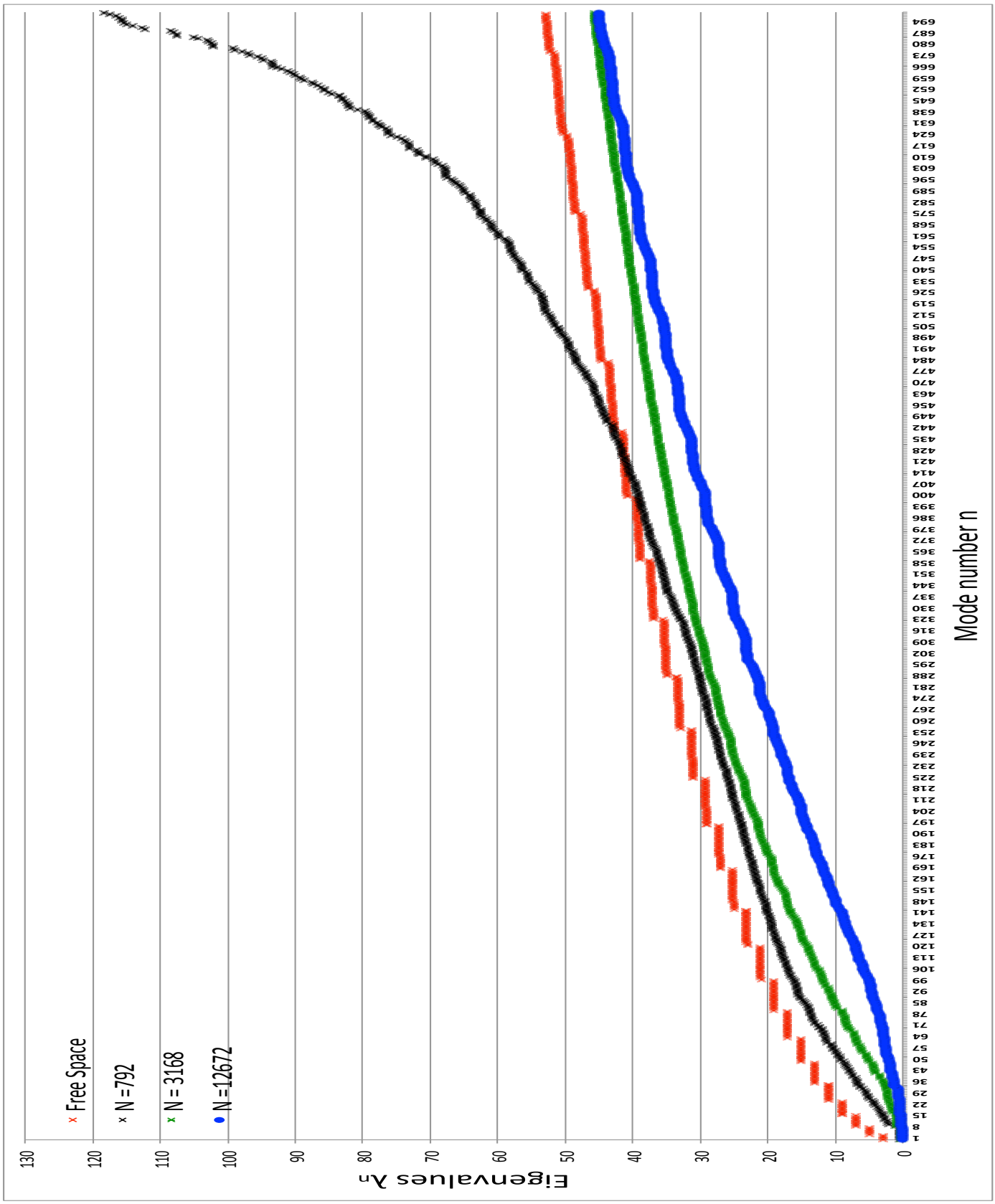

Figure 4.8: Eigenvalues chart for nanoparticle on a SiO_2, which shows the results of three computational values of three meshes. The results with $N = 12672$ compared with the results with the same number of elements from the free space case.

Figure 4.8, we compare the computational results for $N = 12672$ from Figure 4.2 with the corresponding case in Figure 4.6, we see a considerable reduction of the eigenvalues λ for a sphere on a substrate in comparison to a free space case. Referring to equation (4.2), this means that the resonant frequencies for electron oscillations on the sphere will be reduced by the presence of a substrate, which partially screens the Coulomb interactions that drive those oscillations.

4.4 Limitation of the Approximation

The computations have been performed on a laptop with a 2.3 GHz Intel Core i7 processor and 8 GB of RAM running OSX. The matrix storage for the computation of a nanosphere in free space, the matrix storage for the computation of a nanosphere on half-space, and the memory limitation of a storage for both are described in Table 4.6. We notice from the previous two sections that the accuracy of eigenvalues depends on the size of the mesh, however, because of memory limitation, we were not able to generate larger meshes.

Memory calculation	Nansphere in free space	Nanosphere on substrate	Mac OSX
Memory storage	2.78 GB	4.79 GB	8 GB
The maximum for N	32162	16081	8 GB

Table 4.6: Memory limitation

Chapter 5

Conclusion

In this work, we have given a brief historical overview of surface plasmons and localized surface plasmons (LSPR). We have listed some applications for LSPR and we have discussed some aspects of the optical properties of metallic nanoparticles. Using Maxwell's equations, we gave a theoretical description of plasmonics in metallic nanoparticles. After that, we have introduced the BEM historically and we have discussed two popular methods to derive the BIEs. We have discussed a BEM for calculating resonance frequencies of nanoparticles of arbitrary shapes.

We have presented an adaptable simulation tool for numerical solution of the considered systems. An effective BEM for the calculation of resonance frequency is demonstrated through comprehensive computational results for the nanospehical particle that are compared with exact solutions (Mie theory) for spheres. We have shown difference meshes sizes and compared the results with the exact solution. This done for particle on a free space and half space. However, the half space is not compared to the exact solution. We have shown the surface charge densities on the computed sphere addressed compared with the Associated Legendre polynomials.

Our implementation is effective, as it is able to quickly compute numerical solutions. However, we showed the limitation of the approximation and described that to have a better approximation we need more memory to save the huge matrix of the problem concerned. As discussed, the results of small meshes as $N = 792$ are not accurate enough as it diverges from the exact values even for small eigenvalues. The results of a four-time larger mesh are significantly improve the smaller one for small eigenvalues but still diverges for the large eigenvalues. The mesh of $N = 12672$ is noticeably accurate the others for all eigenvalues up to the limit of the mesh.

In future, there are numerous improvements that can be done. For instance, we could apply high order BEM to the same problem we discussed here. In terms of optical point of view it would be exciting to investigate different shapes of nanoparticles such as ellipsoid and two spheres. For the half space it would be interesting to implement our method on other substrates such as metal.

References

[1] M. Pelton and G. Bryant. *Introduction to Metal-Nanoparticle Plasmonics*. Wiley, 2013.

[2] D. Sarid and W. Challener. *Modern Introduction to Surface Plasmons: Theory, Mathematica Modeling, and Applications*. Cambridge University Press, 2010.

[3] J. Homola. "Surface Plasmon Resonance Based Sensors". Vol. 4. Springer Berlin Heidelberg, 2006.

[4] R. Wood. "On a remarkable case of uneven distribution of light in a diffraction grating spectrum". *Philosophical Magazine* 4.21 (1902), pp. 396–402.

[5] R. Schasfoort and A. Tudos, eds. *Handbook of Surface Plasmon Resonance*. The Royal Society of Chemistry, 2008.

[6] L. Rayleigh. "On the Dynamical Theory of Gratings". *Proceedings of the Royal Society of London. Series A* 79.532 (1907), pp. 399–416.

[7] U. FANO. "The Theory of Anomalous Diffraction Gratings and of Quasi-Stationary Waves on Metallic Surfaces (Sommerfeld's Waves)". *J. Opt. Soc. Am.* 31 (1941), pp. 213–222.

[8] R. Ritchie. "Plasma Losses by Fast Electrons in Thin Films". *Phys. Rev.* 106 (5 1957), pp. 874–881.

[9] E. Stern and R. Ferrell. "Surface Plasma Oscillations of a Degenerate Electron Gas". *Phys. Rev.* 120 (1 1960), pp. 130–136.

[10] J. Pitarke and V. Silkin and E. Chulkov and P. Echenique. "Theory of surface plasmons and surface-plasmon polaritons". *Rep. Prog. Phys.* 70 (2007), pp. 1–87.

[11] C. Powell and J. Swan. "Origin of the Characteristic Electron Energy Losses in Aluminum". *Phys. Rev.* 115 (4 1959), pp. 869–875.

[12] C. Powell and J. Swan. "Effect of Oxidation on the Characteristic Loss Spectra of Aluminum and Magnesium". *Phys. Rev.* 118 (3 1960), pp. 640–643.

[13] A. Otto. "Excitation of nonradiative surface plasma waves in silver by the method of frustrated total reflection". *Zeitschrift für Physik* 216.4 (1968), pp. 398–410.

[14] E. Kretschmann and H. Raether. "Radiative Decay of Nonradiative Surface Plasmons Excited by Light". *Z. Naturforsch.* A 23 (1968), 2135–2136.

[15] A. Trügler. "Optical properties of metallic nanoparticles". PhD thesis. Institut für Physik, Fachbereich Theoretische Physik Karl Franzens Universität Graz, 2011.

[16] S. Maier. *Plasmonics: Fundamentals and Applications*. Springer, 2007.

[17] T. Sandu. "Eigenmode Decomposition of the Near-Field Enhancement in Localized Surface Plasmon Resonances of Metallic Nanoparticles". *Plasmonics* 8.2 (2013), pp. 391–402.

[18] I.D. Mayergoyz, D.R. Fredkin, and Z. Zhang. "Electrostatic (Plasmon) Resonances in Nanoparticles". *Physical Review* B 72 (2005), p. 155412.

[19] U. Hohenester and A. Trügler. "MNPBEM - A Matlab toolbox for the simulation of plasmonic nanoparticles". *Computer Physics Communications* B 183 (2012), pp. 370 –381.

[20] C. Pozrikidis. *A Practical Guide to Boundary Element Methods with the Software Library BEMLIB*. Chapman and Hall/CRC, 2002.

[21] Y. Liu. *Fast Multipole Boundary Element Method: Theory and Applications in Engineering*. Cambridge University Press, 2009.

[22] S. Sauter and C. Schwab. *Boundary Element Methods*. Springer, 2010.

[23] A. Jeffrey. *Applied Partial Differential Equations: An Introduction*. Academic Press, 2003.

[24] G. Kakuba. "The Boundary Element Method: Errors and Gridding for Problems with Hot Spots". PhD thesis. Eindhoven University of Technology, 2011.

[25] R. Haberman. *Applied Partial Differential Equations with Fourier Series and Boundary Value Problems*. Pearson Education INC, 2004.

[26] H. C. van de Hulst. *Light Scattering by Small Particles*. Dover Publications, 1981.

[27] J. A. Stratton. *Electromagnetic Theory*. Wiley-IEEE Press, 2007.

[28] J. D. Jackson. *Classical Electrodynamics*. Wiley, 1962.

[29] E. Mesquitaa, R. K. N. D. Rajapakseb, and J. Labakia. "The Indirect-BEM for 3D Elastostatic and Elastodynamic Problems: Constraints, Convergence and Computational Cost". *Mecanica Computacional* XXIX (2010), pp. 4389–4398.

[30] P. Solin, I. Dolezel, and P. Karban. *Integral Methods in Low-Frequency Electromagnetics*. Wiley, 2009.

[31] C. Geuzaine and J. F. Remade. *Gmsh: a three-dimensional finite element mesh generator with built-in pre- and post-processing facilities*. URL: http://geuz.org/gmsh/.

[32] R. Quimby. *Photonics and Lasers*. John Wiley and Sons, Inc., 2006.

[33] C. Moler. *Numerical Computing with MATLAB*. URL: http://www.mathworks.com/moler/.

[34] A. Chou et al. "Predicting the Localized Surface Plasmon Resonances of Spherical Nanoparticles on a Substrate: Electrostatic Eigenmode Method". *The Journal of Physical Chemistry C* 116.50 (2012), pp. 26517–26522.

[35] K. Murata and H. Tanaka. "Surface-wetting effects on the liquid–liquid transition of a single-component molecular liquid". *Nature Communications* 1.16 (2010).

[36] U. Hohenester and J. Krenn. "Surface Plasmon Resonances of Single and Coupled Metallic Nanoparticles: A Boundary Integral Method Approach". *Physical Review* B 72 (2005), p. 195429.

[37] J.M. Montgomery, T.W. Lee, and S.K. Gray. "Theory and Modeling of Light Interactions with Metallic Nanostructures". *Journal Physics: Condensed Matter* 20 (2008), p. 323201.

[38] I. Stakgold and M.J. Holst. *Green's Functions and Boundary Value Problems*. Wiley, 2011.

[39] M. Costabel. *Principles of Boundary Element Methods*. Fachber., TU, 1986.

[40] I.D. Mayergoyz and Z. Zhang. "Numerical Analysis of Plasmon Resonances in Nanoparticles". *IEEE* 42 (2006), pp. 759–762.

[41] S. Kirkup. *The Boundary Element Method in Acoustics: A Development in Fortran*. Integrated Sound Software, 1998.

APPENDICES

Appendix A

Utilities

In this chapter we demonstrate some mathematical background that has been used throughout this thesis.

A.1 Drude Dielectric Function in Metal

Paul Drude proposed important models to describe the reaction between a metallic particle and an electromagnetic field. For more details and historical development of the model see [15]. From the quasi-static approximation which has been discussed formally and by taking the Fourier transform with respect to time only, one can rewrite the Maxwell's equations as follows:

$$\nabla \cdot \tilde{\vec{D}}(\vec{r},\omega) = \tilde{\rho}, \tag{A.1}$$

$$\tilde{\vec{E}}(\vec{r},\omega) = -\nabla\tilde{\Phi}. \tag{A.2}$$

The constitutive relation is

$$\tilde{\vec{D}}(\vec{r},\omega) = \epsilon(\vec{r},\omega)\cdot\tilde{\vec{E}}(\vec{r},\omega), \tag{A.3}$$

where the dielectric constant is $\epsilon(\vec{r},\omega) = \epsilon_0 \cdot \epsilon_r(\vec{r},\omega)$, ϵ_0 is the dielectric permittivity of vacuum and ϵ_r is the relative dielectric constant which can be written as

$$\epsilon_r(\vec{r},\omega) = \begin{cases} 1 & \vec{r} \notin V, \\ \epsilon_D(\omega) & \vec{r} \in V. \end{cases} \tag{A.4}$$

ϵ_D is Drude dielectric function in metal. This equation (A.3) can be written as

$$\tilde{\vec{D}}(\omega) = \epsilon_0\tilde{\vec{E}}(\omega) + \tilde{\vec{P}}(\omega). \tag{A.5}$$

In the time domain $\vec{P}(t)$, which is the density of dipole moments, may be defined as

$$\vec{P}(t) = ne\vec{\chi}(t), \tag{A.6}$$

where n is the density of mobile quasi-free electrons, $e\chi(\vec{t})$ is the dipole moment per electron and e is the electron charge.

Now from Newton's low of motion of a damped oscillator the differential equation for the position of electrons that are moving between heavier, relatively immobile background ions is given by

$$m\frac{\partial^2\vec{\chi}}{\partial t^2}+\gamma\frac{\partial\vec{\chi}}{\partial t}=e\vec{E}, \tag{A.7}$$

where m is electron mass and γ describes a phenomenological damping term. Using the Fourier transform with respect to time only and knowing $\vec{E}(t)=\tilde{\vec{E}}e^{-i\omega t}$, one can rewrite Eq. (A.7) as

$$(-m\omega^2-i\gamma\omega)\tilde{\vec{\chi}}(\omega)=e\tilde{\vec{E}}(\omega), \tag{A.8}$$

which yields

$$\tilde{\vec{\chi}}(\omega)=-\frac{e}{m}\frac{\tilde{\vec{E}}(\omega)}{\omega^2+i\frac{\omega}{\tau}}, \tag{A.9}$$

where $\tau=\frac{m}{\gamma}$ is the relaxation time of the quasi-free electron. Substituting (A.9) in (A.6) but in the frequency domain we get

$$\tilde{\vec{P}}(\omega)=ne\tilde{\vec{\chi}}(\omega)=-\frac{ne^2}{m}\frac{\tilde{\vec{E}}(\omega)}{\omega^2+i\frac{\omega}{\tau}}. \tag{A.10}$$

From equation (A.5) and by using (A.10):

$$\tilde{\vec{D}}(\omega)=\epsilon_0\left(1-\frac{ne^2}{\epsilon_0 m}\frac{1}{\omega^2+i\frac{\omega}{\tau}}\right)\tilde{\vec{E}}(\omega). \tag{A.11}$$

For a loss-less system, $\tau\to\infty$, and we can write the dielectric function of Drude as

$$\epsilon_D(\omega)=1-\frac{\omega_p^2}{\omega^2}, \tag{A.12}$$

where $\omega_p=\sqrt{\frac{ne^2}{\epsilon_0 m}}$ is the plasma frequency of the material containing quasi-free electrons. For instance, the plasma frequency written as

$$\omega_p=2\pi\nu_p, \tag{A.13}$$

Knowing that for gold $\nu_p=2.183\times10^{15}s^{-1}$ and $\nu_p=2.18\times10^{15}s^{-1}$ for silver, ν_p have been adopted from [35].

A.2 Laplace equation in spherical coordinates

We want to find the general solution for the Laplace equation

$$\nabla^2\Phi(\mathbf{r})=0 \tag{A.14}$$

for the potential $\Phi(\mathbf{r})$. In spherical coordinates $\mathbf{r} = (r, \theta, \phi)$, where $0 \leq r < \infty$, $0 \leq \theta \leq \pi$ and $0 \leq \phi < 2\pi$ the Laplacian operator can be written as

$$\nabla^2 = \frac{1}{r^2}\frac{\partial}{\partial r}\left(r^2\frac{\partial}{\partial r}\right) + \frac{1}{r^2}\left[\frac{1}{\sin\theta}\frac{\partial}{\partial\theta}\left(\sin\theta\frac{\partial}{\partial\theta}\right) + \frac{1}{\sin^2\theta}\frac{\partial^2}{\partial\phi^2}\right].$$

Using the method of separation of variables and assuming $\Phi(\mathbf{r}) = R(r)\,Y(\theta,\phi)$ gives the so-called radial equation as

$$\frac{1}{R}\frac{d}{dr}\left(r^2\frac{dR}{dr}\right) = \lambda \tag{A.15}$$

and

$$\frac{1}{Y}\left[\frac{1}{\sin\theta}\frac{\partial}{\partial\theta}\left(\sin\theta\frac{\partial Y}{\partial\theta}\right) + \frac{1}{\sin^2\theta}\frac{\partial^2 Y}{\partial\phi^2}\right] = -\lambda, \tag{A.16}$$

where λ is the first separation constant. The latter equation can be simplified under the assumption that Y has the form $Y(\theta,\phi) = \Theta(\theta)\,P(\phi)$, giving two equations,

$$\frac{\sin\theta}{\theta}\frac{d}{d\theta}\left(\sin\theta\frac{d\Theta}{d\theta}\right) + \lambda\sin^2\theta = m^2 \tag{A.17}$$

and

$$\frac{1}{P}\frac{d^2P}{d\phi^2} = -m^2, \tag{A.18}$$

where m is the second separation variable.

By imposing the periodic boundary condition on the solution of the last equation, $P(\phi) = P(\phi + 2\pi)$, we express its solutions in complex form as $P_m(\phi) = A\,e^{im\phi}$, where $m = 0, \pm1, \pm2, \ldots$. The solutions of the differential equation for function $\Theta(\theta)$ can be shown to be convergent on the interval $0 \leq \theta \leq \pi$ only if $\lambda = l(l+1)$, where $l = 0, 1, 2, 3, \cdots$, whereas m is subject to the constraint

$$-l \leq m \leq l.$$

This solution can be expressed in terms of the so-called Associated Legendre polynomials as $\Theta_{ml}(\theta) = B\,P_l^m(x)$ where $x \equiv \cos(\theta) \in [-1, 1]$. We can write the solution of (A.17) and (A.18) into so-called spherical harmonics $Y_{lm}(\theta,\phi)$, which are written with the normalization constant as

$$Y_{lm}(\theta,\phi) = \Theta_{ml}(\theta)P_m(\phi) = (-1)^{\frac{m+|m|}{2}}\sqrt{\frac{2l+1}{4\pi}\frac{(l-m)!}{(l+m)!}}P_l^m(\cos\theta)\,e^{im\phi}. \tag{A.19}$$

Since the factor $e^{im\phi}$ in the above function only expresses the axial symmetry of our problem, nontrivial dependence on angle θ is given through Associated Legendre polynomials, with several examples given in Table 4.4.

We note that the radial equation now becomes

$$r^2\frac{d^2R}{dr^2} + 2r\frac{dR}{dr} - l(l+1)R = 0,$$

which can be solved with the assumption $R(r) = r^p$ giving a quadratic equation for the parameter p of the form $p^2 + p - l(l+1) = 0$ with the solutions $p = -l - 1$ and $p = l$. Hence, the general solution of the radial part can be written as $R(r) = Cr^{-l-1} + Dr^l$, where $l = 0, 1, 2, \ldots$. Here, the constants C and D may be selected to prevent the divergence of the radial solution as $r \to 0$ or $r \to \infty$, depending on the context.

Finally, we can write the general solution for (A.14) in spherical coordinates in terms of spherical harmonics as

$$\Phi(r, \theta, \phi) = \sum_{l=0}^{\infty} \sum_{m=-l}^{l} \left[C_{lm} r^{-l-1} + D_{lm} r^l \right] Y_{lm}(\theta, \phi). \tag{A.20}$$

Appendix B

MATLAB Codes Used for Computation

We exhibit here some MATLAB's codes that have been used in the calculations throughout this thesis.

B.1 MATLAB Code for Constructing the Matrix for Free-space

The following code is for constructing the matrix. The inputs with the vertices received from GMSH file generate an output, which is a huge matrix of dimension $N \times N$ because in this code N represent the number of triangles.

```
% This function for constructing the matrix
function [ new_f ] = compute_new_f_last(tri)
number_of_triangles = length(tri);
new_f = zeros(number_of_triangles, number_of_triangles);
areas = area_value32(tri);

for k = 1:number_of_triangles

    x1 = tri(k,2);
    y1 = tri(k,3);
    z1 = tri(k,4);

    x2 = tri(k,5);
    y2 = tri(k,6);
    z2 = tri(k,7);

    x3 = tri(k,8);
    y3 = tri(k,9);
    z3 = tri(k,10);
```

```
r_1 = [(x1+x2+x3)/3;
    (y1+y2+y3)/3;
    (z1+z2+z3)/3];

vec1 = [x1-x2;
    y1-y2;
    z1-z2];

vec2 = [x1-x3;
    y1-y3;
    z1-z3];

cross_prod = cross(vec1,vec2);

n = cross_prod/norm(cross_prod,2);
%Since the ridus is one I will consider the real normal
%is equal to the centroid
a = dot(n,r_1);
if  a < 0

    n = -n;

end



for l = 1:number_of_triangles
    if (k ~= l)
        x4 = tri(l,2);
        y4 = tri(l,3);
        z4 = tri(l,4);

        x5 = tri(l,5);
        y5 = tri(l,6);
        z5 = tri(l,7);

        x6 = tri(l,8);
        y6 = tri(l,9);
        z6 = tri(l,10);


        r_2 = [(x4+x5+x6)/3;
            (y4+y5+y6)/3;
            (z4+z5+z6)/3];

        c = r_1 - r_2;
```

```
            new_f(k,l) = dot(n,(c/(norm(c))^3))*areas(l);


        else
            new_f(l,k) = 0;
        end
    end

end
```

B.2 MATLAB Code for Constructing the Matrix for Half-space

The following code is for constructing the matrix. The inputs with the vertices received from GMSH file generate an output, which is a huge matrix of dimension $N \times N$ because in this code N represent the number of triangles.

```
function [ halfspace ] = compute_halfspace(tri )

display('half space Section - start')

number_of_triangles = length(tri);
halfspace = zeros(number_of_triangles, number_of_triangles);
areas = area_value32(tri);
tic;

for k = 1:number_of_triangles

    x1 = tri(k,2);
    y1 = tri(k,3);
    z1 = tri(k,4);

    x2 = tri(k,5);
    y2 = tri(k,6);
    z2 = tri(k,7);

    x3 = tri(k,8);
    y3 = tri(k,9);
    z3 = tri(k,10);


    r_1 = [(x1+x2+x3)/3;
        (y1+y2+y3)/3;
        (z1+z2+z3)/3];
```

```
vec1 = [x1-x2;
    y1-y2;
    z1-z2];

vec2 = [x1-x3;
    y1-y3;
    z1-z3];

cross_prod = cross(vec1,vec2);

n = cross_prod/norm(cross_prod,2);
%since the ridus is one i will consider the real normal
%is equal to the centroid
a = dot(n,r_1);
if  a < 0
    %display ('fixing normal')
    n = -n;
end



for l = 1:number_of_triangles

    x4 = tri(l,2);
    y4 = tri(l,3);
    z4 = tri(l,4);

    x5 = tri(l,5);
    y5 = tri(l,6);
    z5 = tri(l,7);

    x6 = tri(l,8);
    y6 = tri(l,9);
    z6 = tri(l,10);

    %here we fix the half space part

    d = 1;

    r_2 = [(x4+x5+x6)/3;
        (y4+y5+y6)/3;
        (-2*d)-((z4+z5+z6)/3)];


    c = r_1 - r_2;
```

```
        halfspace(k,l) = (2.9/4.9)*dot(n,(c/(norm(c))^3))*areas(l);

    end

end


t_halfspace = toc
display('half space Section - End')
```

Appendix C

Computational Results

In this chapter we present the full results for approach B for $N = 792$ and compare them with those of $N = 3268$ and $N = 12672$.

	N = 792		N = 3168		N=12672				N = 792		N = 3168		N=12672		
l	λ	Error	λ	Error	λ	Error	Mie	l	λ	Error	λ	Error	λ	Error	Mie
1	3.029	0.029	3.007	0.007	3.002	0.002	3	67	16.81	0.188	17.16	0.156	17.05	0.053	17
2	3.03	0.03	3.007	0.007	3.002	0.002	3	68	16.87	0.134	17.17	0.174	17.06	0.058	17
3	3.03	0.03	3.008	0.008	3.002	0.002	3	69	16.9	0.101	17.2	0.196	17.06	0.065	17
4	5.089	0.089	5.023	0.023	5.006	0.006	5	70	17.06	0.064	17.21	0.215	17.07	0.07	17
5	5.094	0.094	5.024	0.024	5.006	0.006	5	71	17.06	0.064	17.22	0.224	17.07	0.072	17
6	5.094	0.094	5.024	0.024	5.006	0.006	5	72	17.17	0.174	17.23	0.235	17.07	0.073	17
7	5.1	0.1	5.026	0.026	5.006	0.006	5	73	17.24	0.241	17.25	0.252	17.08	0.078	17
8	5.103	0.103	5.026	0.026	5.007	0.007	5	74	17.27	0.266	17.28	0.277	17.08	0.084	17
9	7.166	0.166	7.044	0.044	7.011	0.011	7	75	17.38	0.385	17.29	0.288	17.09	0.085	17
10	7.176	0.176	7.046	0.046	7.012	0.012	7	76	17.41	0.414	17.29	0.288	17.09	0.088	17
11	7.187	0.187	7.049	0.049	7.013	0.013	7	77	17.52	0.52	17.31	0.307	17.09	0.091	17
12	7.187	0.187	7.049	0.049	7.013	0.013	7	78	17.65	0.654	17.34	0.345	17.1	0.1	17
13	7.195	0.195	7.052	0.052	7.013	0.013	7	79	17.69	0.686	17.36	0.36	17.1	0.103	17
14	7.205	0.205	7.054	0.054	7.014	0.014	7	80	17.69	0.686	17.36	0.36	17.11	0.106	17
15	7.211	0.211	7.056	0.056	7.014	0.014	7	81	18.03	0.969	19.06	0.055	19.04	0.042	19
16	9.234	0.234	9.067	0.067	9.017	0.017	9	82	18.12	0.877	19.08	0.081	19.04	0.043	19
17	9.259	0.259	9.073	0.073	9.019	0.019	9	83	18.22	0.779	19.11	0.107	19.05	0.053	19
18	9.267	0.267	9.077	0.077	9.02	0.02	9	84	18.29	0.706	19.16	0.163	19.07	0.067	19
19	9.285	0.285	9.08	0.08	9.021	0.021	9	85	18.42	0.583	19.18	0.179	19.07	0.067	19
20	9.285	0.285	9.08	0.08	9.021	0.021	9	86	18.42	0.583	19.19	0.192	19.07	0.07	19
21	9.301	0.301	9.081	0.081	9.021	0.021	9	87	18.53	0.472	19.21	0.21	19.08	0.076	19
22	9.301	0.301	9.089	0.089	9.023	0.023	9	88	18.69	0.312	19.25	0.254	19.09	0.087	19
23	9.346	0.346	9.095	0.095	9.025	0.025	9	89	18.74	0.264	19.25	0.254	19.09	0.089	19
24	9.375	0.375	9.105	0.105	9.027	0.027	9	90	18.79	0.205	19.28	0.279	19.09	0.093	19
25	11.23	0.231	11.09	0.086	11.02	0.024	11	91	18.9	0.103	19.29	0.286	19.1	0.097	19
26	11.29	0.289	11.1	0.1	11.03	0.027	11	92	19.02	0.017	19.31	0.312	19.1	0.101	19
27	11.31	0.31	11.1	0.1	11.03	0.027	11	93	19.02	0.017	19.33	0.328	19.1	0.104	19
28	11.31	0.31	11.11	0.106	11.03	0.029	11	94	19.12	0.119	19.35	0.347	19.11	0.11	19
29	11.34	0.342	11.11	0.109	11.03	0.03	11	95	19.12	0.119	19.35	0.347	19.11	0.11	19
30	11.39	0.391	11.12	0.12	11.03	0.032	11	96	19.29	0.29	19.37	0.374	19.12	0.116	19
31	11.41	0.412	11.12	0.123	11.03	0.033	11	97	19.37	0.366	19.38	0.384	19.12	0.122	19
32	11.44	0.438	11.13	0.132	11.04	0.035	11	98	19.41	0.413	19.44	0.439	19.13	0.132	19
33	11.49	0.494	11.14	0.143	11.04	0.038	11	99	19.44	0.44	19.48	0.476	19.14	0.144	19
34	11.49	0.494	11.15	0.148	11.04	0.039	11	100	19.59	1.409	20.91	0.093	21.02	0.02	21
35	11.57	0.566	11.16	0.165	11.04	0.043	11	101	19.59	1.409	21.07	0.067	21.06	0.057	21
36	13.19	0.192	13.1	0.097	13.03	0.028	13	102	19.8	1.203	21.09	0.093	21.06	0.063	21
37	13.24	0.235	13.11	0.114	13.03	0.033	13	103	19.85	1.15	21.14	0.143	21.07	0.072	21
38	13.29	0.291	13.13	0.126	13.04	0.036	13	104	19.95	1.052	21.14	0.143	21.07	0.072	21
39	13.29	0.291	13.13	0.131	13.04	0.038	13	105	20.1	0.901	21.18	0.181	21.08	0.083	21
40	13.38	0.375	13.15	0.148	13.04	0.042	13	106	20.12	0.883	21.19	0.193	21.09	0.086	21
41	13.4	0.403	13.16	0.156	13.04	0.043	13	107	20.2	0.798	21.22	0.216	21.09	0.09	21
42	13.45	0.452	13.16	0.159	13.04	0.045	13	108	20.22	0.779	21.23	0.232	21.09	0.09	21
43	13.5	0.5	13.18	0.183	13.05	0.051	13	109	20.22	0.779	21.25	0.252	21.1	0.099	21
44	13.5	0.5	13.18	0.183	13.05	0.051	13	110	20.31	0.688	21.28	0.276	21.1	0.103	21
45	13.55	0.554	13.19	0.192	13.05	0.052	13	111	20.5	0.502	21.32	0.32	21.12	0.115	21
46	13.59	0.59	13.2	0.201	13.05	0.054	13	112	20.57	0.427	21.34	0.335	21.12	0.122	21
47	13.62	0.624	13.2	0.201	13.06	0.056	13	113	20.67	0.327	21.34	0.342	21.12	0.122	21
48	13.65	0.654	13.21	0.215	13.06	0.059	13	114	20.67	0.327	21.37	0.371	21.13	0.129	21
49	14.97	0.026	15.09	0.087	15.03	0.029	15	115	20.74	0.263	21.4	0.398	21.13	0.133	21
50	15.07	0.071	15.14	0.136	15.04	0.043	15	116	20.88	0.117	21.44	0.435	21.14	0.141	21
51	15.13	0.132	15.14	0.14	15.04	0.043	15	117	20.88	0.117	21.47	0.473	21.15	0.151	21
52	15.22	0.221	15.17	0.166	15.05	0.05	15	118	21.04	0.038	21.47	0.473	21.16	0.158	21
53	15.24	0.244	15.17	0.171	15.05	0.05	15	119	21.04	0.038	21.53	0.527	21.17	0.166	21
54	15.26	0.257	15.19	0.191	15.06	0.055	15	120	21.14	0.137	21.53	0.534	21.17	0.169	21
55	15.3	0.305	15.19	0.191	15.06	0.058	15	121	21.22	1.785	22.88	0.121	23.03	0.029	23
56	15.4	0.395	15.2	0.198	15.06	0.06	15	122	21.22	1.785	22.96	0.041	23.04	0.043	23
57	15.41	0.411	15.22	0.218	15.06	0.063	15	123	21.34	1.657	23.06	0.058	23.06	0.062	23
58	15.46	0.457	15.23	0.226	15.07	0.066	15	124	21.36	1.641	23.06	0.058	23.07	0.07	23
59	15.52	0.524	15.23	0.235	15.07	0.066	15	125	21.53	1.469	23.07	0.07	23.07	0.075	23
60	15.56	0.564	15.25	0.251	15.07	0.072	15	126	21.53	1.469	23.11	0.108	23.08	0.076	23
61	15.64	0.643	15.25	0.251	15.07	0.072	15	127	21.6	1.4	23.12	0.125	23.09	0.085	23
62	15.71	0.707	15.27	0.267	15.08	0.075	15	128	21.7	1.295	23.15	0.149	23.09	0.091	23
63	15.77	0.775	15.3	0.304	15.08	0.084	15	129	21.82	1.183	23.16	0.164	23.09	0.093	23
64	16.57	0.427	17.1	0.101	17.04	0.042	17	130	21.93	1.072	23.2	0.203	23.11	0.108	23
65	16.66	0.338	17.12	0.124	17.05	0.047	17	131	21.93	1.072	23.27	0.271	23.12	0.121	23
66	16.71	0.295	17.15	0.148	17.05	0.051	17	132	21.98	1.022	23.3	0.297	23.12	0.125	23

Table C.1: Computational Results for N=792, 3168 and 12672

	N = 792		N = 3168		N=12672				N = 792		N = 3168		N=12672		
l	λ	Error	λ	Error	λ	Error	Mie	l	λ	Error	λ	Error	λ	Error	Mie
133	21.98	1.022	23.31	0.308	23.13	0.128	23	199	26.59	2.414	28.7	0.304	29.06	0.059	29
134	22.13	0.867	23.36	0.363	23.14	0.144	23	200	26.65	2.354	28.72	0.28	29.08	0.08	29
135	22.13	0.867	23.38	0.382	23.15	0.149	23	201	26.65	2.354	28.79	0.211	29.08	0.08	29
136	22.23	0.768	23.41	0.408	23.15	0.152	23	202	26.66	2.342	28.83	0.167	29.08	0.085	29
137	22.23	0.768	23.42	0.416	23.16	0.159	23	203	26.83	2.167	28.83	0.167	29.1	0.098	29
138	22.4	0.602	23.44	0.438	23.16	0.161	23	204	26.83	2.167	28.92	0.081	29.11	0.113	29
139	22.41	0.59	23.48	0.479	23.18	0.176	23	205	26.89	2.111	28.97	0.031	29.11	0.113	29
140	22.41	0.59	23.53	0.533	23.18	0.183	23	206	26.98	2.02	28.99	0.012	29.13	0.129	29
141	22.63	0.371	23.55	0.546	23.19	0.191	23	207	26.98	2.02	29.02	0.016	29.14	0.141	29
142	22.63	0.371	23.59	0.591	23.19	0.195	23	208	27.06	1.938	29.04	0.043	29.15	0.145	29
143	22.65	0.35	23.63	0.633	23.21	0.214	23	209	27.19	1.806	29.09	0.09	29.16	0.16	29
144	22.84	2.155	24.64	0.358	24.99	0.015	25	210	27.33	1.674	29.16	0.165	29.18	0.176	29
145	22.84	2.155	24.82	0.181	25.02	0.022	25	211	27.33	1.674	29.23	0.226	29.18	0.182	29
146	22.93	2.074	24.83	0.168	25.04	0.035	25	212	27.36	1.637	29.24	0.24	29.2	0.199	29
147	22.93	2.074	25	0.002	25.07	0.07	25	213	27.46	1.541	29.24	0.24	29.21	0.21	29
148	22.96	2.036	25	0.002	25.08	0.08	25	214	27.46	1.541	29.26	0.261	29.21	0.214	29
149	23.04	1.963	25.08	0.081	25.09	0.089	25	215	27.63	1.365	29.31	0.314	29.23	0.227	29
150	23.1	1.903	25.08	0.081	25.1	0.097	25	216	27.67	1.335	29.35	0.346	29.23	0.228	29
151	23.1	1.903	25.1	0.101	25.1	0.097	25	217	27.67	1.335	29.38	0.383	29.24	0.245	29
152	23.29	1.708	25.18	0.177	25.12	0.116	25	218	27.8	1.201	29.42	0.424	29.25	0.252	29
153	23.29	1.708	25.18	0.177	25.12	0.116	25	219	27.8	1.201	29.49	0.489	29.25	0.255	29
154	23.46	1.541	25.19	0.191	25.13	0.129	25	220	28.02	0.984	29.49	0.489	29.25	0.255	29
155	23.53	1.467	25.22	0.224	25.13	0.131	25	221	28.1	0.902	29.52	0.522	29.28	0.284	29
156	23.53	1.466	25.29	0.286	25.14	0.141	25	222	28.1	0.902	29.56	0.558	29.3	0.299	29
157	23.53	1.466	25.29	0.291	25.14	0.144	25	223	28.1	0.901	29.62	0.624	29.3	0.303	29
158	23.64	1.361	25.34	0.344	25.15	0.153	25	224	28.21	0.787	29.72	0.723	29.32	0.324	29
159	23.82	1.184	25.38	0.377	25.17	0.168	25	225	28.23	2.767	30.02	0.983	30.99	0.009	31
160	23.95	1.046	25.41	0.41	25.18	0.178	25	226	28.3	2.698	30.32	0.675	31	0.002	31
161	23.95	1.046	25.42	0.424	25.18	0.178	25	227	28.49	2.506	30.38	0.624	31.02	0.02	31
162	23.99	1.005	25.45	0.447	25.19	0.189	25	228	28.53	2.466	30.43	0.566	31.04	0.042	31
163	24.02	0.975	25.51	0.511	25.2	0.198	25	229	28.53	2.466	30.45	0.548	31.04	0.044	31
164	24.02	0.975	25.54	0.538	25.21	0.208	25	230	28.54	2.458	30.53	0.474	31.08	0.081	31
165	24.17	0.825	25.56	0.564	25.22	0.222	25	231	28.65	2.347	30.57	0.425	31.08	0.081	31
166	24.3	0.7	25.6	0.602	25.22	0.222	25	232	28.65	2.347	30.67	0.334	31.09	0.088	31
167	24.4	0.598	25.67	0.675	25.25	0.246	25	233	28.83	2.175	30.73	0.274	31.1	0.095	31
168	24.4	0.598	25.68	0.68	25.25	0.254	25	234	28.83	2.175	30.8	0.196	31.1	0.103	31
169	24.59	2.413	26.56	0.442	26.97	0.027	27	235	28.84	2.157	30.81	0.192	31.13	0.13	31
170	24.59	2.413	26.69	0.31	27.02	0.023	27	236	28.94	2.057	30.87	0.125	31.14	0.138	31
171	24.69	2.305	26.82	0.182	27.04	0.042	27	237	28.94	2.057	30.9	0.102	31.15	0.155	31
172	24.83	2.174	26.82	0.182	27.05	0.048	27	238	28.96	2.036	30.9	0.102	31.16	0.164	31
173	24.83	2.174	26.88	0.121	27.06	0.064	27	239	29.1	1.903	30.99	0.007	31.17	0.167	31
174	24.88	2.124	26.91	0.09	27.08	0.075	27	240	29.1	1.898	30.99	0.007	31.18	0.181	31
175	25	2.002	26.93	0.072	27.09	0.085	27	241	29.1	1.898	31.01	0.008	31.2	0.201	31
176	25	2.002	27.04	0.04	27.11	0.11	27	242	29.24	1.756	31.08	0.083	31.2	0.201	31
177	25.13	1.875	27.06	0.059	27.12	0.123	27	243	29.32	1.677	31.08	0.083	31.21	0.21	31
178	25.13	1.875	27.07	0.07	27.12	0.123	27	244	29.34	1.656	31.12	0.118	31.23	0.229	31
179	25.13	1.865	27.12	0.119	27.13	0.132	27	245	29.34	1.656	31.12	0.118	31.23	0.229	31
180	25.3	1.697	27.16	0.159	27.14	0.142	27	246	29.58	1.415	31.2	0.199	31.25	0.252	31
181	25.37	1.634	27.18	0.182	27.15	0.153	27	247	29.62	1.383	31.27	0.268	31.26	0.259	31
182	25.37	1.634	27.23	0.232	27.16	0.162	27	248	29.62	1.383	31.27	0.268	31.26	0.259	31
183	25.53	1.47	27.26	0.261	27.17	0.168	27	249	29.71	1.287	31.37	0.368	31.28	0.281	31
184	25.53	1.47	27.32	0.318	27.17	0.173	27	250	29.71	1.287	31.39	0.389	31.29	0.287	31
185	25.62	1.376	27.35	0.352	27.18	0.185	27	251	29.75	1.253	31.42	0.424	31.3	0.297	31
186	25.62	1.376	27.39	0.393	27.2	0.201	27	252	29.88	1.117	31.44	0.445	31.3	0.303	31
187	25.71	1.29	27.39	0.393	27.2	0.201	27	253	29.88	1.117	31.58	0.581	31.34	0.337	31
188	25.71	1.29	27.41	0.411	27.22	0.219	27	254	30.03	0.967	31.58	0.581	31.35	0.351	31
189	25.79	1.207	27.49	0.486	27.22	0.22	27	255	30.03	0.967	31.59	0.59	31.37	0.371	31
190	25.9	1.095	27.49	0.486	27.23	0.233	27	256	30.14	2.864	31.68	1.324	32.94	0.057	33
191	25.96	1.036	27.55	0.554	27.24	0.239	27	257	30.21	2.792	31.9	1.097	32.97	0.034	33
192	26.06	0.943	27.59	0.591	27.25	0.248	27	258	30.21	2.792	32.08	0.915	32.98	0.017	33
193	26.11	0.89	27.63	0.626	27.26	0.256	27	259	30.28	2.722	32.23	0.772	33.02	0.015	33
194	26.25	0.752	27.67	0.67	27.28	0.277	27	260	30.28	2.722	32.23	0.772	33.02	0.015	33
195	26.25	0.752	27.71	0.712	27.29	0.285	27	261	30.43	2.567	32.31	0.694	33.04	0.044	33
196	26.31	2.687	28.3	0.699	28.96	0.037	29	262	30.59	2.413	32.31	0.694	33.06	0.058	33
197	26.44	2.56	28.51	0.486	29.02	0.017	29	263	30.59	2.413	32.38	0.623	33.07	0.072	33
198	26.46	2.536	28.7	0.304	29.02	0.022	29	264	30.78	2.224	32.38	0.623	33.09	0.092	33

	N = 792		N = 3168		N=12672				N = 792		N = 3168		N=12672		
l	λ	Error	λ	Error	λ	Error	Mie	l	λ	Error	λ	Error	λ	Error	Mie
265	30.87	2.125	32.43	0.574	33.09	0.092	33	331	36.16	0.836	35.67	1.333	37.02	0.023	37
266	30.91	2.092	32.49	0.509	33.11	0.113	33	332	36.32	0.678	35.67	1.333	37.04	0.039	37
267	30.91	2.092	32.51	0.494	33.13	0.13	33	333	36.32	0.678	35.75	1.248	37.06	0.06	37
268	30.93	2.065	32.56	0.443	33.14	0.135	33	334	36.45	0.553	35.78	1.222	37.07	0.075	37
269	31.1	1.905	32.62	0.382	33.14	0.135	33	335	36.45	0.553	35.78	1.22	37.07	0.075	37
270	31.1	1.905	32.67	0.326	33.16	0.163	33	336	36.46	0.536	35.85	1.146	37.09	0.094	37
271	31.15	1.851	32.67	0.326	33.16	0.163	33	337	36.5	0.5	35.9	1.104	37.1	0.101	37
272	31.15	1.851	32.76	0.243	33.18	0.18	33	338	36.69	0.307	35.9	1.104	37.15	0.147	37
273	31.18	1.819	32.81	0.187	33.2	0.201	33	339	36.77	0.233	36	1.003	37.15	0.147	37
274	31.36	1.639	32.84	0.164	33.21	0.21	33	340	36.83	0.165	36.01	0.992	37.17	0.166	37
275	31.36	1.639	32.84	0.155	33.23	0.235	33	341	36.96	0.041	36.01	0.992	37.18	0.184	37
276	31.44	1.564	32.92	0.084	33.23	0.235	33	342	37.05	0.054	36.06	0.937	37.21	0.205	37
277	31.44	1.564	32.96	0.045	33.25	0.253	33	343	37.11	0.109	36.11	0.893	37.21	0.21	37
278	31.51	1.494	33.01	0.006	33.25	0.253	33	344	37.3	0.295	36.13	0.872	37.22	0.224	37
279	31.51	1.494	33.06	0.056	33.27	0.267	33	345	37.43	0.43	36.2	0.795	37.22	0.224	37
280	31.66	1.336	33.08	0.079	33.28	0.284	33	346	37.45	0.452	36.2	0.795	37.25	0.254	37
281	31.66	1.336	33.12	0.117	33.3	0.295	33	347	37.45	0.452	36.24	0.757	37.25	0.254	37
282	31.88	1.117	33.2	0.199	33.3	0.304	33	348	37.55	0.55	36.31	0.691	37.28	0.281	37
283	31.88	1.117	33.28	0.282	33.32	0.32	33	349	37.61	0.615	36.31	0.691	37.28	0.281	37
284	32.08	0.925	33.35	0.35	33.34	0.337	33	350	37.61	0.615	36.35	0.646	37.32	0.322	37
285	32.14	0.862	33.35	0.35	33.36	0.364	33	351	37.71	0.715	36.4	0.595	37.34	0.336	37
286	32.23	0.769	33.38	0.385	33.39	0.394	33	352	37.74	0.743	36.42	0.584	37.34	0.336	37
287	32.31	0.691	33.45	0.455	33.43	0.435	33	353	37.81	0.809	36.48	0.52	37.37	0.371	37
288	32.38	0.617	33.56	0.564	33.5	0.501	33	354	37.81	0.809	36.52	0.476	37.39	0.389	37
289	32.38	2.617	33.6	1.399	34.93	0.067	35	355	37.93	0.929	36.6	0.396	37.39	0.389	37
290	32.5	2.502	33.62	1.38	34.94	0.058	35	356	37.93	0.929	36.67	0.33	37.4	0.403	37
291	32.5	2.502	33.8	1.199	34.98	0.022	35	357	37.96	0.965	36.67	0.327	37.41	0.412	37
292	32.72	2.279	33.86	1.136	34.99	0.014	35	358	38.05	1.049	36.67	0.327	37.43	0.431	37
293	32.72	2.279	33.9	1.099	35.03	0.029	35	359	38.05	1.049	36.75	0.248	37.47	0.475	37
294	32.88	2.122	33.96	1.041	35.03	0.029	35	360	38.22	1.219	36.87	0.13	37.49	0.491	37
295	32.96	2.035	33.96	1.041	35.04	0.042	35	361	38.22	0.781	36.88	2.12	38.86	0.142	39
296	33.06	1.94	34.02	0.979	35.05	0.048	35	362	38.32	0.676	36.88	2.12	38.87	0.131	39
297	33.12	1.885	34.1	0.904	35.05	0.048	35	363	38.32	0.676	36.91	2.087	38.88	0.121	39
298	33.31	1.691	34.1	0.902	35.07	0.071	35	364	38.49	0.511	37.03	1.974	38.92	0.083	39
299	33.36	1.635	34.23	0.771	35.08	0.083	35	365	38.54	0.464	37.07	1.928	38.94	0.064	39
300	33.46	1.544	34.23	0.771	35.1	0.097	35	366	38.54	0.464	37.07	1.928	38.95	0.05	39
301	33.47	1.527	34.27	0.73	35.12	0.119	35	367	38.74	0.256	37.11	1.89	38.95	0.046	39
302	33.58	1.423	34.3	0.699	35.13	0.132	35	368	38.74	0.256	37.14	1.855	38.96	0.039	39
303	33.73	1.267	34.3	0.699	35.14	0.144	35	369	38.8	0.195	37.14	1.855	39	0.003	39
304	33.82	1.183	34.38	0.623	35.16	0.157	35	370	38.98	0.017	37.23	1.769	39.02	0.017	39
305	33.96	1.038	34.4	0.603	35.17	0.175	35	371	39.02	0.024	37.27	1.726	39.02	0.017	39
306	33.96	1.038	34.45	0.548	35.18	0.185	35	372	39.03	0.026	37.27	1.726	39.05	0.048	39
307	34.2	0.801	34.48	0.523	35.21	0.206	35	373	39.03	0.026	37.29	1.706	39.06	0.062	39
308	34.23	0.77	34.53	0.469	35.21	0.215	35	374	39.14	0.139	37.41	1.592	39.09	0.094	39
309	34.28	0.716	34.53	0.469	35.23	0.232	35	375	39.19	0.191	37.41	1.592	39.1	0.1	39
310	34.46	0.536	34.55	0.45	35.25	0.251	35	376	39.19	0.191	37.51	1.489	39.14	0.138	39
311	34.51	0.491	34.68	0.32	35.27	0.275	35	377	39.23	0.227	37.51	1.489	39.14	0.138	39
312	34.81	0.19	34.71	0.289	35.28	0.284	35	378	39.31	0.31	37.58	1.425	39.16	0.165	39
313	34.91	0.093	34.78	0.218	35.3	0.303	35	379	39.46	0.458	37.64	1.362	39.19	0.187	39
314	35.06	0.057	34.79	0.213	35.3	0.303	35	380	39.61	0.609	37.68	1.323	39.19	0.194	39
315	35.06	0.061	34.79	0.213	35.32	0.324	35	381	39.65	0.654	37.68	1.323	39.21	0.211	39
316	35.06	0.061	34.83	0.172	35.35	0.346	35	382	39.65	0.654	37.73	1.268	39.23	0.23	39
317	35.14	0.145	34.95	0.053	35.36	0.355	35	383	39.67	0.672	37.73	1.268	39.23	0.23	39
318	35.22	0.218	35	0.002	35.36	0.36	35	384	39.67	0.672	37.77	1.233	39.24	0.243	39
319	35.26	0.261	35.06	0.063	35.38	0.38	35	385	39.94	0.94	37.79	1.213	39.27	0.267	39
320	35.26	0.261	35.12	0.125	35.4	0.399	35	386	40.08	1.075	37.85	1.148	39.27	0.271	39
321	35.35	0.35	35.12	0.125	35.42	0.418	35	387	40.2	1.201	37.93	1.066	39.29	0.288	39
322	35.35	0.35	35.16	0.164	35.43	0.432	35	388	40.45	1.447	37.95	1.047	39.31	0.311	39
323	35.4	0.4	35.2	0.204	35.46	0.464	35	389	40.53	1.532	37.95	1.047	39.32	0.32	39
324	35.46	1.542	35.25	1.746	36.88	0.12	37	390	40.59	1.592	38.01	0.993	39.36	0.359	39
325	35.66	1.341	35.32	1.685	36.92	0.079	37	391	40.59	1.592	38.05	0.955	39.38	0.377	39
326	35.72	1.281	35.4	1.603	36.94	0.061	37	392	40.79	1.785	38.05	0.955	39.39	0.39	39
327	35.74	1.262	35.4	1.603	36.97	0.032	37	393	40.8	1.802	38.1	0.903	39.42	0.417	39
328	35.75	1.249	35.44	1.56	36.98	0.016	37	394	40.96	1.959	38.16	0.838	39.43	0.427	39
329	35.92	1.081	35.56	1.442	37	0.002	37	395	41.05	2.054	38.18	0.821	39.46	0.461	39
330	36.02	0.977	35.56	1.442	37	0.002	37	396	41.09	2.094	38.26	0.743	39.47	0.467	39

	N = 792		N = 3168		N=12672				N = 792		N = 3168		N=12672		
l	λ	Error	λ	Error	λ	Error	Mie	l	λ	Error	λ	Error	λ	Error	Mie
397	41.13	2.132	38.31	0.685	39.47	0.467	39	463	48.3	5.297	40.77	2.234	43.2	0.195	43
398	41.13	2.132	38.34	0.658	39.48	0.483	39	464	48.34	5.339	40.78	2.219	43.2	0.204	43
399	41.17	2.168	38.39	0.609	39.52	0.517	39	465	48.41	5.41	40.78	2.219	43.22	0.217	43
400	41.42	0.423	38.39	2.609	40.74	0.262	41	466	48.41	5.41	40.79	2.206	43.23	0.231	43
401	41.57	0.57	38.44	2.557	40.8	0.2	41	467	48.55	5.548	40.79	2.206	43.25	0.246	43
402	41.61	0.607	38.48	2.516	40.85	0.146	41	468	48.57	5.567	40.92	2.085	43.25	0.246	43
403	41.61	0.607	38.55	2.452	40.87	0.127	41	469	48.79	5.789	40.92	2.085	43.27	0.266	43
404	41.68	0.684	38.6	2.405	40.89	0.11	41	470	48.79	5.789	40.97	2.031	43.33	0.329	43
405	41.76	0.759	38.6	2.405	40.91	0.091	41	471	48.9	5.898	40.98	2.024	43.33	0.329	43
406	41.9	0.898	38.62	2.384	40.91	0.091	41	472	49.3	6.301	40.98	2.024	43.35	0.355	43
407	41.9	0.898	38.71	2.287	40.95	0.048	41	473	49.39	6.391	41.06	1.938	43.39	0.386	43
408	41.92	0.919	38.74	2.256	40.95	0.048	41	474	49.5	6.499	41.06	1.938	43.4	0.4	43
409	41.98	0.983	38.74	2.256	40.96	0.038	41	475	49.53	6.529	41.14	1.862	43.42	0.419	43
410	42.08	1.084	38.82	2.182	40.98	0.016	41	476	49.67	6.674	41.2	1.797	43.43	0.426	43
411	42.22	1.22	38.85	2.147	41.02	0.023	41	477	49.92	6.921	41.2	1.797	43.46	0.46	43
412	42.59	1.595	38.85	2.147	41.02	0.023	41	478	50.2	7.203	41.24	1.761	43.46	0.46	43
413	42.64	1.641	38.87	2.129	41.05	0.047	41	479	50.31	7.31	41.32	1.682	43.48	0.478	43
414	42.78	1.784	38.94	2.064	41.07	0.066	41	480	50.46	7.459	41.32	1.681	43.51	0.507	43
415	42.78	1.784	38.98	2.016	41.08	0.076	41	481	50.57	7.565	41.32	1.681	43.53	0.534	43
416	42.86	1.861	39	1.999	41.08	0.08	41	482	50.77	7.767	41.34	1.659	43.57	0.572	43
417	42.86	1.861	39.08	1.918	41.13	0.128	41	483	50.95	7.946	41.41	1.586	43.63	0.631	43
418	42.86	1.864	39.08	1.918	41.15	0.152	41	484	50.99	5.987	41.52	3.481	44.58	0.423	45
419	42.86	1.864	39.13	1.87	41.16	0.164	41	485	51.14	6.141	41.52	3.481	44.67	0.329	45
420	43.01	2.007	39.13	1.87	41.18	0.178	41	486	51.45	6.455	41.53	3.475	44.69	0.306	45
421	43.15	2.147	39.17	1.831	41.21	0.208	41	487	51.73	6.726	41.55	3.45	44.76	0.241	45
422	43.4	2.4	39.2	1.803	41.21	0.208	41	488	51.78	6.776	41.55	3.45	44.78	0.221	45
423	43.6	2.596	39.26	1.741	41.23	0.228	41	489	51.86	6.863	41.64	3.363	44.81	0.19	45
424	43.6	2.596	39.3	1.701	41.25	0.25	41	490	52.07	7.074	41.64	3.363	44.84	0.165	45
425	43.96	2.956	39.36	1.638	41.26	0.258	41	491	52.19	7.192	41.72	3.277	44.84	0.165	45
426	43.98	2.976	39.41	1.585	41.29	0.293	41	492	52.22	7.222	41.72	3.277	44.86	0.136	45
427	44.08	3.083	39.46	1.54	41.31	0.305	41	493	52.45	7.449	41.75	3.246	44.89	0.108	45
428	44.28	3.283	39.49	1.512	41.32	0.323	41	494	52.53	7.53	41.83	3.173	44.91	0.089	45
429	44.37	3.369	39.49	1.512	41.33	0.329	41	495	52.98	7.981	41.83	3.173	44.91	0.089	45
430	44.37	3.372	39.54	1.457	41.35	0.354	41	496	53.01	8.007	41.9	3.099	44.94	0.062	45
431	44.47	3.474	39.61	1.393	41.39	0.391	41	497	53.02	8.018	41.9	3.099	44.97	0.034	45
432	44.57	3.573	39.65	1.345	41.41	0.412	41	498	53.02	8.022	41.94	3.06	44.97	0.034	45
433	44.71	3.709	39.67	1.329	41.43	0.427	41	499	53.18	8.178	41.97	3.026	45	5E-04	45
434	44.93	3.93	39.67	1.329	41.43	0.427	41	500	53.18	8.183	41.99	3.011	45.02	0.025	45
435	44.93	3.93	39.72	1.28	41.45	0.45	41	501	53.27	8.275	42.09	2.91	45.02	0.025	45
436	44.94	3.936	39.79	1.208	41.45	0.45	41	502	53.41	8.407	42.09	2.91	45.05	0.053	45
437	44.95	3.948	39.79	1.208	41.5	0.503	41	503	53.41	8.407	42.15	2.847	45.06	0.056	45
438	44.95	3.948	39.84	1.156	41.52	0.518	41	504	53.42	8.425	42.15	2.847	45.06	0.056	45
439	45.15	4.152	39.93	1.07	41.53	0.531	41	505	53.5	8.505	42.2	2.805	45.11	0.113	45
440	45.28	4.277	39.93	1.07	41.57	0.567	41	506	53.51	8.507	42.2	2.805	45.14	0.137	45
441	45.38	2.385	39.98	3.021	42.69	0.307	43	507	53.56	8.561	42.26	2.744	45.14	0.14	45
442	45.6	2.601	39.98	3.021	42.78	0.224	43	508	54.04	9.041	42.26	2.736	45.14	0.14	45
443	45.61	2.612	40.01	2.987	42.78	0.224	43	509	54.29	9.292	42.39	2.614	45.17	0.175	45
444	45.66	2.659	40.09	2.907	42.83	0.172	43	510	54.32	9.318	42.39	2.614	45.23	0.228	45
445	45.79	2.791	40.11	2.889	42.83	0.166	43	511	54.32	9.318	42.4	2.597	45.24	0.244	45
446	45.79	2.791	40.13	2.872	42.83	0.166	43	512	54.49	9.491	42.4	2.597	45.24	0.244	45
447	45.81	2.812	40.24	2.764	42.86	0.144	43	513	54.58	9.58	42.46	2.536	45.27	0.265	45
448	45.93	2.931	40.24	2.764	42.9	0.102	43	514	54.96	9.963	42.5	2.504	45.29	0.293	45
449	46.01	3.009	40.24	2.759	42.9	0.102	43	515	55.33	10.33	42.53	2.466	45.33	0.332	45
450	46.03	3.034	40.24	2.755	42.95	0.051	43	516	55.39	10.39	42.6	2.397	45.35	0.348	45
451	46.22	3.219	40.24	2.755	42.97	0.035	43	517	55.45	10.45	42.6	2.397	45.37	0.371	45
452	46.39	3.394	40.34	2.66	42.97	0.035	43	518	55.51	10.51	42.68	2.322	45.38	0.384	45
453	46.61	3.607	40.43	2.568	42.98	0.021	43	519	55.51	10.51	42.68	2.322	45.4	0.404	45
454	46.74	3.744	40.44	2.556	43.01	0.007	43	520	55.79	10.79	42.68	2.322	45.43	0.427	45
455	46.95	3.946	40.45	2.555	43.02	0.015	43	521	56.16	11.16	42.76	2.241	45.43	0.43	45
456	47.04	4.044	40.45	2.555	43.04	0.04	43	522	56.28	11.28	42.76	2.241	45.44	0.44	45
457	47.39	4.387	40.53	2.469	43.06	0.065	43	523	56.44	11.44	42.83	2.17	45.45	0.452	45
458	47.45	4.455	40.57	2.431	43.06	0.065	43	524	56.53	11.53	42.83	2.17	45.52	0.519	45
459	47.53	4.534	40.61	2.389	43.12	0.117	43	525	56.53	11.53	42.86	2.135	45.53	0.535	45
460	47.66	4.665	40.64	2.364	43.13	0.133	43	526	56.55	11.55	42.9	2.102	45.57	0.568	45
461	48.03	5.032	40.68	2.32	43.15	0.148	43	527	56.84	11.84	42.95	2.047	45.62	0.616	45
462	48.19	5.192	40.68	2.32	43.17	0.173	43	528	56.99	11.99	43	1.996	45.68	0.681	45

	N = 792		N = 3168		N=12672				N = 792		N = 3168		N=12672		
l	λ	Error	λ	Error	λ	Error	Mie	l	λ	Error	λ	Error	λ	Error	Mie
529	57.08	10.08	43	3.996	46.54	0.46	47	595	69.34	20.34	45.2	3.797	48.93	0.066	49
530	57.36	10.36	43.07	3.925	46.55	0.453	47	596	69.52	20.52	45.2	3.797	48.99	0.014	49
531	57.62	10.62	43.08	3.917	46.64	0.359	47	597	70.49	21.49	45.26	3.739	48.99	0.013	49
532	57.73	10.73	43.08	3.917	46.68	0.325	47	598	70.54	21.54	45.29	3.711	48.99	0.013	49
533	57.74	10.74	43.12	3.884	46.69	0.305	47	599	70.54	21.54	45.29	3.711	49.04	0.042	49
534	57.97	10.97	43.15	3.846	46.73	0.269	47	600	71.06	22.06	45.38	3.621	49.07	0.068	49
535	58.14	11.14	43.21	3.792	46.73	0.269	47	601	71.73	22.73	45.38	3.621	49.09	0.087	49
536	58.14	11.14	43.21	3.792	46.76	0.238	47	602	71.82	22.82	45.47	3.533	49.09	0.087	49
537	58.17	11.17	43.23	3.765	46.81	0.192	47	603	71.9	22.9	45.51	3.49	49.1	0.102	49
538	58.2	11.2	43.23	3.765	46.81	0.192	47	604	72.53	23.53	45.51	3.49	49.14	0.144	49
539	58.2	11.2	43.34	3.657	46.81	0.188	47	605	73.03	24.03	45.56	3.444	49.14	0.144	49
540	58.39	11.39	43.34	3.657	46.83	0.167	47	606	73.08	24.08	45.56	3.444	49.19	0.19	49
541	58.39	11.39	43.4	3.6	46.87	0.128	47	607	73.09	24.09	45.64	3.359	49.21	0.21	49
542	58.49	11.49	43.44	3.564	46.9	0.103	47	608	73.23	24.23	45.64	3.359	49.23	0.233	49
543	58.79	11.79	43.44	3.564	46.9	0.103	47	609	73.29	24.29	45.72	3.28	49.24	0.241	49
544	58.92	11.92	43.55	3.446	46.93	0.07	47	610	73.57	24.57	45.72	3.28	49.24	0.241	49
545	59.78	12.78	43.55	3.446	46.97	0.03	47	611	73.86	24.86	45.73	3.27	49.29	0.294	49
546	59.82	12.82	43.56	3.436	47	4E-04	47	612	74.32	25.32	45.73	3.27	49.29	0.294	49
547	59.82	12.82	43.56	3.436	47.02	0.023	47	613	75.03	26.03	45.81	3.195	49.33	0.334	49
548	60.14	13.14	43.67	3.33	47.03	0.029	47	614	75.82	26.82	45.81	3.195	49.37	0.371	49
549	60.17	13.17	43.67	3.33	47.03	0.029	47	615	76.2	27.2	45.9	3.099	49.38	0.385	49
550	60.56	13.56	43.68	3.316	47.09	0.091	47	616	76.3	27.3	45.9	3.099	49.43	0.426	49
551	60.66	13.66	43.73	3.27	47.09	0.091	47	617	76.52	27.52	45.92	3.077	49.44	0.443	49
552	60.89	13.89	43.73	3.27	47.09	0.093	47	618	76.9	27.9	45.96	3.037	49.49	0.493	49
553	60.91	13.91	43.81	3.188	47.14	0.141	47	619	77.12	28.12	45.99	3.01	49.52	0.52	49
554	60.91	13.91	43.85	3.146	47.17	0.166	47	620	77.49	28.49	45.99	3.01	49.53	0.527	49
555	61.23	14.23	43.85	3.146	47.19	0.187	47	621	77.57	28.57	46.03	2.969	49.58	0.584	49
556	61.55	14.55	43.97	3.033	47.19	0.187	47	622	78.14	29.14	46.03	2.969	49.62	0.625	49
557	61.66	14.66	43.98	3.024	47.2	0.195	47	623	78.56	29.56	46.05	2.945	49.65	0.649	49
558	62.22	15.22	44.07	2.934	47.21	0.214	47	624	78.58	29.58	46.1	2.899	49.72	0.721	49
559	62.46	15.46	44.07	2.934	47.21	0.214	47	625	78.88	27.88	46.21	4.79	50.28	0.721	51
560	62.52	15.52	44.11	2.891	47.26	0.264	47	626	78.95	27.95	46.25	4.749	50.38	0.617	51
561	62.52	15.52	44.11	2.891	47.29	0.289	47	627	79.21	28.21	46.25	4.749	50.45	0.555	51
562	62.56	15.56	44.12	2.877	47.29	0.289	47	628	79.39	28.39	46.3	4.696	50.45	0.555	51
563	62.57	15.57	44.14	2.857	47.33	0.332	47	629	79.67	28.67	46.3	4.696	50.5	0.5	51
564	62.89	15.89	44.18	2.821	47.36	0.364	47	630	81.59	30.59	46.35	4.648	50.53	0.472	51
565	63.22	16.22	44.25	2.752	47.38	0.383	47	631	81.98	30.98	46.35	4.648	50.53	0.472	51
566	63.22	16.22	44.25	2.748	47.41	0.411	47	632	82.05	31.05	46.4	4.604	50.62	0.384	51
567	63.33	16.33	44.25	2.748	47.41	0.411	47	633	82.39	31.39	46.4	4.596	50.62	0.384	51
568	63.51	16.51	44.31	2.688	47.43	0.431	47	634	82.56	31.56	46.4	4.596	50.63	0.371	51
569	63.88	16.88	44.35	2.645	47.46	0.458	47	635	82.93	31.93	46.42	4.579	50.69	0.311	51
570	63.93	16.93	44.35	2.645	47.49	0.485	47	636	83.1	32.1	46.56	4.442	50.7	0.297	51
571	64.08	17.08	44.45	2.551	47.52	0.517	47	637	83.11	32.11	46.59	4.41	50.72	0.282	51
572	64.18	17.18	44.45	2.551	47.54	0.537	47	638	83.49	32.49	46.59	4.41	50.75	0.25	51
573	64.7	17.7	44.45	2.546	47.58	0.58	47	639	83.55	32.55	46.61	4.394	50.76	0.237	51
574	64.82	17.82	44.48	2.515	47.69	0.692	47	640	84.56	33.56	46.61	4.394	50.81	0.188	51
575	65.12	18.12	44.52	2.479	47.71	0.705	47	641	85.02	34.02	46.63	4.369	50.81	0.188	51
576	65.13	16.13	44.6	4.398	48.42	0.578	49	642	85.62	34.62	46.69	4.306	50.82	0.176	51
577	65.21	16.21	44.6	4.398	48.5	0.495	49	643	85.62	34.62	46.7	4.296	50.84	0.161	51
578	65.52	16.52	44.64	4.363	48.59	0.409	49	644	86.37	35.37	46.7	4.296	50.84	0.161	51
579	66.09	17.09	44.7	4.297	48.6	0.398	49	645	86.71	35.71	46.75	4.255	50.89	0.115	51
580	66.37	17.37	44.71	4.288	48.6	0.398	49	646	87.3	36.3	46.77	4.234	50.92	0.077	51
581	66.64	17.64	44.78	4.222	48.65	0.349	49	647	87.66	36.66	46.77	4.234	50.94	0.064	51
582	66.72	17.72	44.78	4.222	48.69	0.312	49	648	88.73	37.73	46.87	4.127	50.98	0.015	51
583	66.97	17.97	44.79	4.209	48.69	0.312	49	649	89.29	38.29	46.87	4.127	50.98	0.015	51
584	67.04	18.04	44.79	4.209	48.72	0.284	49	650	89.91	38.91	46.88	4.122	51.01	0.01	51
585	67.72	18.72	44.85	4.15	48.74	0.26	49	651	90.21	39.21	46.88	4.122	51.04	0.036	51
586	67.72	18.72	44.94	4.059	48.75	0.252	49	652	90.66	39.66	46.97	4.033	51.07	0.065	51
587	67.8	18.8	44.97	4.025	48.75	0.246	49	653	91.17	40.17	47	3.999	51.08	0.081	51
588	67.85	18.85	44.97	4.025	48.77	0.226	49	654	91.23	40.23	47	3.999	51.08	0.081	51
589	67.96	18.96	44.98	4.018	48.8	0.2	49	655	91.85	40.85	47.05	3.95	51.12	0.116	51
590	68.09	19.09	45.03	3.971	48.84	0.162	49	656	92	41	47.12	3.883	51.14	0.141	51
591	68.17	19.17	45.04	3.963	48.84	0.162	49	657	92.8	41.8	47.12	3.875	51.14	0.141	51
592	68.22	19.22	45.08	3.918	48.87	0.13	49	658	93.33	42.33	47.12	3.875	51.18	0.182	51
593	68.72	19.72	45.08	3.918	48.91	0.086	49	659	93.34	42.34	47.14	3.857	51.21	0.214	51
594	68.77	19.77	45.17	3.833	48.91	0.086	49	660	93.36	42.36	47.17	3.829	51.23	0.227	51

	N = 792		N = 3168		N=12672				N = 792		N = 3168		N=12672		
l	λ	Error	λ	Error	λ	Error	Mie	l	λ	Error	λ	Error	λ	Error	Mie
661	93.55	42.55	47.17	3.829	51.25	0.251	51	727	178.9	125.9	49.16	3.839	53.65	0.647	53
662	94.82	43.82	47.25	3.753	51.26	0.259	51	728	182.8	129.8	49.16	3.839	53.67	0.675	53
663	94.88	43.88	47.3	3.703	51.31	0.313	51	729	183.5	128.5	49.16	5.836	54.01	0.989	55
664	96.64	45.64	47.3	3.703	51.34	0.345	51	730	200.5	145.5	49.19	5.814	54.09	0.909	55
665	96.96	45.96	47.31	3.686	51.34	0.345	51	731	203.6	148.6	49.19	5.814	54.18	0.822	55
666	97.07	46.07	47.32	3.683	51.36	0.357	51	732	204.3	149.3	49.24	5.762	54.19	0.811	55
667	97.91	46.91	47.32	3.683	51.42	0.415	51	733	209.5	154.5	49.24	5.762	54.25	0.752	55
668	99.24	48.24	47.42	3.583	51.42	0.415	51	734	209.8	154.8	49.32	5.677	54.28	0.718	55
669	102.1	51.08	47.42	3.583	51.46	0.456	51	735	219.9	164.9	49.36	5.638	54.34	0.661	55
670	102.2	51.24	47.43	3.575	51.49	0.487	51	736	223.2	168.2	49.36	5.638	54.36	0.643	55
671	102.4	51.36	47.46	3.539	51.54	0.536	51	737	227.2	172.2	49.37	5.632	54.39	0.614	55
672	102.9	51.88	47.46	3.539	51.55	0.552	51	738	233.3	178.3	49.37	5.632	54.39	0.614	55
673	102.9	51.93	47.55	3.453	51.59	0.593	51	739	237.7	182.7	49.45	5.548	54.48	0.525	55
674	104.4	53.37	47.57	3.431	51.63	0.626	51	740	238.2	183.2	49.47	5.533	54.48	0.525	55
675	105	54.05	47.61	3.391	51.66	0.659	51	741	238.4	183.4	49.47	5.533	54.49	0.514	55
676	107.6	54.59	47.61	5.391	52.17	0.826	53	742	239.7	184.7	49.55	5.449	54.5	0.499	55
677	107.9	54.92	47.65	5.35	52.3	0.695	53	743	250.9	195.9	49.57	5.432	54.55	0.447	55
678	108	54.97	47.68	5.319	52.32	0.68	53	744	257.7	202.7	49.63	5.369	54.55	0.447	55
679	108.4	55.42	47.68	5.319	52.36	0.642	53	745	259.4	204.4	49.68	5.324	54.58	0.421	55
680	112.3	59.28	47.72	5.283	52.41	0.586	53	746	263.9	208.9	49.68	5.324	54.6	0.401	55
681	112.6	59.61	47.79	5.214	52.41	0.586	53	747	275	220	49.73	5.273	54.6	0.401	55
682	114.1	61.12	47.79	5.214	52.45	0.548	53	748	275.1	220.1	49.73	5.273	54.64	0.357	55
683	115	62.02	47.84	5.159	52.5	0.495	53	749	276	221	49.78	5.219	54.64	0.357	55
684	115.4	62.43	47.87	5.126	52.51	0.488	53	750	276.2	221.2	49.78	5.219	54.7	0.299	55
685	115.7	62.7	47.94	5.059	52.51	0.488	53	751	278.1	223.1	49.85	5.153	54.7	0.299	55
686	116	62.99	47.94	5.059	52.55	0.45	53	752	280.6	225.6	49.85	5.153	54.74	0.263	55
687	116.6	63.6	47.95	5.053	52.55	0.45	53	753	283.3	228.3	49.87	5.126	54.78	0.218	55
688	117.5	64.48	47.97	5.032	52.62	0.378	53	754	289	234	49.87	5.126	54.82	0.181	55
689	117.5	64.53	48.04	4.964	52.62	0.378	53	755	313.9	258.9	49.93	5.07	54.83	0.168	55
690	118.8	65.82	48.05	4.949	52.65	0.348	53	756	331.3	276.3	50	4.996	54.83	0.168	55
691	120.4	67.38	48.11	4.885	52.67	0.332	53	757	339.3	284.3	50	4.996	54.86	0.139	55
692	120.7	67.72	48.11	4.885	52.72	0.284	53	758	352.1	297.1	50.01	4.99	54.9	0.1	55
693	121.4	68.42	48.14	4.862	52.72	0.284	53	759	398.7	343.7	50.12	4.876	54.92	0.079	55
694	123.4	70.36	48.2	4.801	52.72	0.28	53	760	406.1	351.1	50.12	4.876	54.93	0.075	55
695	124.1	71.14	48.21	4.786	52.76	0.24	53	761	415.3	360.3	50.15	4.852	54.99	0.014	55
696	124.6	71.62	48.21	4.786	52.82	0.185	53	762	416.5	361.5	50.15	4.852	54.99	0.014	55
697	125	71.99	48.29	4.715	52.82	0.185	53	763	450.1	395.1	50.18	4.816	55	0.003	55
698	125.5	72.5	48.29	4.713	52.83	0.174	53	764	477.3	422.3	50.18	4.816	55.07	0.072	55
699	126.8	73.81	48.29	4.713	52.87	0.134	53	765	516.7	461.7	50.24	4.757	55.07	0.072	55
700	128.4	75.42	48.33	4.674	52.91	0.086	53	766	533.2	478.2	50.24	4.757	55.08	0.084	55
701	131.4	78.44	48.4	4.605	52.93	0.07	53	767	574	519	50.27	4.733	55.12	0.12	55
702	131.4	78.44	48.4	4.605	52.93	0.07	53	768	578.8	523.8	50.27	4.733	55.16	0.161	55
703	132.7	79.75	48.42	4.581	52.95	0.053	53	769	588.4	533.4	50.36	4.642	55.17	0.171	55
704	135.4	82.39	48.51	4.494	52.99	0.014	53	770	588.6	533.6	50.36	4.642	55.17	0.171	55
705	135.5	82.54	48.52	4.485	53.01	0.01	53	771	611.9	556.9	50.4	4.599	55.23	0.226	55
706	137.5	84.52	48.55	4.453	53.01	0.01	53	772	643.4	588.4	50.4	4.599	55.23	0.226	55
707	139.7	86.71	48.55	4.453	53.05	0.055	53	773	744	689	50.41	4.591	55.27	0.272	55
708	141	87.95	48.58	4.416	53.07	0.067	53	774	839	784	50.49	4.513	55.27	0.272	55
709	143.7	90.65	48.63	4.369	53.08	0.083	53	775	842.3	787.3	50.51	4.486	55.36	0.356	55
710	151.1	98.13	48.65	4.353	53.1	0.103	53	776	857.3	802.3	50.51	4.486	55.36	0.356	55
711	151.7	98.73	48.65	4.353	53.13	0.13	53	777	896.8	841.8	50.56	4.438	55.4	0.396	55
712	152.2	99.2	48.68	4.323	53.18	0.183	53	778	974.2	919.2	50.61	4.394	55.41	0.413	55
713	152.5	99.5	48.72	4.284	53.18	0.183	53	779	1026	971.5	50.66	4.342	55.42	0.423	55
714	153.4	100.4	48.73	4.269	53.21	0.209	53	780	1054	998.9	50.66	4.342	55.48	0.48	55
715	153.5	100.5	48.73	4.269	53.24	0.236	53	781	1078	1023	50.76	4.237	55.49	0.492	55
716	153.7	100.7	48.74	4.257	53.26	0.256	53	782	1114	1059	50.78	4.216	55.56	0.555	55
717	156	103	48.74	4.257	53.3	0.296	53	783	1371	1316	50.78	4.216	55.63	0.633	55
718	157.7	104.7	48.87	4.129	53.32	0.318	53	784	1734	1677	50.79	6.212	55.66	1.336	57
719	157.7	104.7	48.87	4.129	53.35	0.346	53	785	1805	1748	50.81	6.19	55.85	1.146	57
720	165.1	112.1	48.91	4.089	53.35	0.346	53	786	2152	2095	50.81	6.19	56	1	57
721	167.9	114.9	48.91	4.089	53.38	0.383	53	787	3170	3113	50.87	6.13	56.08	0.918	57
722	170.7	117.7	48.92	4.082	53.45	0.448	53	788	8795	8738	50.91	6.093	56.08	0.918	57
723	172.5	119.5	48.98	4.023	53.47	0.47	53	789	10030	9973	50.92	6.083	56.11	0.891	57
724	173	120	49.02	3.978	53.53	0.531	53	790	36450	36393	50.96	6.036	56.16	0.841	57
725	174.1	121.1	49.1	3.898	53.53	0.531	53	791	48095	48038	50.96	6.035	56.2	0.805	57
726	176.2	123.2	49.12	3.882	53.6	0.603	53	792	N/A	N/A	N/A	N/A	N/A	N/A	N/A